

Deep Space Optical Terminal

Design study on a lunar laser communication system

MSc Thesis Aerospace Engineering
Rooderick J. Ciggaar

Deep Space Optical Terminal

Design study on a lunar laser communication
system

by

Rooderick J. Ciggaar

to obtain the degree of Master of Science
at the Delft University of Technology,
to be defended publicly on December 8, 2023 at 09:30 AM.

Student number: 4626230
Project duration: March 1, 2023 – December 8, 2023
Thesis committee: Prof. Dr. E. K. A. Gill, TU Delft, committee chair
Dr. Ir. R. Saathof, TU Delft, supervisor
Ir. E. Bertels, Ispispace, supervisor
Dr. S. Speretta TU Delft, external committee member

Cover: The ESO VLT in Paranal, Chile fires a laser guide star into the
heart of the Milky Way. (ESO/Yuri Beletsky)
Style: TU Delft Report Style, with modifications by Daan Zwaneveld

An electronic version of this thesis is available at <http://repository.tudelft.nl/>.

Preface

TU Delft's seal in figure 1 depicts a fiery torch which symbolizes the ancient Greek myth of Prometheus, who stole fire from the gods as a gift to mankind. Fire in this regard stands for knowledge and technology. Quite similar, TU Delft's gift to society is technological development. Another parallel can be made to the Deep space Optical Terminal (DOT). Once operational, the terminal would effectively form a celestial beacon of light unlocking new scientific knowledge and technology.

First of all I would like to thank my supervisors, Dr. Ir. Rudolf Saathof of the TU Delft and Ir. Eric Bertels of Isispace for their valuable guidance and expertise. I would like to thank Isispace and in particular Jeroen Rotteveel for the opportunity to perform my thesis on this amazing innovative subject. Equivalently, I would like to thank my family, Esther, Christiaan, Isabeau and Pim for their continuous support. Similarly I would like to thank my space study mates for the good times, big shoutout to Frankie, Ludo and Carla. Shoutout to my Rijnlands homies 'Ouwe jongens krentenbrood'. Last but not least I would like to thank Dr. Stéphanie Cazaux for the opportunity to work on Enceladus exploration for a while and I would like to thank Ir. Barry Zandbergen for his wise teachings.



Figure 1: TU Delft seal [138].

*Rooderick J. Ciggaar
Delft, November 2023*

List of Abbreviations

4QD	Four quadrant	DPSK	Differential phase shift keying
AO	Adaptive optics	DSD	Deep Space Deployer
AOCS	Attitude and orbital control system	DSN	Deep space network
APD	Avalanche photodiode	DSOC	Deep space optical communication
ASE	Amplified spontaneous emission	DTE	Directly to Earth
ASM	Attached synchronization marker	ECC	Error correction coding
AU	Astronomical unit	EDFA	Erbium doped fiber amplifier
BER	Bit error rate	EDRS	European data relay system
BO	Backend optics	Eff	Efficiency
BPSK	Binary phase shift keying	EIRP	Effective isotropic radiated power
BS	Beamsplitter	EM	Electromagnetic
CAD	Computer Aided Design	Er	Erbium
CCSDS	Consultative Committee for Space Data Systems	ESA	European Space Agency
CE	Control electronics	ESO	European Southern Observatory
CFLOS	Cloud free line of sight	EYDFA	Erbium Ytterbium doped fiber amplifier
CMD	Command	FEC	Forward error correction
Comm	Communications	FOV	Field of view
COTS	Commercial of the shelf	FPGA	Field programmable gate array
CPA	Coarse pointing assembly	Freq	Frequency
CR	Coding rate	FSM	Fast steering mirror
CRC	Cyclic redundancy check	FSO	Free space optics
CSM	Codeword sync marker	Gb	Gigabit
CTE	Coefficient of thermal expansion	Gbps	Gigabit per second
DBS	Dichroic beamsplitter	GEO	Geostationary orbit
DFB	Distributed feedback laser	HPE	High photon efficiency
DL	Downlink	HW	Hardware
DLA	Downlink laser assembly	IAC	International Astronautical Congress
DOCOMAS	Deep space optical communication architecture study	IF	Interface
DOT	Deep space optical terminal	IM/DD	Intensity modulated direct detection
		IMU	Inertial measurement unit
		InGaAs	Indium-Gallium-Arsenide

IOD	In orbit demonstration	PAA	Point ahead angle
ISL	Intersatellite link	PAM	Point ahead mirror
JAXA	Japan Aerospace Exploration Agency	PAT	Pointing, acquisition and tracking
JPL	Jet Propulsion Laboratory	PD	Photodiode
KPLO	Korean Pathfinder Lunar Orbiter	ph	photon
L5	Lagrange point 5	PMT	Photomultiplier tube
LADEE	Lunar Atmosphere and Dust Environment Explorer	PPM	Pulse position modulation
LCRD	Laser communications relay demonstration	PSD	Power spectral density
LCT	Laser communication terminal	PSK	Phase shift keying
LD	Laser diode	PTAP	Peak to average power ratio
LEO	Low earth orbit	PU	Power unit
LLCD	Lunar laser communications demonstration	QAM	Quadrature amplitude modulation
LLO	Low lunar orbit	QE	Quantum efficiency
LLR	Log likelihood ratio	QPSK	Quadrature phase shift keying
LOS	Line of sight	Retro	Retroreflector mirror
LRO	Lunar reconnaissance orbiter	RF	Radiofrequency
MAB	Main asteroid belt	RMS	Root mean square
Mbps	Megabit per second	RQ	Research question
MCT	Mercury Cadmium Telluride	Rx	Receiver
MEPS	Modular electronic power system	SAR	Synthetic aperture radar
MOPA	Master Oscillator Power Amplifier	Sat	Satellite
MZM	Mach-Zehnder Modulator	SC	Spacecraft
NASA	National Aeronautics and Space Administration	SCPPM	Serially concatenated pulse position modulation
NEO	Near earth orbit	SE	Systems engineering
NIR	Near Infrared	SGAC	Space Generation Advisory Council
NRHO	Near rectilinear halo orbit	SH	Stakeholder
O2O	Orion to Optical	Si	Silicon
OBC	Onboard computer	SMTF	Synchronization marked transfer frame
ODSN	optical deep space network	SNR	Signal to noise ratio
OGS	Optical Ground Station	SNSPD	Superconducting nanowire single photon detector
OH	Optical head	SOTA	State of the art
OOK	On-off-keying	SPC	Single photon counter
		SPL	Solar Pumped Laser
		SQ	Sub-question

SR	System requirement	UHD	Ultra high definition
SW	Software	UL	Uplink
SWAP	Size, weight and power	VLT	Very Large Telescope
TBD	To be determined	WFE	Wavefront error
TM	Telemetry	xDFA	Doped fiber amplifier
TRL	Technology readiness level	Yb	Ytterbium
Tx	Transmitter		

Summary

The future will see an increase in missions headed for deep space. Advanced payloads and crewed missions will require higher data rates in more efficient spacecraft. Conventional space communication is facilitated through RF technology. Although it has a lot of space heritage and is very reliable, doubts arise on its future sustainability because of limited bandwidth, inefficiency and a saturated spectrum. Deep space optical communication (DSOC) can mitigate all these issues and may present a sustainable solution. Many near Earth optical communications systems have already been demonstrated in orbit while only two DSOC systems have been launched up to now. These include the 'Lunar Laser Communications Demonstration' (LLCD) terminal and the 'Deep Space Optical Communications' (DSOC) terminal aboard the Psyche mission to the main asteroid belt (MAB). The Dutch NXTGEN high-tech program aims to stimulate the high-tech industry in the Netherlands, including optical communication among other fields of expertise. Isispace is part of this program and wants to increase its system knowledge on DSOC technology. Hence in this thesis work performed at Isispace, a concept is generated for the link and opto-mechanical design of a **Deep space Optical Terminal (DOT)**, which is meant to be able of high data rate optical communication between the Moon and Earth.

Applications for DOT were explored in several use cases, the first of which a lunar science mission. Main priorities for this use case are a high downlink data rate with low bit error rate. The second use case included a 'live' video call to a lunar orbital or surface station. Main priorities for this case are a high availability with low latency, in order to keep the call as live as possible. Additionally, a hypothetical lunar platform spacecraft was modelled on which DOT could be mounted. These applications resulted in stakeholder requirements, from which system requirements were derived. These were the focus of the thesis. The methodology applied was based on a systems engineering approach using the V-model for product development. Several systems engineering tools were used in the process of coming to a concept design.

The first design iteration focused on achieving a link design that is able to meet correlated system requirements. Several constraints had to be taken into account here which include the optical ground station, assumed to be TNO's at the Waalsdorpervlakte, having a diameter of 0.8 meter, adaptive optics capacity and 200 W uplink power at a wavelength of 1064 nanometer. Another constraint is noise experienced by the optical link. A very conservative noise power level has been assumed here for all noise sources, that is approximately one order of magnitude larger than similar optical system designs assume for just the daylight background radiance. The first critical link parameter is wavelength. Two trades were performed for the up and downlink, which resulted in choices of 1064 and 1550 nm respectively. These choices comply with the Consultative Committee for Space Data Systems (CCSDS) protocol for interoperability in space data systems. For coding, serially concatenated pulse position modulation (SCPPM) has been chosen which is currently one of the, if not the most efficient coding scheme available, approaching capacity limit within one dB. Regarding modulation, several schemes were considered in a trade-off, which ultimately resulted in a choice for pulse position modulation (PPM), compliant with the SCPPM coding scheme. PPM seems to be the best option primarily because of its unrivalled power efficiency, adaptability and resilience to atmospheric turbulence. In order to meet the downlink data requirement, modulation and coding was determined to have a 16-PPM modulation order, a 0.125 nanosecond slot time and a coding rate of 2/3, achieving 1067 Mbit/s. In order to meet the uplink data requirement, modulation and coding was determined to have a 4-PPM modulation order, a 2 nanosecond slot time and a coding rate of 2/3, achieving 33 Mbit/s. Lower performance settings are also possible in case of sub-optimal link conditions. As for pointing, it was decided to aim for a maximum loss of 2 dB as recommended by NASA and others for deep space applications. Using a TNO fine steering mirror in combination with an aperture equal or smaller than 10 cm would allow this. The link will encounter several factors along its path to the receiver. These include link gains and losses. The link equation determines received power as a function of these factors and transmitted power. When the required receiver power is known along with these factors, transmitter or in this case

DOT terminal characteristics can be determined. An SCPPM deep space Poisson channel simulation was set up in Matlab. The goal of this was to model the link including modulation and coding with different levels of optical transmit power. This produces bit error rate (BER) curves as a function of this power. In combination with one of the system requirements determining maximum BER and the link budget, required optical effective isotropic radiated power (EIRP) was determined for DOT to be 134 dBm. A constant EIRP curve was produced at steady pointing loss as a function of transmit power and diameter aperture. DOT terminal design parameters, which lie on this curve, were determined in the second design iteration.

The second design iteration focused on the opto-mechanical system design including subsystems. It was decided to split the system into five subsystems: the Control Electronics (CE), the Modem, the Downlink Laser Assembly (DLA), the Optical Head (OH) and the Power Unit (PU). Each subsystem has its own tasks and interactions with the others which ultimately define the total system capability. The CE will control data flows that are to be up and downlinked by the terminal. It furthermore controls the other subsystems and acts a main interface of the terminal to the spacecraft. The modem is where data translation happens between digital bits and the physical SCPPM scheme. The downlink laser is generated in the DLA. Use of PPM modulation goes very well with average power limited lasers and fiber amplifiers. A powerful laser will have to be created and modulated at a clock rate of 8 GHz using a binary input vector from the modem. A high extinction ratio is preferred to maintain a high peak to average power (PTAP) ratio. The best architecture seems to be a Master Oscillator Power Amplifier (MOPA) with external modulator. This would include a continuous wave distributed feedback (DFB) seed laser at several tens of mW power, externally modulated by a Lithium Niobate electro-optic modulator with extinction ratio over 30 dB. The modulated low power laser is then amplified using multiple fiber amplifier stages with optical isolators, amplified spontaneous emission (ASE) filters and photodiode (PD) taps for monitoring quality and safety. The OH couples, guides, expands and condenses transmit and receive beams. It crosses the spacecraft (SC) skin with the backend optics (BO) located inside, which is firmly connected to the Course Pointing Assembly (CPA) located just outside the SC, mounted in a vibration isolation frame. The BO includes an optical assembly where the fiber coupled downlink beam is free space coupled, pointed ahead, verified, and stabilized before being sent to the CPA. The uplink beam is received from the CPA, stabilized and detected by an avalanche photodiode (APD) array in terms of spatial orientation and data communication. Spatial data is sent to the CE for pointing and tracking purposes and the data signal is sent to the modem for decoding. The CPA includes an off axis Coudé telescope mounted in a two axis gimbal frame, achieving hyper-hemispherical range. The optimal aperture diameter proved to be 10 centimeter. This means an average optical power of 1.5 W is required with a peak power of 30 W, when using 16-PPM. Tracking will be supported by several different methods along the disturbance frequency spectrum. The Power Unit (PU) is meant to collect power from the spacecraft platform before distributing it to the DOT subsystems. Isispace's Modular Electric Power System (iMEPS) would be a feasible candidate for this. It includes a battery for storage, management, conditioning and distribution units.

The integrated system was reviewed, combining the link and opto-mechanical design iterations. A product tree was produced which illustrates the setting of the DOT system within a hypothetical spacecraft. The link analysis and design results were combined in a link budget for the maximum downlink data rate case. Size, weight and power budgets for all subsystems were estimated based on models, literature and market analysis. Uncertainty factors for each respective subsystem were taken into account, similar to methods used at Isispace, for the calculation of a worst case scenario. This resulted in total estimation for the system of approximately 28 liters, 20 kg and 85 W for size, mass and power use respectively. A high level interface diagram is produced which highlights DOT subsystems, internal interactions between subsystems and external interactions with the spacecraft and space in terms of data, power and optical link. Derived specifications for the subsystems were listed and summarized which were found as a result of the design iterations.

The system requirements were subsequently verified in order to check if design steps were taken properly. Verification methods included design review and analysis of results. All system requirements were complied with. The thesis is concluded by revisiting the main research questions and its sub-questions. There are several points of discussion. This thesis mainly highlights the link and opto-

mechanical design aspects of the terminal while there are many more relevant aspects, which were not part of the scope. This thesis is very theoretical and further research would require practical experiments for more verification and validation of the system. The thesis is validated in a sense that it meets the initial need statement, however the concept design itself is not due to the theoretical nature of this report. Furthermore, this thesis focuses on the application of systems engineering for a DSOC design. Given its multidisciplinary nature, there was not enough time to specialize into every field concerned with DSOC. Hence, some generalized assumptions were made for certain aspects of the terminal within the design iterations.

It is recommended to tackle the problem of limited availability of optical communication due to atmospheric sensitivity by expanding existing optical ground system infrastructure. Additionally, increasing laser efficiencies of these systems would enable even higher data rates in the future. The initiative for boosted DSOC development lies at government agencies that can create demand for DSOC in exploration missions. The industry, where the momentum lies, will automatically follow to meet that demand. DSOC development should be a high priority since it is of significant relevance for future exploration missions. It will collaterally prove to be a contribution to other important research fields not only focused on space, but for Earth applications as well.

Contents

Preface	i
Summary	v
1 Introduction	1
1.1 Current state of technology	1
1.2 Research plan	2
1.3 Scope	3
1.4 Thesis layout	4
2 Applications	5
2.1 Use cases	5
2.1.1 Analysis	5
2.1.2 Conclusion	6
2.2 Reference platform	6
3 Requirements	9
3.1 Stakeholder requirements	9
3.2 System requirements	9
4 Methodology	11
4.1 Steps taken	11
4.2 V-model	11
4.3 Systems engineering tools	12
4.4 Software tools	13
5 Link design	14
5.1 Constraints	14
5.1.1 Optical ground station	14
5.1.2 Noise	15
5.2 Wavelength	15
5.2.1 Downlink trade	16
5.2.2 Uplink trade	16
5.3 Coding	17
5.4 Modulation	19
5.4.1 Modulation trade	19
5.4.2 Downlink settings	20
5.4.3 Uplink settings	21
5.4.4 Lower modulation settings	21
5.5 Pointing	21
5.5.1 Acquisition	23
5.5.2 Pointing loss	24
5.6 Link analysis	25
5.6.1 Link equation	25
5.6.2 CCSDS SCPPM Poisson channel simulation	26
5.6.3 EIRP	27
6 Opto-mechanical design	30
6.1 Control electronics	30
6.2 Modem	31
6.3 Downlink laser assembly	32
6.4 Optical head	33

6.5	Power unit	40
7	System design	42
7.1	Product tree	42
7.2	Link Budget	43
7.3	SWAP budgets	43
7.3.1	Control electronics	43
7.3.2	Modem	44
7.3.3	Downlink laser assembly	45
7.3.4	Optical head	46
7.3.5	Power unit	46
7.3.6	Summary	46
7.4	Interfaces	48
7.5	Derived specifications	48
8	Verification	50
9	Conclusion	51
9.1	Conclusion	51
9.2	Discussion	52
9.3	Recommendations	52
	References	53
A	Matlab codes	60
A.1	BER plots	60
A.2	Data rates	61
A.2.1	Downlink	61
A.2.2	Uplink	61
A.3	Pointing	62
A.3.1	Pointing loss vs. geometric loss	62
A.3.2	Required pointing accuracy vs. Diameter	62
A.4	SCPPM deep space Poisson simulation	63
A.5	3D EIRP plot	64
A.6	2D EIRP plots	64
B	Redundant chapter: Challenges and opportunities	66
B.1	Challenges	66
B.1.1	Laser and amplifier efficiency	66
B.1.2	Pointing	66
B.1.3	Modulation slot time	66
B.1.4	Geographic diversity	67
B.1.5	Atmospheric turbulence	67
B.1.6	Photon counting uplink detector	67
B.1.7	Low spectral efficiency PPM	67
B.2	Opportunities	67
B.2.1	Fast steering dichroic beam splitters	67
B.2.2	Solar pumped lasers	68
B.2.3	Multidimensional pulse position modulation	70
B.2.4	Multifunctional uplink detector	71
B.2.5	Isispace deep space deployer and optical relay	72
C	Redundant work	75
C.1	Downlink detector	75
D	Simulations	77

List of Figures

1	TU Delft seal [138].	i
1.1	EDRS ISL with RF downlinks [102].	2
1.2	Envisioned DOT terminal on a lunar orbiter [40].	3
4.1	V-model of systems engineering [44].	12
5.1	TNO optical ground station in the Hague [32].	14
5.2	Atmospheric loss as function of wavelength and several popular wavelengths used for optical communication [2].	15
5.3	Information block size [14].	17
5.4	SCPPM as prescribed by the CCSDS [14].	18
5.5	BER versus SNR of various considered modulation schemes.	20
5.6	Achievable data rate as function of slot time and PPM order at constant coding rate of 2/3.	21
5.7	Uplink data rates vs slot time and PPM order at 2/3 CR.	22
5.8	Nested uplink channels.	22
5.9	Typical optical terminal PAT system [50].	23
5.10	Link acquisition process [65].	23
5.11	Pointing loss vs. geometric loss trade for optimal aperture diameter.	24
5.12	Required pointing accuracy as function of preset pointing loss and aperture diameter.	25
5.13	The process of estimating active SCPPM slots at the receiver [20].	27
5.14	BER as function of signal photons for maximum downlink rate.	28
5.15	3D plot of constant EIRP surface as function of three system variables.	28
5.16	DOT required EIRP.	29
5.17	DOT required EIRP compared with LLCD and DSOC EIRP lines and their respective design points.	29
6.1	High level architecture of O2O modem [26].	32
6.2	Concept MOPA architecture.	33
6.3	Backend optics.	35
6.4	Power spectral density for SILEX spacecraft platform vibration [131].	36
6.5	Disturbance stabilization spectral coverage.	36
6.6	Point ahead angle [13].	37
6.7	Body mounted and moving head CPAs.	38
6.8	Single mirror and periscope CPA.	38
6.9	CPA and telescope mounted in a vibration isolation frame.	39
6.10	Redundant double inverse telescope assembly concept.	40
6.11	Isispace MEPS elements [57].	41
7.1	DOT product tree.	42
7.2	LLCD space terminal subsystems with the CE left, Modem above and OH below [9].	44
7.3	LLCD modem design [25].	45
7.4	O2O modem [26].	45
7.5	Solidworks model of the OH.	46
7.6	Solidworks model of all DOT subsystems scaled on a $1m^2$ plate.	47
7.7	High level interface overview.	48
B.1	Fast steering dichroic beam splitter performing PA.	68
B.2	TNO FSM [72].	68
B.3	SPL used for terrestrial FSO [144].	69

B.4	Terrestrial solar irradiance spectrum along with absorption spectrum of the Ce:Nd:YAG pump medium used in [79].	69
B.5	Multiwavelength PPM (MWPPM) [27].	70
B.6	Multidimensional PPM	71
B.7	Binary substrate 4QD APD array. The green circle represents uplink beam and the red circle the downlink beam PAA verification.	71
B.8	Data rates as function of slot time and PPM order.	73
B.9	CCSDS SCPPM deep space Poisson simulation for Saturn.	73
B.10	Comparison of EIRP for several DSOC terminals.	74
C.1	SNSPD mechanism [94].	76
D.1	SCPPM max datarate simulation 1.	77
D.2	SCPPM max datarate simulation 2.	78
D.3	SCPPM max datarate simulation 3.	78
D.4	SCPPM max datarate simulation 4.	79
D.5	SCPPM max datarate simulation 5.	79

List of Tables

2.1	Use case derived link requirements.	7
2.2	DOT hypothetical platform analysis.	7
2.3	Reference lunar platforms.	8
3.1	DOT stakeholder requirements.	9
3.2	DOT system requirements.	10
4.1	Software tools used during the thesis	13
5.1	Various noise estimation approaches [19][122][32].	15
5.2	Downlink wavelength trade.	16
5.3	Uplink wavelength trade.	17
5.4	Modulation scheme trade.	19
5.5	DOT modulation and data rate settings.	23
5.6	Link equation terms. NB: TBD values calculated later on in this report.	26
6.1	Uplink detector trade.	34
6.2	Aperture diameter trade.	37
6.3	CPA trade.	39
7.1	DOT downlink budget.	43
7.2	DOT size budget with estimation model uncertainties causing the margin. Variables A, B and C have uncertainties of 5, 10 and 15% respectively.	47
7.3	DOT mass budget with estimation model uncertainties causing the margin. Variables A, B and C have uncertainties of 5, 10 and 15% respectively.	47
7.4	DOT power budget with estimation model uncertainties causing the margin. Variables A, B and C have uncertainties of 5, 10 and 15% respectively.	47
7.5	Maximum SWAP budget.	48
7.6	Derived system specifications.	49
8.1	System requirements compliance matrix.	50
9.1	DOT link design.	51
C.1	Downlink detector trade.	75

1

Introduction

In recent years, more initiatives for deep space exploration missions have sprung up. Several countries are aiming for the lunar south pole, chasing resources [83][61]. Crewed deep space exploration will continue on the Moon through the Artemis program [80]. Initiated by NASA, the program will return humans to the moon and establish a permanent orbital station through Gateway [43], before expanding lunar surface infrastructure. The Moonlight and LunaNet lunar orbital communication constellations are meant to support this program [29][38].

NASA and SpaceX even have a long term goal of setting foot on Mars [80][124]. Additionally, there is an increasing amount of missions aiming for the outer solar system with three flagship missions to Europa, Uranus and Enceladus [81][5][103]. Missions are thus going deeper into space. Simultaneously, technological development enables payloads to gather more high quality data, which is to be downlinked to Earth in sometimes limited transmission windows [74][133].

Communication in space is conventionally done through radio-frequency (RF) techniques. It is very reliable because of atmospheric transparency at these frequencies. It still is the primary method for (deep) space communication [12]. The Mars Reconnaissance Orbiter (MRO) for example is meant to search for evidence of water on Mars. It is therefore equipped with several instruments to study surface features including the high resolution camera HiRISE. A single image made by this camera may be up to 28 Gbit in size, which is reduced to 11.2 Gbit after data compression [86]. With a maximum downlink rate of 6 Mbit/s using RF however, a single image transfer may take more than 30 minutes [60]. Another example is the Lunar Reconnaissance Orbiter (LRO). Launched in 2011 and still operational, the orbiter has a daily payload data generation rate of 572 Gbit. With a maximum downlink rate of 100 Mbit/s, daily data offload takes approximately 95 minutes [68].

This presents a problem since payload data generation rates will only increase and spacecraft will need to be more efficient in support of future sustainable and commercial exploration. Doubts are increasing regarding sustainability of RF technology for future applications for several reasons. It has limited bandwidth and achievable data rates. Its spectrum is becoming saturated, and its wide beamwidth is relatively inefficient at large deep space ranges. Optical or **laser communication** on the other hand, which operates at much smaller wavelengths in the near infrared (NIR) part of the spectrum, can mitigate these problems. It has a larger bandwidth with higher data rates, its narrow beam width causes a smaller chance of interference and thus its spectrum is yet unregulated. This smaller beam width furthermore yields a higher system efficiency at large deep space ranges [65]. RF may not be able to meet future (deep) space mission needs and optical might be the solution [63][140].

1.1. Current state of technology

The first ever established space optical communication link was performed by JAXA's ETS-VI GEO satellite in 1995, achieving a 1 Mbit/s downlink. In 2001, ESA demonstrated the first ever inter-satellite

link (ISL) over a distance of 40,000 km at 50 Mbit/s. In 2014, ESA launched the European Data Relay System (EDRS), the first operational laser communication system consisting of multiple GEO satellites capable of 1.8 Gbit/s [48], which is depicted in figure 1.1. Regarding DSOC, not a lot of systems have been demonstrated yet. Early 2013, NASA used a laser uplink to transmit an image of the Mona Lisa to the Lunar Orbiter Laser Altimeter (LOLA) instrument aboard the Lunar Reconnaissance Orbiter (LRO). Later on in 2013, a DSOC terminal was part of NASA's Lunar Atmosphere and Dust Environment Explorer (LADEE) mission called the Lunar Laser Communication Demonstration (LLCD) [9]. The mission set a DSOC record with 622 Mbit/s downlink and 22 Mbit/s uplink to lunar orbit [75].

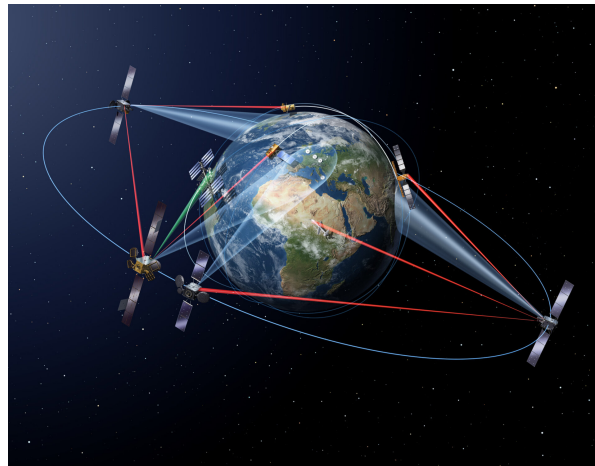


Figure 1.1: EDRS ISL with RF downlinks [102].

The Psyche mission launched in October 2023 will explore the main asteroid belt (MAB) metallic asteroid 16 Psyche [62]. It has an optical terminal called 'DSOC' which will demonstrate high data rate optical links beyond Mars. The technology demonstration recently achieved 'first light', which means the first duplex link has been established [98]. The European Space Agency (ESA) is also planning to apply a DSOC terminal on its space weather mission to the Sun-Earth Lagrange 5 point (L5) [122]. Both ESA and NASA are additionally planning to construct optical satellite networks around the moon with Moonlight [38] and LunaNet [29].

1.2. Research plan

The high-tech industry is one of the primary economic motors in the Netherlands. The NXTGEN high-tech program initiated by the ministry of economic affairs is meant to achieve more collaboration and technological development in several fields within this sector in order to maintain Dutch leadership. Laser communication is one of these fields. Main expertise on this currently resides at TNO, however many more companies, institutes and academics are getting involved in this consortium. This includes Isispace which intends to participate and leverage this collaboration. A need statement has therefore been formulated:

Isispace intends to participate in the development of deep space optical communication terminals as part of the Dutch NXTGEN high-tech program. In order to do this the company needs to expand its expertise into the field of opto-mechanical systems design for deep space optical terminals.

Isispace already has a lot of experience in satellite avionics and RF technology. Regarding DSOC, the company wants to expand its knowledge on optical link design and opto-mechanical systems. To meet this need, a thesis statement has been formulated:

*This exploratory thesis aims to generate a concept design of the optical link and opto-mechanics of a **Deep space Optical Terminal**, which is meant to be able of high data rate communication between*

the Moon and Earth.

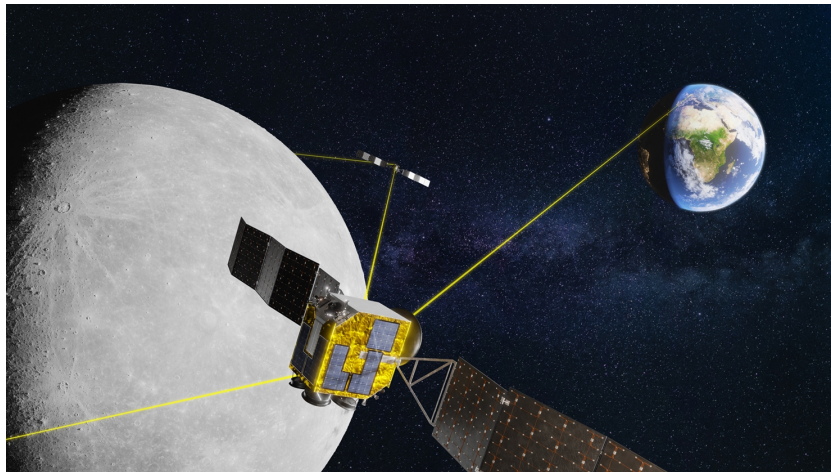


Figure 1.2: Envisioned DOT terminal on a lunar orbiter [40].

The envisioned DOT is depicted in figure 1.2. In order to support the thesis statement, a thesis research question has been formulated:

What optical link and opto-mechanical design is needed for a terminal aboard a lunar orbital spacecraft, enabling high data rate optical communication with Earth?

The following sub-questions (SQ) will guide the author in the process of answering the research question:

- SQ1: What are the system requirements for a spacecraft terminal that facilitates an optical communication link between the Moon and Earth?
- SQ2: What link design is needed for an optical communication system between the Moon and Earth?
- SQ3: What are the opto-mechanical subsystems of the optical communication terminal aboard the lunar orbital spacecraft?

The first SQ discusses explicitly what exactly is required of the system in terms of functions and characteristics. The system requirements (SR) follow up on the stakeholders requirements. Once these requirements are clear, design can start. In this case with the second SQ discussing the link design that supports fulfilment of the system requirements. The third SQ discusses the physical opto-mechanical design that is required to realize the link design discussed in SQ2. The sub-questions thus naturally follow up on each other.

1.3. Scope

The focus of this thesis is the system link design and the opto-mechanical part of the space terminal in lunar orbit. Emphasis lies on link analysis, design choices and the subsystems required to realize the link. Models are used to illustrate variations in design variables. Required subsystems, their components and budgets are discussed. The design process is discussed using systems engineering methods and tools.

Naturally, constraints imposed by connected elements like the optical ground station (OGS) and spacecraft (SC) platform have been mentioned shortly but not extensively. Potential mission operational details have been discussed roughly in the uses cases but are considered outside the current scope. Housing, thermal control and mechanical SC interfaces have not been discussed as these depend on specific applications. The system requirements defined in chapter 3 will only include the

system requirements relevant within the scope of the research question of link and opto-mechanical design and will therefore not include every system requirement.

1.4. Thesis layout

Chapter 1 intended to give an introduction to the subject, the current state of technology and to the research plan of this thesis. Chapter 2 will follow with use cases and a hypothetical platform on which the terminal could be mounted. These will generate stakeholder requirements from which subsequently system requirements are derived, answering SQ1 in chapter 3. Chapter 4 elaborates on the system engineering methodologies applied during the thesis project. It explains how this thesis report is setup in a V-model format where chapter 5 is the first design iteration following the system requirements. This chapter answers SQ2 by discussing the envisioned link design needed to meet the correlated system requirements. Chapter 6 follows up with the second design iteration, answering SQ3, discussing the physical opto-mechanical design and subsystems required to support discussed link design. Chapter 7 integrates and reviews both design iterations into a single system. Verification of the system requirements happens in chapter 8. Finally, chapter 9 will conclude the research and sub-questions, discuss and review the work performed in this thesis and finally make recommendations.

2

Applications

In this chapter, two potential use cases for DOT will be highlighted, along with a hypothetical spacecraft platform on which DOT could be mounted. These support derivation of the stakeholder and system requirements which are leading the design iterations. Use cases will be evaluated on four link parameters deemed to be relevant for users: Bandwidth, latency, bit error rate (BER) and availability. The reference platform application is meant to generate mass and power requirements for DOT.

2.1. Use cases

This section will discuss two use cases for DOT. The use cases include:

- A lunar science orbiter with two data heavy payloads onboard, including a synthetic aperture radar and a hyper-spectral imager. Large amounts of data are generated by these which have to be offloaded daily, while maintaining high quality.
- An ultra HD (UHD) 4K 'live' video call to cis-lunar space, either to a crewed orbital station or the lunar surface.

2.1.1. Analysis

This subsection will analyse both cases in more detail to support derivation of relevant link requirements.

Science downlink

Synthetic Aperture Radar (SAR) is a form of radar used to produce 2D or 3D images of objects and landscapes [52]. Typical SAR images cover an area of about 100x100 km with a raw data size of about 60 to 300 Mbit [7]. These instruments can produce large amounts of data. ICEYE's SAR operates only for about 120 s/ orbit because of this. Typical downlink rates for SAR missions are for example 100 Mbit/s for ICEYE's SAR, 500 Mbit/s for CARBSAR and up to >1 Gbit/s for Capella space [54]. JAXA is even aiming for 2 Gbit/s in their newest SAR [115]. Uplink rates are much smaller because this is only used for commands.

The second payload is a hyperspectral imager. These instruments also capture images, but for each pixel, its radiant intensity along a wide range of the electromagnetic spectrum is captured. This produces 'data cubes' for each image as a function of x, y and λ (wavelength) along the axes, producing large amounts of data in the process like for example the PRISMA satellite of the Italian Space Agency (ASI) [69]. The instrument produces up to 600 Mbit/s when imaging, requiring a downlink rate of 155 Mbit/s. HypSIPI, another hyperspectral satellite by the Jet Propulsion Laboratory (JPL) uses a downlink rate of 800 Mbit/s and assumes an average link time per orbit of 10 min, as the satellite payload generates 5000 Gbit per day on average [47].

The two payloads are assumed to have an operational time of approximately 120 seconds per orbit. A data generation rate of 600 Mbit/s would then result in 144 Gbit/orbit and 1728 Gbit per earth day. This amount of data should be fully downlinked within one day to keep data flow steady state. To make

an estimation of required data flow, a parallel assumption with the LLCD mission will be made. This mission performed approximately 5 link sessions per earth day, each with duration around 20 minutes [107][116]. If the same link time is used as for DOT, an average downlink rate of 288 Mbit/s is required.

Latency is not a high priority in the science case. Minimum latency is already set to be 1.3 seconds due to the lightspeed constraint. Additional signal processing, distribution and interleaving will contribute even more. Latency could be traded against data quality and in the science case, data quality is of higher priority. The most important thing is that the scientific data arrives as accurate as possible, thus with the least errors as possible. This is why the optical terminal has to have a low Bit Error Rate (BER) in the order of 10^{-6} , after error correction. This value for BER is often handled in DSOC [50][8][65][90][31]. Availability of the satellite is less of a priority in the science case, but this depends on data generation rate and the mission concept of operations since the generated data has to be downlinked to make place for new data production. As already mentioned, around 1.7 Tbit/day of data will be generated. Assuming a bandwidth of around 288 Mbit/s and a complete daily downlink of all generated data, an availability is required of 6.9%.

Live video call

An Ultra HD 4K stream takes approximately up to 30 Mbit/s bandwidth one way [8][46]. This would be needed for both up and downlink. Required availability will be relatively high in order to facilitate an uninterrupted link. In the small time frame of an hour long call, it is estimated that a downtime of maximum 1 minute is allowed. This means an availability of 98.3 % is required. This will be difficult to achieve with one satellite. Instead, a constellation or network might be needed to support this high availability. Such a network may contain different satellites from various manufacturers in different countries. Interoperability and international standards are therefore important to achieve for such a network to succeed.

In order to produce a video call as live as possible, this scenario requires a low latency. That means signal processing will have to be minimized just like the number of involved network devices because each adds more latency. Referring to the LLCD mission, one way data transfer to the moon had a latency of 3.4 seconds. Reducing interleaving intervals from 1 second in LLCD, to milliseconds, can significantly lower latency to about 2.5 seconds. This would include time of flight, data and video processing, earth transfer and a margin. However, decreasing interleaving interval may affect data quality because of atmospheric distortion and scintillation. NASA recently released a preliminary requirements document for its Lunanet relay system. Here it specified a requirement that latency for real time video transfer between Earth and the moon shall be no more than three seconds [29], which is consistent with the 2.5 seconds defined here.

Compared to the first case concerning high quality science data, BER is more flexible in this application. Not only because small errors during a video call are not critical, but also because error correction techniques increase latency. A lower latency may be traded against higher BER.

2.1.2. Conclusion

Table 2.1 shows a summary of the use case analysis. The required downlink rate of 288 Mbit/s for the science mission is almost 3 times higher than the currently active maximum downlink rate from lunar orbit by the LRO, still only half of that demonstrated by the LLCD. Latency in the science downlink is not the biggest priority and is assumed to have a maximum equal to that of the LLCD system in 2013. For the video call, availability is of high importance to allow for a continuous connection. A BER value similar to that of the science mission is mentioned which, as discussed, is often handled for DSOC in literature.

2.2. Reference platform

This section will discuss a potential application of DOT on a hypothetical spacecraft platform, which is modelled based on previous lunar missions, in order to determine system requirements in terms of mass and power. An analysis based on volume was unfortunately not possible due to lack of data. DOT is envisioned to improve on system budgets relative to similar systems. This is important to en-

Table 2.1: Use case derived link requirements.

Aspect	Science downlink	Video call
Bandwidth	288 Mbit/s down	30 Mbit/s up and down
Latency	3.4 s	2.5 s
BER	10^{-6} after ECC	10^{-6} after ECC
Availability	6.9%	98.3%

able more efficient systems for future exploration missions.

Four recent lunar missions were taken into consideration. These include the Lunar Atmosphere and Dust Environment Explorer (LADEE), the Lunar Reconnaissance Orbiter (LRO), the Korean Pathfinder Lunar Orbiter (KPLO) and the Chandrayaan-2 orbiter. Their specifics are listed in table 2.3.

An estimation is made for a hypothetical spacecraft platform on which DOT could be used based on payload characteristics of these similar missions and subsequent extrapolation. Two payloads are assumed for the hypothetical platform, just like the science use case, which seems to be the minimum for a lunar mission. Assuming the minimum amount of payloads will result in lower end baseline mass and power requirements for DOT. This means DOT will be applicable for both small and large deep space platforms.

The average payload instrument mass is 9.17 kg considering all platforms in the table. Two payloads times average payload mass gives 18.3 kg total payload mass for the reference platform. Taking the average payload mass to SC mass ratio of 0.09255 gives a total SC mass of 198.2 kg. Then taking the average payload instrument power consumption of 17.19 W and doubling it gives the total payload power use of 34.4 W. Then using the average payload power consumption to average SC power ratio of 0.147 gives a total average power of 233.9 W for the hypothetical SC.

It is envisioned that DOT will relatively improve on LLCD regarding system power and mass budget. Using the LLCD mass to SC mass ratio of 0.12 as a baseline, DOT would have to have a mass less than 24 kg. Furthermore using the LLCD optical terminal power consumption ratio to total SC average power of 0.383 as a baseline, DOT has to use less than 89.6 W. These calculations are summarized in table 2.2.

The applications for DOT discussed in this chapter will produce requirements that are elaborated on in the next chapter on stakeholder and system requirements.

Table 2.2: DOT hypothetical platform analysis.

DOT hypothetical spacecraft	Mass	Power
Payloads	18.3 kg	34.4 W
Spacecraft	198 kg	234 W
DOT	24.0 kg	89.6 W

Table 2.3: Reference lunar platforms.

	Specifi- cation	LADEE	LRO	KPLO	Chandrayaan-2 (orbiter)
General	Mission	<i>study the pristine state of the lunar atmosphere and dust environment prior to significant human activities [67]</i>	<i>Map the Moon's surface, identify landing sites, locate resources, study lunar radiation environment [68]</i>	<i>Development of critical technologies for lunar exploration, identify future landing sites, survey lunar resources [92]</i>	<i>Demonstrate new technologies for future planetary missions, deploy lunar lander-rover and enhance science objectives of Chandrayaan-1 with improved resolution [22]</i>
	Launch	2013 [67]	2009 [68]	2022 [139]	2019 [22]
	Dry mass	248 kg [4]	949 kg [68]	550 kg [66]	682 kg [104]
	Average orbital power	295 W	824 W	760 W [66]	1000 W
	Lifetime	160 days	1+13 years (and counting)	1 year	7.5 years
Payloads	# of data generating instruments	3	7	6	8
	Daily data generation rate	10-100 Gbit	572 Gbit	10-100 Gbit	
	Total payload mass	18.9 kg	91.7 kg	40 kg	85 kg [22][104][24]
	Total payload power use	41.5 W [4]	124 W [21]	52.6 W	228 W [23][28][127]
Comms system	Type	Optical	RF	RF	RF
	Max data rate	622 Mbit/s down [9]	100 Mbit/s down [21]	8.5 Mbit/s	8.4 Mbit/s
	Mass	30 kg [106]	61 kg		
	Power consumption	113 W [119]	120 W		
	Power transmitted	0.5 W [25]	40 W [136]		

3

Requirements

This chapter will discuss identified requirements, thereby elaborating on SQ1. The goal of this chapter is to come to a set of system requirements that is used for the design iterations in this thesis. These requirements will not include every important system requirement but just those that fall within the thesis scope of terminal link and opto-mechanical design.

3.1. Stakeholder requirements

The identified stakeholder requirements are listed in table 3.1. DOT-SH-01 was derived by the first use case. This stakeholder requirement is especially applicable to a lunar scientific research satellite with several data generating payloads onboard. DOT-SH-02 was derived from the second use case where DOT would facilitate a 'live' video call between the Earth and for example astronauts on the lunar surface or in orbit. For this second use case, a high availability is important. To enable this, interoperability between communication relay satellites might be necessary. To this end, but also to comply with regulations, DOT-SH-03 was identified. Finally, DOT-SH-04 was formulated, driven by technological development and improvement upon similar systems.

Table 3.1: DOT stakeholder requirements.

Requirement code	Stakeholder requirement	Justification
DOT-SH-01	DOT shall be able to downlink large amounts of high quality data through high data rate optical communication from the Moon to Earth	Required for next generation exploration payloads
DOT-SH-02	DOT shall be able to support an ultra HD 4K live video call through high data rate optical communication between the Moon and Earth	Required for future crewed lunar exploration
DOT-SH-03	DOT shall comply with international standards for communication in space	This will facilitate spacecraft interoperability in future networks
DOT-SH-04	DOT shall be competitive with regards to similar systems in terms of system budgets	Development of higher system efficiencies is important for future sustainable deep space exploration

3.2. System requirements

Table 3.2 lists the system requirements that were derived from the stakeholder requirements. These system requirements are the focus for this particular thesis and will lead the design iterations.

DOT-SR-01 has been derived from DOT-SH-01. Although the use cases concluded that approximately 288 Mbit/s on average would be needed for science offload, Isispace mentioned in an earlier paper in collaboration with TNO that they are aiming for a downlink rate of 400 up to 1000 Mbit/s in the future [32]. Thus one Gbit/s will be used for this system requirement. DOT-SR-02 was also derived

Table 3.2: DOT system requirements.

Requirement code	System requirement	Justification	Parent stakeholder requirement	Verification by
DOT-SR-01	DOT shall be able to downlink 1 Gbit/s through optical communication from the Moon to Earth	Required for science data offload, will also cover live video call downlink	DOT-SH-01	Design review
DOT-SR-02	BER shall be equal or lower than 10^{-6} for the optical downlink from the Moon to Earth after error correction	Accepted level of communication quality	DOT-SH-01	Design review
DOT-SR-03	DOT shall be able to receive 30 Mbit/s of high data rate optical uplink from Earth	Required for live video call	DOT-SH-02	Design review
DOT-SR-04	DOT design shall follow CCSDS high photon efficiency standards	Interoperability will benefit integrated networks and international cooperations	DOT-SH-03	Design review
DOT-SR-05	DOT shall consume less than 89.6 Watt of power	Technology development and economic reasons	DOT-SH-04	Analysis
DOT-SR-06	DOT shall have a mass less than 24 kg	Technology development and economic reasons	DOT-SH-04	Analysis

from DOT-SH-01, where this SR states required level of data quality. DOT-SR-03 was derived from DOT-SH-02 to facilitate a live video call. This would be required for both up and downlink. For the downlink however this data rate is expected to be covered by DOT-SR-01. Hence only the uplink is mentioned in DOT-SR-03. DOT-SR-04 was derived from DOT-SH-03. The Consultative Committee for Space Data Systems (CCSDS) has defined an international standard for optical communication especially in deep space scenarios for high photon efficiency (HPE) applications. Finally, DOT-SR-05 and 06 were derived from DOT-SH-04. The reference spacecraft analysis in chapter 2 provided a mass and power budget ceiling where DOT has to stay underneath in order to be competitive and improve relative to existing systems.

4

Methodology

The objective of this thesis is to create a concept design for the link and opto-mechanics of a deep space optical terminal. Such a terminal is a complex system of subsystems and interfaces requiring expertise from different disciplines. Hence the methodology used includes systems engineering (SE) practices. First, the steps taken in the thesis process will be discussed. This is followed by an explanation of the SE process applied to this thesis report. Finally the SE and software tools used in the process will be highlighted.

4.1. Steps taken

The first phase of the thesis revolved around a literature study on the subject. DSOC is heavily multidisciplinary and thus broad research was performed into relevant fields. Additionally system architectures were studied along with past and future missions. Optical link budgets were explored and experimented with in order to get a feeling for relevant link variables. This was followed by use cases. How would DOT be used in what setting, which parameters are important and with what magnitude? Answers to these questions are important to know how the system should function and to what extent. Elaborate study was done into data science and communication. Modulation schemes were explored and experimented with. This was to important find out how certain data rates could be achieved at certain quality levels. Data science and link design are closely interconnected. That is why this was followed up by more research into the latter. Models were produced using formulas and assumptions found in literature and similar systems.

Critical design choices were identified along with performance criteria. Trade-offs were done to make optimal choices. Simulations of the deep space channel were performed. The results of which were combined with link budget and trade-off decisions. Required optical terminal performance was determined as a result. A final trade-off was done that determined key terminal design specifications. The next phase focused on architecture and opto-mechanical design, where the system was divided into subsystems. Required subsystem tasks were formulated and components were identified. System budgets were estimated. Computer aided design (CAD) models were made for complex subsystems. High level subsystem interfaces and flows were identified.

4.2. V-model

In this thesis, the V-model has been applied as systems engineering (SE) process. It was chosen because it is often used in product development[44]. The product in this case is the current thesis in the form of a concept design report for a deep space optical terminal. The model is shown in figure 4.1. The first part of the thesis focused on identification of a need. The need being leveraging of Isispace expertise on DSOC. This leveraging is achieved through concept design of the DSOC terminal. Subsequently, identified stakeholder requirements on this terminal by use cases led to system requirements one level deeper which are the focus of this thesis. The first design iteration used these system

requirements to model, trade and analyse critical parameters of the link design. A link performance description was made. Afterwards in the second design iteration, the opto-mechanical design was made concrete by defining subsystems, their tasks, components and performance. This thesis will not go any deeper than the system requirements in the second level of the V. The identified subsystem design specifications and performance description are a result of the design iterations represented by the horizontal arrow to the right of system requirements in figure 4.1. Verification of the system requirements in the opposite direction follows to check if the design iterations have been performed properly. Going upwards on the right side of the V-model leads to system capability. In this case, the block is represented by the conclusion of this thesis. The conclusion is validated as it meets the initial need of leveraging Ispac expertise on DSOC technology by answering the RQ and SQs. The other way around, the conclusion can be seen as result of the upper level horizontal design arrow going to the right from system need, represented by the entire thesis project. The applied V-model will be revisited throughout the thesis.

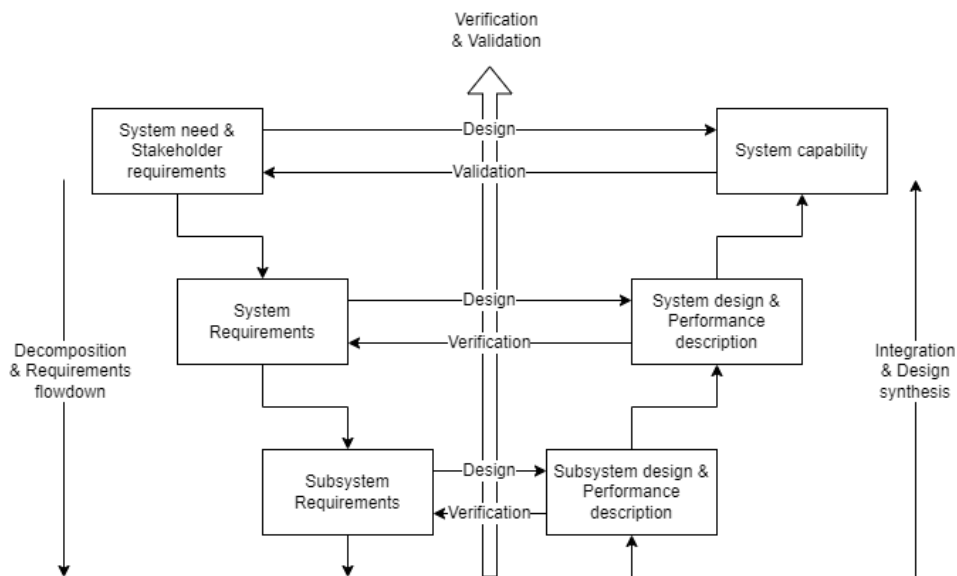


Figure 4.1: V-model of systems engineering [44].

4.3. Systems engineering tools

Several systems engineering tools were used in the process of which a need statement was the first one. It answers the question why this thesis has been performed. Second, use cases are a typical SE tool used in product development. Actual scenario's where the product is used are simulated, thereby producing and clarifying required system capabilities. In the design iterations graphical trade-off tables were used to make decisions on system parameters and architectures. These tables offer a clear overview of the advantages and disadvantages of certain choices, compared with others, along certain criteria. Feasible design choices were identified along with performance criteria. Options were evaluated, quantitative scores were assigned where possible and otherwise qualitative judgements were made. These added up in scores which determined design choices. Size, Weight and Power (SWAP) budgets were estimated based on engineering models, State-Of-The-Art and historical data. These budgets are useful to get insight into system and subsystem SWAP values. Furthermore, a high level interface diagram was produced to indicate quantified flows and interactions between the subsystems of DOT. A system's capability is only defined by the interactions between its subsystems and thus the importance of interfaces can not be underestimated.

Table 4.1: Software tools used during the thesis

<i>Tool used</i>	<i>Purpose</i>
Mendeley	Literature study, Bibliography
Overleaf	Reporting
Excel	Link budgets, SWAP budgets, Data gathering, Trade-offs
Matlab	Simulations, Models
Solidworks	Modelling, SWAP estimation, Visual representation
Draw.io	Schematics, Diagrams
Powerpoint	Visual presentations

4.4. Software tools

Several software tools were used during the thesis, these are listed in table 4.1. Excel, Matlab and Solidworks were especially used a lot for the design iterations. Excel was essential for making link budgets, SWAP budgets, data gathering and performing system trade-offs. Matlab was especially useful to visualize system models and perform deep space Poisson simulations. These simulations enabled an essential part of the link analysis and terminal design. Other software tools mainly had a supporting role.

The system requirements have been identified in chapter 3, answering SQ1. This chapter explained the methodology used in this thesis. The next chapter will discuss the first design iteration on the link design, building on the system requirements, thereby addressing SQ2.

5

Link design

This chapter will discuss the envisioned link design for DOT, thereby answering SQ2. It will highlight tools, models and simulations used in the process. In the V-model in figure 4.1, this and the next chapter on opto-mechanical design would represent the design arrow moving to the right to system design and performance description, coming from system requirements.

5.1. Constraints

This section discusses several (external) constraints, outside the scope that focuses on terminal design, that will still have to be taken into account while designing the optical terminal.

5.1.1. Optical ground station

Although this thesis revolves around the design of an optical space terminal, it is important to specify the optical ground station (OGS) connecting with DOT to a certain extent to perform proper link analysis.

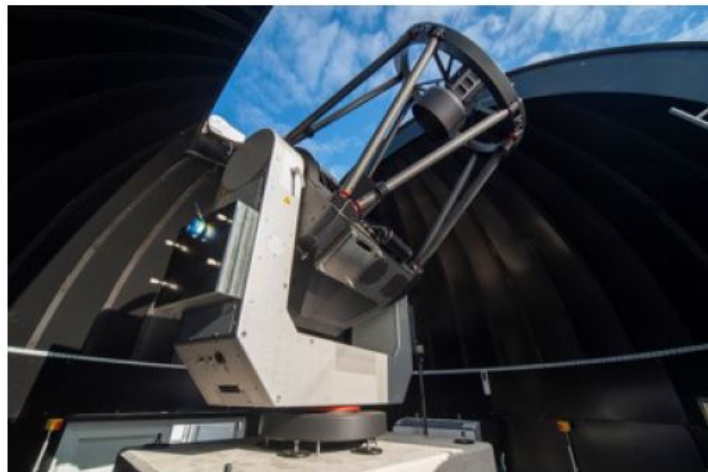


Figure 5.1: TNO optical ground station in the Hague [32].

The OGS assumed to be used for DOT is TNO's at the Waalsdorpervlakte in the Hague, the Netherlands as seen in figure 5.1. This OGS has a telescope receiver aperture of 0.8 m diameter. It is equipped with adaptive optics (AO). An earlier collaboration by Isispace and TNO specified OGS up-link power of 200 W with 1064 nm wavelength [32]. Note that this OGS is assumed as example for this thesis because of previous collaborations between TNO and Isispace. The actual intended OGS is not yet definitive.

5.1.2. Noise

The optical link will experience and accumulate a certain amount of noise along its way. The noise sources include but are not limited to shot noise, thermal noise, dark noise, background noise etc. The optical communication link will experience background noise both ways from several sources. These sources include the blue sky, sun, moon, stars, and Earth. The LLCD mission considered blue sky radiance and lunar background radiation in its noise simulation. For blue sky radiance a value of 41.2 pW/m^2 was assumed and for lunar background a value of 132 pW/m^2 [19]. Taking into account a receiver aperture of 0.8 m for DOT, this sums up to a total background noise power of 87.1 pW. It is unclear what telescope settings have been used here (filter, FOV). However, it does give an indication of what to expect.

Another planned mission of ESA for optical comms to the Sun-Earth lagrange L5 point monitoring space weather assumes a background radiance of $5 \text{ W/m}^2/\mu\text{m/sr}$ [122]. In the Ispace/TNO paper [32], another noise analysis is performed with the same receiver telescope assumed to be used for DOT. A sky radiance of $50 \text{ W/m}^2/\mu\text{m/sr}$ is assumed, along with filter bandwidth of 10 nm, viewing angle $7.85\text{E-}9 \text{ sr}$. This results in a background noise power of 986 pW, more than an order of magnitude larger than the LLCD case and the L5 mission. The authors do admit the assumed radiance value is on the high side. Used wavelengths in this paper were 1550 and 1064 for down and uplink respectively, similar to mentioned missions. For the DOT downlink, the 986 pW will be assumed to account for all noise sources in the link as it was deemed difficult to effectively estimate all separate noise sources. Hence these will be considered under the label background noise with an order of magnitude margin compared to the discussed similar systems.

Table 5.1: Various noise estimation approaches [19][122][32].

System approach	Downlink noise power for DOT	Notes
NASA LLCD	87.1 pW	Blue sky and lunar background radiance
ESA L5	98.6 pW	Background radiance
TNO/Ispace	986 pW	All noise sources

5.2. Wavelength

Wavelength is a system parameter that affects a lot of functionalities. It is often seen that free space optical (FSO) wavelengths operate in the spectral region over $1 \mu\text{m}$ where solar radiation is relatively smaller than in the visible band and where a few high transmission bands exist [13]. Commonly used wavelengths include 1064 nm and 1550 nm. This is because these are situated within atmospheric transmission windows, shown in figure 5.2. Another reason for these wavelengths is their high TRL and the terrestrial heritage in glassfiber networks of 1550 nm.

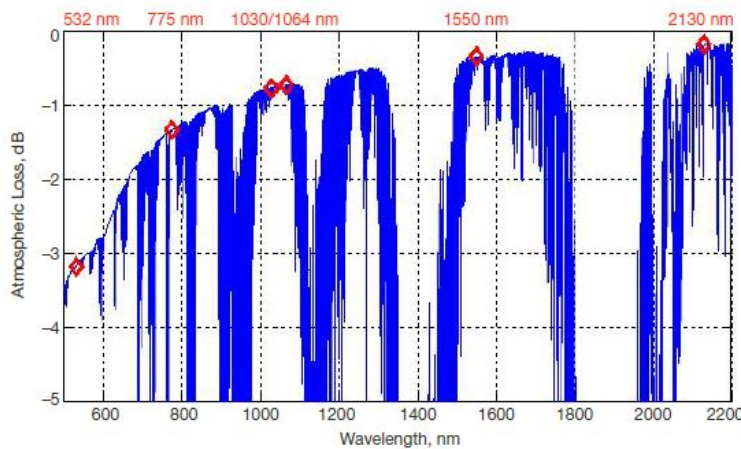


Figure 5.2: Atmospheric loss as function of wavelength and several popular wavelengths used for optical communication [2].

The figure highlights several wavelengths where atmospheric loss is lowest. 2130 nm has the lowest atmospheric attenuation, followed by decreasing wavelength maxima in the graph. Several other factors are important when selecting system wavelength. These include TRL, interoperability, background noise, eye safety etc.

5.2.1. Downlink trade

For the optical downlink, the CCSDS recommends to use 1550 nm [15]. In this subsection however, an independent trade-off has been made to select the best wavelength for the system. The downlink trade can be seen in table 5.2.

In this trade-off, and others later on, an excellent score of green is given to the highest performing option in a criterion, blue is considered good and given to the second best, yellow is deemed correctable and red is given to unknown or unacceptable performance. Quantitative data is used where possible, otherwise qualitative or relative scores are given. Criteria were given weights that are determined by the number of criteria in a trade-off and by relative importance.

Table 5.2: Downlink wavelength trade.

Downlink		Wave-lengths >						Comments
Criteria V	Weight (1-8)	1030	1064	1530	1550	1570	2130	
SPC Technology	-	SNSPD	SNSPD	SNSPD	SNSPD	SNSPD	SNSPD	
SPC detector eff.	8	>60%	85%	95%	98%	>80%	-	
Atmospheric loss	4	-	-	+	+	+	++	Relative
Transmitter gain (dB)	3	109.69	109.40	106.25	106.14	106.03	103.38	At constant 10 cm D
Laser TRL	6	-	+	+	++	+	-	COTS seed lasers
Background flux	2	5.8	5.6	2.3	2.5	2.3	0.85	MODTRAN
Interoperability	5	-	+	-	+	-	-	Lasercom heritage and CCSDS
Pointing loss (dB)	7	-4.6	-4.3	-2.1	-2	-2	-1.1	Matlab
Eye safety	1	Retina	Retina	Cornea	Cornea	Cornea	Cornea	
Score		39	63	69	92	75	52	Red = 0, yellow = 1, blue = 2, green = 3

The preferred wavelength is 1550 nm, similar and compliant to the CCSDS protocol. This is mainly because of its high detector efficiency, TRL and interoperability. Practically, it is seen that other wavelengths in the vicinity of 1.5 μm are also often used, which also complies with the trade-off scores.

5.2.2. Uplink trade

For the uplink, the CCSDS recommends either use of 1030, 1064 or 1070 nm. These lie relatively close to each other so performance differences aren't big but nevertheless present. A trade-off can be seen in table 5.3. The preferred wavelength is 1064 nm along with an InGaAs detector, primarily because of high detection efficiency, interoperability and high market TRL, which is good when using COTS components. Often used Si based detectors work up to approximately 1100 nm maximum so the higher wavelengths of the three will not perform optimally with those. InGaAs detectors perform better around these wavelengths [13]. An additional benefit of InGaAs detectors is that they can perform PAA verification when using a downlink wavelength of 1550 nm. A downside is higher dark count rate.

Table 5.3: Uplink wavelength trade.

Uplink		Wave-lengths >						Comments
Criteria V	Weight (1-7)	775	1030	1064	1064	1070	1550	
SPC Technology	-	Si APD	Si APD	Si APD	InGaAs APD	InGaAs APD	InGaAs APD	
SPC detector eff.	7	57%	30%	20%	75%	75%	75%	
SPC dark count	1	120 Hz	1 kHz	1 kHz	20 kHz	20 kHz	200 kHz	
Downlink isolation	2	Yes	Yes	Yes	No	No	No	With 1550 nm downlink
PAA verification	4	No	No	No	Yes	Yes	Yes	Detector sensitivity
Average laser power [W]	6	50	250	200	200	200	100	SOTA lasers
Atmospheric loss	3	1.3	0.78	0.73	0.73	0.73	0.34	
Interoperability	5	-	-	+	+	-	+	Lasercom heritage and CCSDS
Score		31	44	48	70	60	64	Red = 0, yellow = 1, blue = 2, green = 3

5.3. Coding

For high photon efficiency (HPE) deep space applications, the CCSDS prescribes serially concatenated pulse position modulation (SCPPM) [14] as a combined coding and modulation scheme. It is summarized in figure 5.4. This type of coding is currently one of the, if not the most efficient ones, approaching capacity limit within one dB [90]. Therefore this coding will be used for DOT. Below a short summary is given of the coding method.

Input data enters the coding layer in CCSDS transfer frames. An attached synchronization marker (ASM) is added to each frame, 32 bits long, resulting in synchronization marked transfer frames (SMTFs). These are sliced to produce information blocks of size k , which is determined by coding rate r as seen in figure 5.3. K sized information blocks are pseudo-randomized by digit-wise modulo 2 addition, its sequence determined by information blocks. Cyclic redundancy check (CRC) bits, 32 of which, are then added to the pseudo randomized blocks for error correction purposes, followed by two zeroes as termination bits. These packages are also called SCPPM encoder input blocks and consist of a randomized information block along with CRC and termination bits, having a size of the right column in figure 5.3.

Code Rate	Information block size	Length of information blocks with CRC-32 and 2-binary-digit termination added
r	k	\hat{k}
1/3	5006	5040
1/2	7526	7560
2/3	10046	10080

Figure 5.3: Information block size [14].

The blocks enter the outer SCPPM encoder where they are convolutionally encoded. This means they are filled to their usual size of 15120 with error correction bits. Encoding initially produces a 1/3 code and then may be punctured, removing redundancy bits, resulting in a 1/2 or 2/3 code. This is followed by a block interleaver, which scrambles the bit sequence.

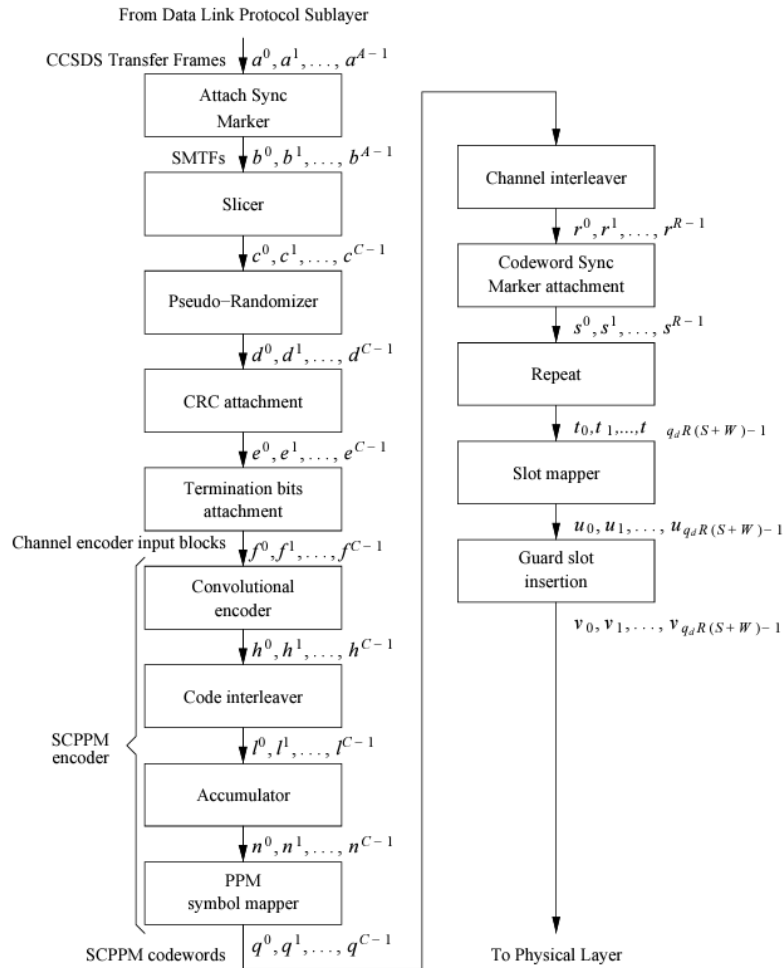


Figure 5.4: SCPPM as prescribed by the CCSDS [14].

The data enters the inner SCPPM code where it is accumulated and mapped to PPM symbols according to PPM order. Output of SCPPM encoding are PPM codewords ranging between 0 and $M-1$, each coding for $\log_2(M)$ bits. Another round of channel interleaving is performed, scrambling the PPM codewords to mitigate burst error link degradation. This is followed by codeword sync marker (CSM) attachment. Finally the PPM codewords are mapped to their designated slots within M sized binary vectors, each having $M-1$ zeroes and one 1. Simultaneously $M/4$ guard slots are inserted at the end of each M slot sized symbol, resulting in binary vector symbols of size $5M/4$ with one active slot and $(M-1)+M/4$ inactive slots. This is done for clock retrieval on the receiving end and improves laser and detector performance. It is then sent to the physical layer, where laser carving happens by an electro-optic modulator. At the receiver end of the system, decoding happens in reverse, using CSMs to synchronize the codewords. PPM symbols are deinterleaved and decoded, data is derandomized. SMTFs are synchronized by ASMs resulting in initial transfer frames again. Redundancy bits additionally identify and correct errors, to a certain extent, in the transferred data stream [14].

5.4. Modulation

In order for light to carry information, its characteristics will have to be altered in some way. This section will perform a trade-off to determine the best modulation method for DOT.

5.4.1. Modulation trade

Several modulation formats have been considered for DOT, these include On-Off-Keying return-to-zero (OOKrz), Binary Phase Shift Keying (BPSK), Differential Phase Shift Keying (DPSK), Quadrature Amplitude Modulation (QAM) and Pulse Position Modulation (PPM). Each have their advantages and disadvantages, which will be reviewed along relevant performance criteria.

DOT will be operating from lunar orbit. Its operational environment is therefore on the edge of deep space and near Earth. This complicates things because the standard modulation format for deep space applications is PPM due to its power efficiency, robust and noise resilient characteristics. However, the required downlink data rate of one Gbit/s is considered high, and higher data rates are often correlated to modulation formats used for near Earth environments. These include OOK and coherent modulation schemes as BPSK and DPSK. The CCSDS has prescribed recommended standards for these like the high photon efficiency (HPE) blue book for photon starved scenarios [15], often deep space, which recommends using PPM. Another is the optical high data rate (HDR) orange book, which prescribes coherent modulation like BPSK, DPSK and QPSK [16]. CCSDS does not however specify when to use either of these books.

Table 5.4: Modulation scheme trade.

Modulation		Schemes >					Comments
Criteria V	Weight (1-6)	16-QAM	BPSK	DPSK	16-PPM	OOKrz	
E_b/N_0	6	14.5	10.5	16.5	4.50	13.5	Theoretical SNR at BER E-6
Implementation complexity	1	High, requires oscillator and variable amplitude HW/SW	Medium, requires local oscillator	Medium, consecutive symbol dependence	Medium, requires symbol and slot sync	Low, simplest modulation scheme	Coding and HW/SW complexity
Resilience to atmos. turbulence	3	Phase shift and scintillation sensitive	Phase shift sensitive	Phase shift sensitive but higher resilience due to differential dependence	Low spectral efficiency and high peak power, scintillation sensitive	Low peak power, scintillation sensitive	
Data rate	5	4 Gbps	1 Gbps	1 Gbps	200 Mbps	1 Gbps	At constant Ts of 1 nanosecond
Space experience	4	None	GEO	GEO	Cislunar	LEO	
Adaptive modulation	2	Yes, order can be changed, does require more HW complexity	No	No	PPM order easily variable	No	At constant Ts
Score		25	36	30	51	28	Red = 0, yellow = 1, blue = 2, green = 3

A modulation tradeoff was performed to determine the most feasible scheme for DOT, seen in table 5.4. The schemes were reviewed on listed weighted criteria, the weights based on relative importance,

and subsequently given scores. PPM scores highest, primarily because of its unrivalled power efficiency, which is considered to be the most important criterion. A Matlab model depicting theoretical BER performance as function of signal to noise ratio (SNR) for various modulation schemes can be seen in figure 5.5, the used formulas acquired from [36][84]. PPM clearly performs best, dominating on the left side of the graph at low SNR while achieving low BER. PPMs low spectral efficiency on the one hand allows for laser buffering capacity for high peak powers and noise resilience but on the other hand inhibits high data rates. The fact that the scheme has already been tested in cis-lunar environment also is an advantage. Changing between orders is easily facilitated which makes the scheme adaptive and even more robust to environmental challenges. The high required data rate of one Gbit/s on the other hand will require pushing the limits of the PPM scheme.

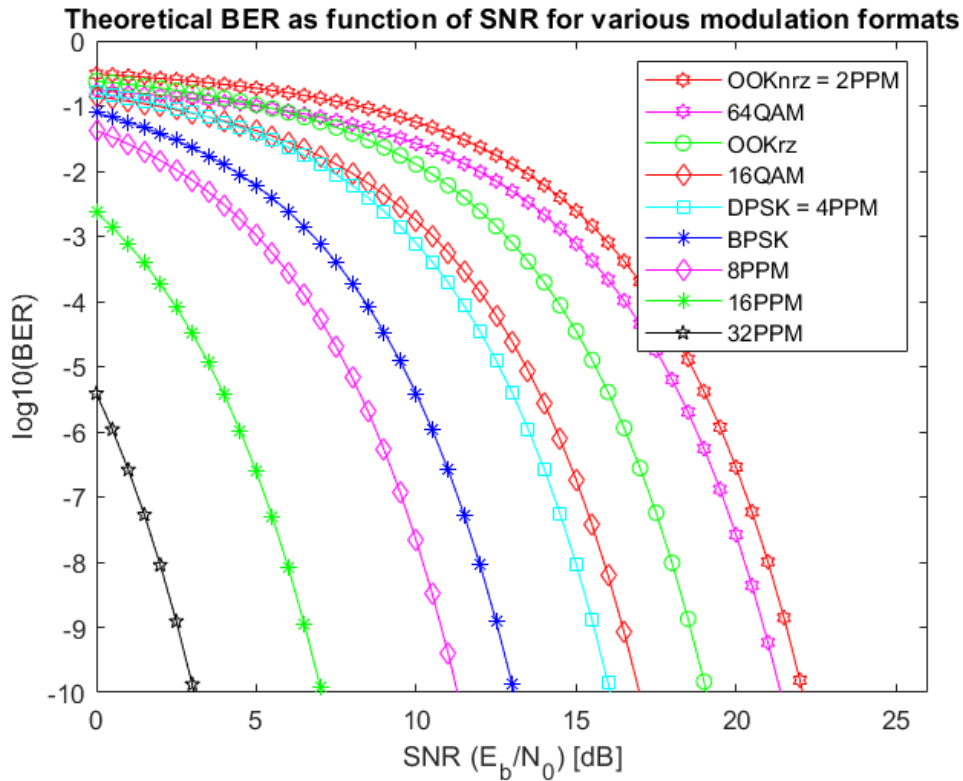


Figure 5.5: BER versus SNR of various considered modulation schemes.

5.4.2. Downlink settings

The CCSDS standard recommends using slot times ranging from 0.125, 0.25, 0.5, 1, 2, 4, 8, 16, 32, 64, 128, 256, or 512 ns [15]. To achieve the required downlink rate of a Gbit/s at a maximum power efficiency, the smallest allowable slot time of 0.125 ns will be needed in combination with maximum coding rate of 2/3 and PPM order 16. This can be seen in figure 5.6, which shows a Matlab simulation of achievable data rates for several PPM orders as function of slot times, at a constant coding rate (CR). With these modulation settings, a net downlink data rate of 1067 Mbit/s is achieved. A lower PPM order could achieve even higher data rates, however this is not needed according to the system requirements. Furthermore, a lower order would require a higher average laser power to achieve the same SNR. Higher PPM orders decrease data rates but simultaneously increase slot SNR (at the same average transmit power). This may be used for a more robust link in sub-optimal link conditions. Optional robust modulation settings are seen in table 5.5.

A slot time of 0.125 ns means a laser and detector jitter of max 12.5 ps is needed according to CCSDS, requiring a maximum jitter of 10% slot time for both. In combination with 16 PPM, this gives a symbol time of 2.5 ns, and a symbol rate of 400 MHz, which is thus the average laser repetition rate.

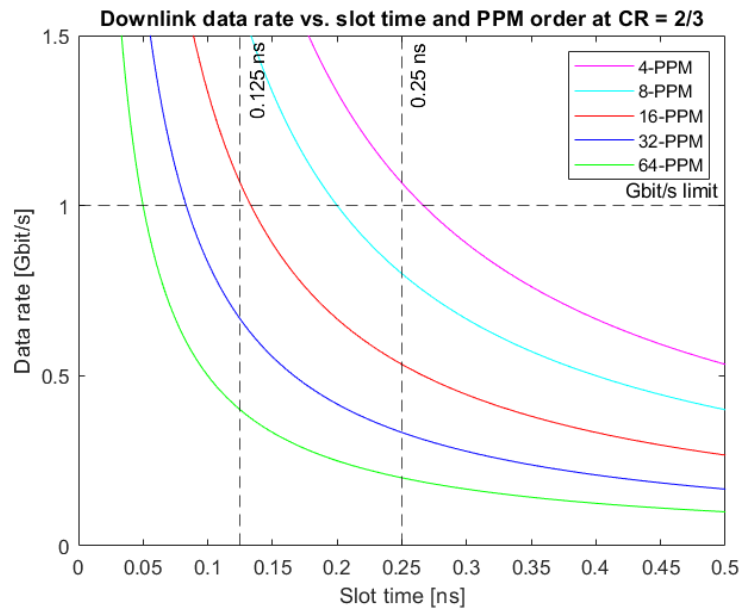


Figure 5.6: Achievable data rate as function of slot time and PPM order at constant coding rate of 2/3.

The slot clock is very high with 8 GHz, requiring high performance (de)modulators. A laser transmitter with modulation speed >10 GHz is currently in development at TNO which would suffice [32]. Guard slots will support synchronization and ease detector performance requirements but dead time still is only 0.5 ns, lower than any existing detector reset time, which means blocking loss could occur. This is mitigated by using multiple detector elements, error correction methods and interleaving. The LLCSD system used slot times of 0.2 ns for example and did not even have guard slots while performing perfectly fine.

5.4.3. Uplink settings

Uplink data rate has been determined to be able of reaching 30 Mbit/s. Conventionally, beacon lasers from OGS to space terminals are used to help in pointing, acquisition and tracking (PAT). To ease SWAP and complexity, it is proposed to use a nested uplink design [15], where acquisition, low rate uplink command and high rate telemetry are integrated in one beam, see figure 5.8. It does on the other hand ask more of modulators and electronics. The outer layer will consist of a square synchronization wave with a frequency of 3.8 kHz. As prescribed by CCSDS, nested inside will be a low rate command channel. Approximately 1.9 kbit/s, 2 PPM with 100% guard time, $65.5 \mu\text{s}$ slot time, and coding rate 0.5. The high rate data channel is nested even deeper. A 4-PPM, 2 ns slot time, 2/3 CR is able to achieve data rate of 33 Mbit/s. A smaller slot time of 1 ns will not be possible due to uplink detector timing jitter constraints and a 4 ns slot time will not be able to achieve required data rate. It will require modems capable of (de)coding multiple layers of data. The system requires a timing jitter smaller than 200 ps.

5.4.4. Lower modulation settings

Apart from the highest data rate settings for down and uplink, lower rate settings are possible with higher PPM orders, lower coding rates and longer slot times. These lower rate settings will be beneficial in sub-optimal environmental conditions and offer a more robust communication link. Proposed modulation settings can be seen in table 5.5.

5.5. Pointing

At lunar distances, a high accuracy pointing, acquisition and tracking (PAT) system will be needed. For deep space, required root mean square (RMS) pointing accuracies go below $1 \mu\text{rad}$ [8]. PAT systems are complex systems including sensors, actuators and control loops as shown in figure 5.9. Rough pointing is commonly performed by a course pointing assembly (CPA) in the case of a gimbaled

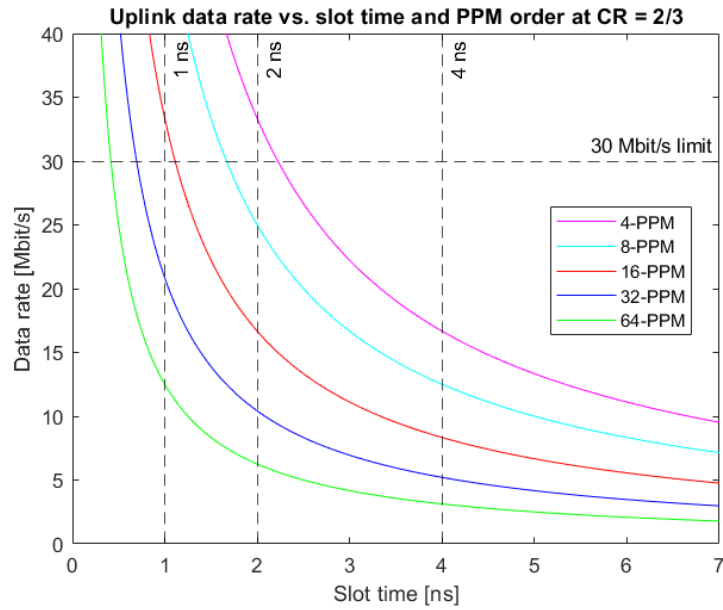


Figure 5.7: Uplink data rates vs slot time and PPM order at 2/3 CR.

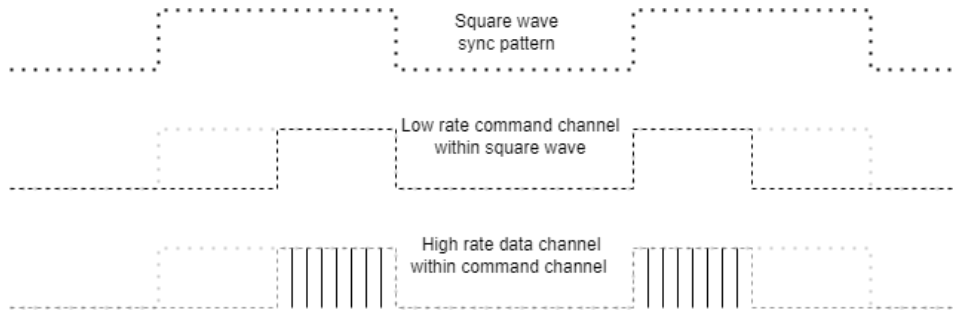
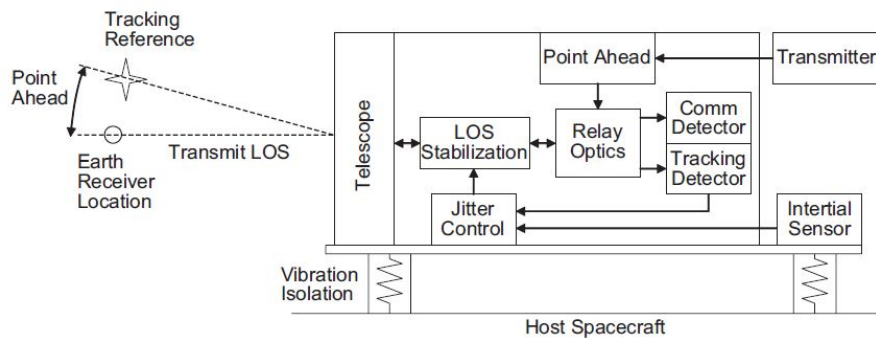


Figure 5.8: Nested uplink channels.

terminal or by the spacecraft AOCS system in a body pointing format. Fine pointing is often performed through fine pointing actuated mirrors in the optical assembly. Initial acquisition requires operational sequences and interactions in close collaboration between the terminal and OGS many kilometers apart, in order to acquire a steady link before data communication begins. Tracking the link is essential for data quality and continuity. This often happens by closed loop tracking where the uplink intensity spot is measured by a spatial four quadrant (4QD) detector and fed through a control loop that actuates the PAT subsystem, in order to keep the spot in the middle of the detector and catch as many uplink photons as possible. In duplex systems, the downlink is sent along the exact same path except for a calculated point ahead angle that accounts for differences in relative velocities between the space terminal and OGS. In this particular section, the acquisition sequence and pointing losses will be discussed, as deemed relevant for the link design. Tracking and point ahead angle shall be discussed in the next chapter on the terminal opto-mechanical design.

Table 5.5: DOT modulation and data rate settings.

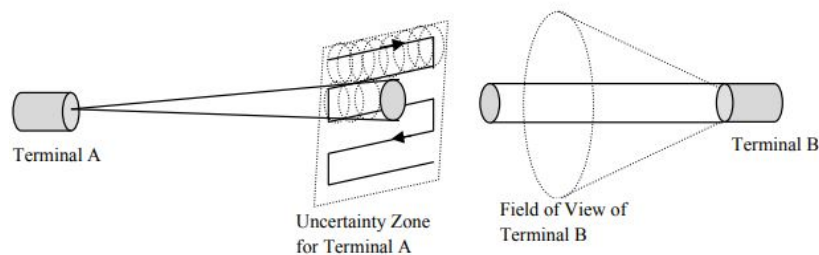
Mode	Clock rate (GHz)	Tslot (ns)	PPM order	Coding rate	Datarate (Mbit/s)	Notes
<i>Downlink</i>						
Ultra	8	0.125	16	2/3	1067	
Turbo	8	0.125	16	1/2	800	
Fast	8	0.125	16	1/3	533.3	
Cruise	8	0.125	32	1/3	333.3	
Nominal	4	0.25	32	1/3	166.7	
Safe	2	0.5	32	1/3	83.33	
<i>Uplink</i>						
Fast	0.5	2	4	2/3	33.33	1.9 Kbit/s command
Nominal	0.5	2	4	1/2	25	1.9 Kbit/s command

**Figure 5.9:** Typical optical terminal PAT system [50].

5.5.1. Acquisition

Link acquisition generally includes a standard operational sequence, with minor deviations between different optical systems. Steps include [32][2][65]:

1. RF is used to schedule an optical communications window because of its currently higher availability and reliability.
2. CPA and optionally the whole spacecraft are pointed roughly in the OGS direction using SC ephemeris.
3. OGS beams uplink square wave within a large FOV.
4. DOT scans the probability region, acquires the link, starts tracking and beams downlink towards OGS taking into account point ahead angle, see figure 5.10.
5. OGS receives downlink and starts tracking.
6. Data communication starts while both ends continue tracking the link.

**Figure 5.10:** Link acquisition process [65].

To be more independent from the SC platform and to implement redundancy, the optical terminal could potentially be equipped with its own startracker instead of relying on the spacecraft AOCS. This would allow independent attitude determination and could provide more pointing accuracy.

5.5.2. Pointing loss

System pointing loss is a function of static pointing loss, average jitter loss and jitter induced scintillation loss [111]. These are dependent on the terminal static pointing error, system pointing jitter, outage probability and beam divergence which is a function of wavelength and aperture diameter. Several assumptions are made as starting point for modelling. These are $3 \mu\text{rad}$ for static error, $1 \mu\text{rad}$ for pointing jitter using a TNO FSM [72], outage probability of 10^{-3} [50][114], a 1550 nm wavelength and a Gaussian beam [111].

Pointing loss is often traded against geometric loss in order to determine optimal aperture diameter of the terminal. Pointing loss increases with diameter and smaller beamwidths while geometric loss decreases with diameter because the beam stays tight. Such a trade can be seen in figure 5.11. The diameter with least total loss would be about 14 cm with a pointing loss of 4 dB according to the figure. Pointing loss can be reduced by choosing a smaller aperture with larger beam divergence at a cost of more geometric loss. It seems better to keep pointing loss low instead of geometric loss because the latter can be accounted for by increasing average laser power. While a relatively high pointing loss will cause scintillation and variations in received power intensity due to beam wander, degrading link and data quality. The trade in figure 5.11 can only be performed when the PAT system static and jitter RMS are known. Although this trade is a good approximation to obtain a value for the aperture, it does not take into account other system constraints like SWAP and laser power.

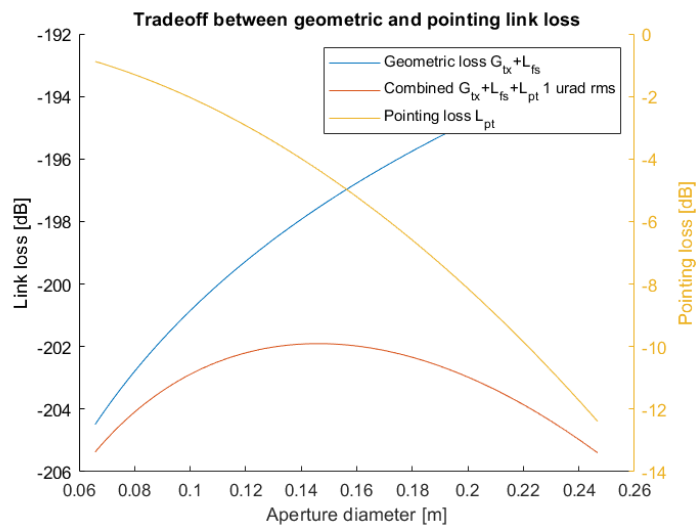


Figure 5.11: Pointing loss vs. geometric loss trade for optimal aperture diameter.

Another way of looking at this is to determine system variables following a preset maximum pointing loss. NASA and others for example recommend keeping deep space pointing loss less than 2 dB [50][31][51][17], because performance degrades very rapidly beyond this point. This value is hence also used in similar deep space simulations [3]. In this case aperture diameter and required system accuracy are a function of pointing loss. For example, a 2 dB predetermined pointing loss with earlier mentioned $1 \mu\text{rad}$ system accuracy would require an aperture of 10 cm according to figure 5.12. Diameter can be chosen larger at a cost of a higher required accuracy at constant loss. For the rest of this thesis, the 2 dB pointing loss maximum shall be handled along with an accuracy of $1 \mu\text{rad}$ of the TNO FSM system. As for pointing, this means DOT aperture diameter shall preferably be equal or less than 10 cm .

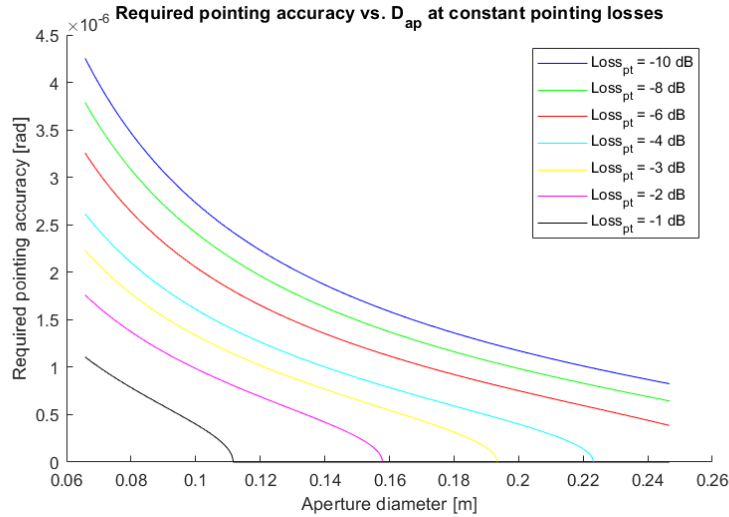


Figure 5.12: Required pointing accuracy as function of preset pointing loss and aperture diameter.

5.6. Link analysis

Link conditions are challenging. Lunar range is approximately 3.84E8 [m]. This means geometric free space loss is significant, about -310 [dB]. Additionally the link will have to cross the turbulent atmosphere before reaching the detector. In this section, the optical link will be analysed and modelled in order to determine a performance description for the terminal. First, the link equation will be discussed.

5.6.1. Link equation

Free space optical links are governed by the link equation 5.1, which is a formula for power at the receiving end. A clarification of used symbols and their magnitudes can be seen in table 5.6. The table includes some values TBD which are determined later on in this analysis.

$$P_{rx} = (P_{tx}G_{tx}\eta_{tx}L_{pt})L_{fs}L_{atm}L_{wfe}L_{imp}L_{scin}G_R\eta_R\eta_{det} \quad (5.1)$$

The first couple of terms in this equation between brackets are design characteristics of the DOT space terminal and their product is called the effective isotropic radiated power (EIRP), which is the beamed out directional optical power [2], its formula given by 5.2.

$$EIRP = P_{av}G_{tx}\eta_{tx}L_{pt} \quad (5.2)$$

The required terminal EIRP is the main design variables to determine using this link analysis. The EIRP is used later to determine terminal average transmit power and aperture diameter, from transmitter gain. The EIRP can only be determined when the rest of the terms in the link equation are known. Rewriting the link equation and replacing received power with required signal photons, which is easier to work with, results in equation 5.3 [51].

$$EIRP = \frac{n_s E_{ph}}{L_{fs}L_{atm}L_{wfe}L_{imp}L_{scin}G_R\eta_R\eta_{det}} \quad (5.3)$$

These terms are calculated where possible and otherwise realistic assumptions are made. An overview of the terms is seen in table 5.6. Required signal photon rate at the receiver is a function of SNR at predefined BER of 10^{-6} and the amount of noise photons. This will be determine later using Matlab. Photon energy is calculated at a wavelength of 1550 nm. Free space loss is calculated with wavelength and lunar range. Atmospheric transmission is assumed to be 0.7 according to similar values used in literature [116][123][122][18][101]. Wavefront error (WFE) is assumed to be 0.8 for a diffraction limited system because of adaptive optics (AO) at the TNO OGS. For link margin, often 3 dB is included in the budget, while [50] additionally recommends 2 dB for hardware and electronics implementation loss, which is also done here. Scintillation loss was calculated as function of outage probability (10^{-3}) and (high) scintillation index of 0.2 [111][50]. Receiver gain is a function of OGS aperture diameter

and wavelength. Receiver efficiency was taken from literature [50][116][101]. Detector efficiency was assumed to be 85%, accounting for detector losses. Pointing loss is taken within EIRP and assumed to be 2 dB as earlier mentioned. Transmitter efficiency is assumed to be 0.7 from literature, including losses concerned with optics, telescope and loss caused by Gaussian illumination in combination with a finite aperture [50][116][122][18][101].

Table 5.6: Link equation terms. NB: TBD values calculated later on in this report.

Link factor	Abbreviation	Value	Value [dB]
Average transmit power	P_{tx}	TBD [W]	TBD
Transmitter gain	G_{tx}	TBD	TBD
Signal photon rate	n_s	TBD [ph/s]	TBD
Photon energy (downlink)	E_{ph}	1.28E-19 [J]	-
Pointing loss	L_{pt}	0.63	-2
Free space loss	L_{fs}	1.03E-31	-310
Atmospheric loss	L_{atm}	0.7	-1.55
Wavefront error loss	L_{wfe}	0.8	-0.97
Link margin and HW implementation loss	L_{imp}	.32	-5
Scintillation loss	L_{scin}	0.47	-3.27
Receiver gain	G_{rx}	2.63E12	124
Receiver efficiency	η_{rx}	0.5	-3.01
Transmitter efficiency	η_{tx}	0.7	-1.55
Detector efficiency	η_{det}	0.85	-0.7

5.6.2. CCSDS SCPPM Poisson channel simulation

To determine required EIRP, first the signal photon rate is calculated, which is a function of SNR, thus BER, PPM order, and noise power. The earlier found value of 986 pW for noise power, together with photon energy and slot times of 0.125 ns give an average of 0.96 noise photons per slot, rounded up to 1. This is consistent with upper level noise limits found in similar simulations in literature [50][90].

A Matlab simulation was performed for a CCSDS compliant SCPPM deep space Poisson channel [85]. The usual Gaussian distribution cannot be applied in photon starved situations. Instead, Poisson channels are useful in modelling discrete time independent statistical probabilistic events, such as photon arrival counts [58]. First, SCPPM data is randomly generated, formatted taking into account coding rate and CRC is added. The data frames enter an SCPPM encoder and subsequently are PPM modulated. It then passes through the Poisson channel described below.

K is the slot photon count, λ_s is signal rate in photons per second, λ_b is noise photons per second, T_s is slot time, M is PPM order. In this simulation, λ_s is the variable input which represents different levels of optical power used for signal transmission. Signal photons per pulse is given by equation 5.4 [90].

$$n_s = \frac{5M\lambda_s T_s}{4} \quad (5.4)$$

While noise photon per slot is modeled as 5.5

$$n_b = \lambda_b T_s \quad (5.5)$$

The probability of receiving k photons in an inactive slot is given by 5.6

$$p_0(k) = \frac{e^{-n_b} n_b^k}{k!} \quad (5.6)$$

While the probability of receiving k photons in an active slot is given by 5.7

$$p_1(k) = \frac{e^{-(n_s+n_b)}(n_s+n_b)^k}{k!} \tag{5.7}$$

The log likelihood ratio of each slot is given by 5.8

$$LLR = \log\left(\frac{p_1(k)}{p_0(k)}\right) = k \log\left(1 + \frac{n_s}{n_b}\right) - n_s \tag{5.8}$$

The ratio of probabilities for an active/inactive slot at slot photon count k is used to calculate the log likelihood ratio (LLR) of each slot. This is then used by the SCPPM decoder to estimate if a slot with specific amount of received photons is in fact an active slot or inactive slot, see figure 5.13. PPM symbols are decoded and data is reassembled. This data is compared with initial authentic data to calculate the BER before plotting error results as a function of signal intensity.

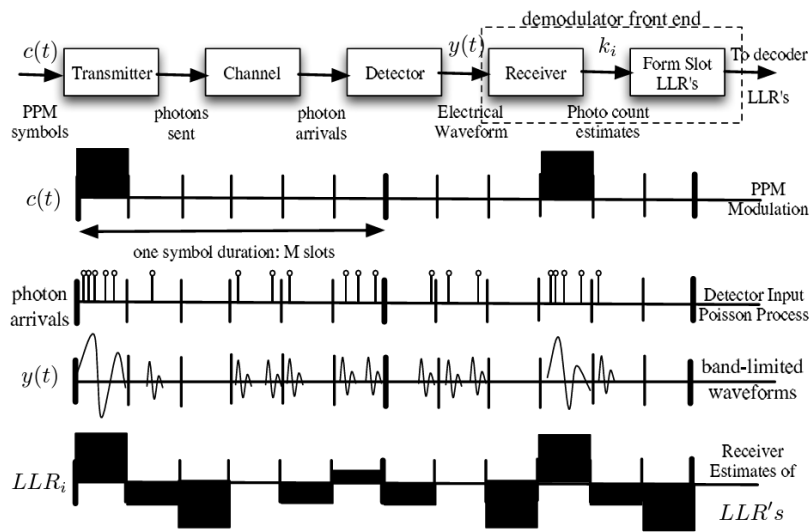


Figure 5.13: The process of estimating active SCPPM slots at the receiver [20].

Input parameters achieving a theoretical downlink of 1067 mbps included 16 PPM, 0.125 ns, 2/3 coding rate, 1 noise ph/slot. the result of which is shown in figure 5.14. As can be seen, the required BER of 10^{-6} would be reached at a signal photon flux of 3 dB photons/ns, or 5 ph/PPM symbol, 2.10^9 ph/s. This simulation takes a whole working day, so only a few were done. They were all consistent and the one in the figure was the most representative. The shape of the curve was as expected similar to figure 5.5, which is also BER as function of signal intensity. The signal input for equation 5.3 is thus determined and EIRP can be calculated.

5.6.3. EIRP

Now the required signal power to achieve sufficient BER at Gbit/s settings is known, EIRP is calculated with equation 5.3. This results in a value of 134 dBm. A 3D plot was made in 5.15, visualizing the constant EIRP surface as function of the three variables P_{tx} , G_{tx} and L_{pt} at constant transmitter efficiency. A small aperture (wide beam) and large pointing loss would require high laser power and large aperture with negligible loss very little laser power.

Taking a slice out of of this plot at an assumed 2 dB pointing loss maximum results in the graph seen in figure 5.16. At an average power of 1 W, the terminal would require an aperture diameter of 12 cm. While at 1.5 W, a diameter of 10 cm would suffice to achieve required EIRP. Figure 5.17 includes a plot that shows the same required EIRP for DOT but compared with EIRP's of other DSOC systems and their design points. DOT EIRP lies between that of LLCD and DSOC. This is caused by a combination

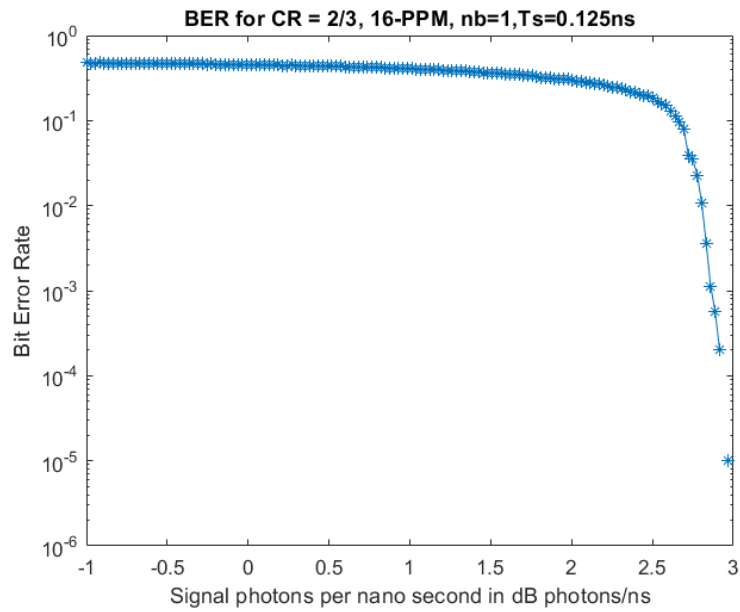


Figure 5.14: BER as function of signal photons for maximum downlink rate.

of data rate and link distance. DOT has the same link distance as LLCD but higher data rate, which requires more laser power to achieve sufficient SNR, so higher EIRP is needed. While it has higher data rate but much smaller distance than DSOC, which thus needs higher EIRP.

Where the DOT link design has been discussed in this chapter, the next chapter will elaborate on design of the opto-mechanical system and subsystems required to realize this link.

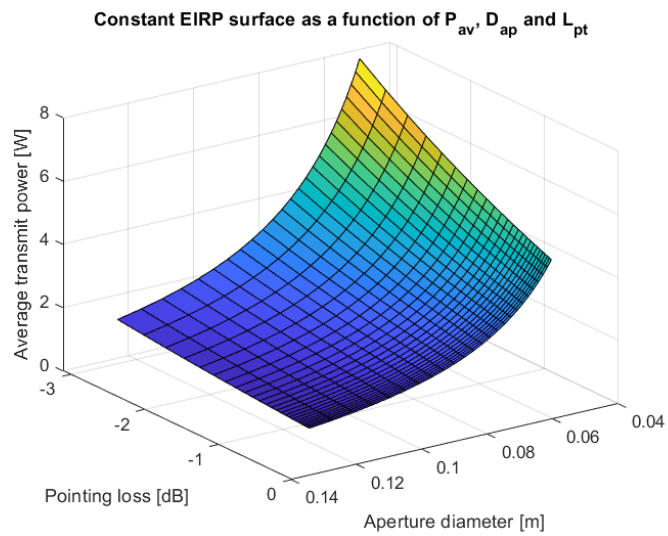


Figure 5.15: 3D plot of constant EIRP surface as function of three system variables.

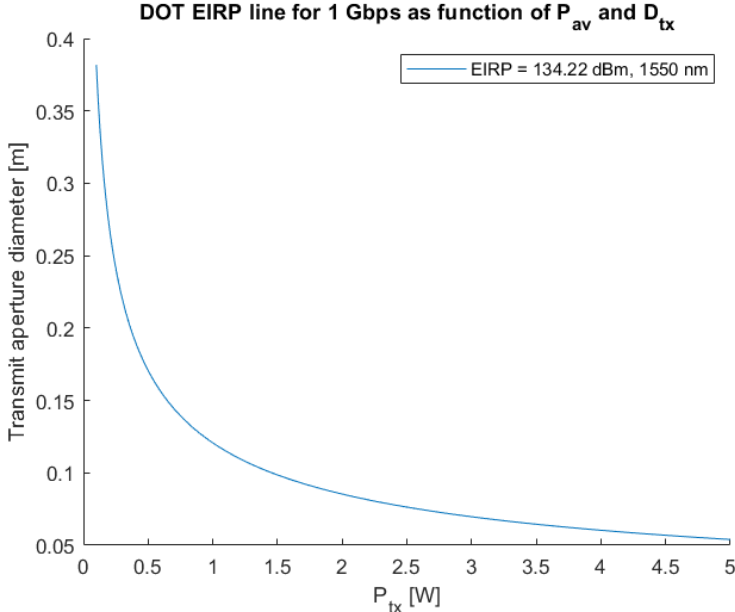


Figure 5.16: DOT required EIRP.

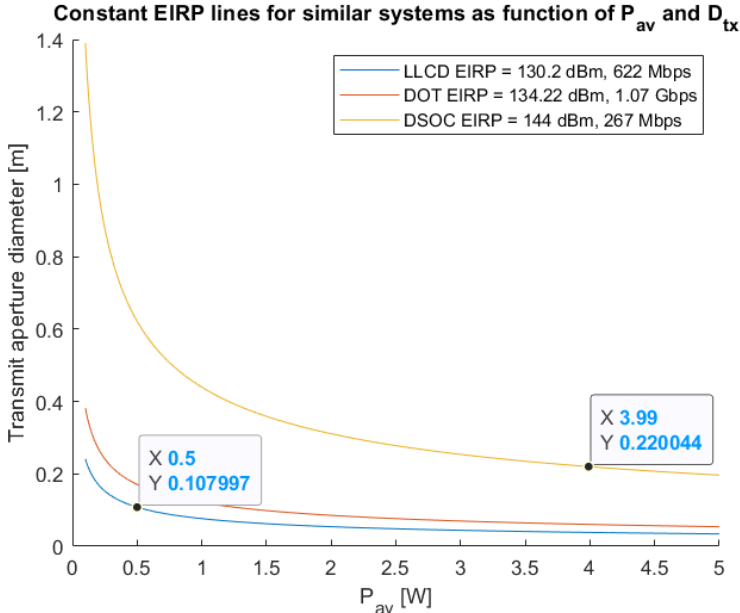


Figure 5.17: DOT required EIRP compared with LLCD and DSOC EIRP lines and their respective design points.

6

Opto-mechanical design

This chapter will elaborate on a concept opto-mechanical design for the subsystems of the optical terminal, thereby answering SQ3. It was decided to divide DOT into several subsystems with different functionalities, the following subsystems have been defined:

- Control electronics (CE)
- Modem
- Downlink laser assembly (DLA)
- Optical head (OH)
- Power unit (PU)

Although each subsystem will be discussed in the following sections, main focus lies on the opto-mechanical subsystems of the DLA and OH in line with the scope, and will thus be discussed more elaborately than the others.

6.1. Control electronics

As main point of contact towards the spacecraft, the CE are practically the brains of DOT. It is meant to monitor and control all subsystems, it processes data flows, reads sensors and controls actuators. A list of tasks assigned to the CE can be seen below:

- Data interface (up and downlink) towards SC
- Monitor and control power distribution towards subsystems
- Schedule link window with SC
- Manage link window and operational sequence
- Manage data flows to and from modem
- Convert data to and from CCSDS transfer frames and SC usable data format
- Monitor link quality using various inputs and environmental conditions
- Control data rates and link parameters fitting with link conditions to uphold quality
- Control modem, OH and DLA operations
- Monitor all subsystem performances and intervene if necessary
- Monitor, process and control all PAT loops in cooperation with subsystems and SC
- Control and monitor actuators within the OH

Key performance parameters for the Control Electronics (CE) include data rates, interfaces, formats, and processor capacity. High data rates will pass through the CE, which have to be conditioned and distributed. Apart from managing data flows, the CE will collect data from different subsystems and sensors which have to be processed and subsequently execute control operations to keep certain variables within predefined limits. Control loops will be required for thermal control, fine and coarse pointing, data quality, downlink optical power, uplink power, subsystem power distribution etc. These

control loops will be interconnected. To facilitate this, the CE needs sensory in and output gates combined with digital control loops, which may also interact with link data flow management. Control loop bandwidths will typically go up to several kHz [17].

CE hardware will resemble an onboard computer (OBC) since many of the conventional systems controlled by an OBC are included within the DOT system. It should be taken into account that lunar environment experiences larger radiation levels and thus the OBC will have to be resilient to these. This counts for all DOT hardware.

6.2. Modem

The modem is where data translation happens. Data to be downlinked enters the modem from the CE. It is framed, coded and modulated in the SCPPM method including error correction coding (ECC) and interleaving. Output of the system is a signal that tells the electro-optic modulator in the DLA how to temporally carve the laser beam. Regarding the uplink, an electrical signal similar to DLA input enters the modem from the OH where photon to electrical conversion has already happened, buried in a layer of noise. The modem retrieves signal clock(s), demodulates and decodes to produce data packages to be sent towards the CE. A list of modem tasks can be seen below:

- Import downlink data from the CE in transfer frames
- Perform SCPPM coding and modulation fitting the data rate and link conditions
- Pass on binary output vector indicating pulsed slots towards DLA
- Import noisy uplink signal from uplink detector in OH
- Retrieve signal clocks
- Filter noise
- Retrieve signal slots
- SCPPM decode and demodulate
- Pass on uplink data to the CE

The modem will require high datarate Gbit/s ethernet capacity. Data will be framed according to CCSDS protocol, then SCPPM coded, interleaved and modulated, probably within a Field Programmable Gate Array (FPGA). These devices allow customization of its digital integrated circuit by programming links between logic blocks. It is used for adaptive systems that can be modified remotely over time in case system design needs an update. They can be optimized to efficiently perform high data rate SCPPM coding in as little time as possible, reducing latency which is preferably as low as possible. Radiation hardened reconfigurable FPGAs are often used in aerospace engineering and are available COTS [93]. The FPGA will have to be accompanied with a memory unit to facilitate interleaving operations as part of SCPPM coding, the required size of which scales with interleaving time intervals. These intervals may vary instead of being constant to adapt according to fluctuations in atmospheric scintillation.

Regarding uplink, the raw electrical signal from the detector array in the OH enters the modem. A filter and low noise amplifier will probably be needed to condition the signal before passing the clock retriever, synchronizing both symbols and slots. The signal then enters an FPGA where together with the recovered clock, demodulation and decoding happens. The FPGAs are central in the modem and all elements within it will support and complement the FPGAs to achieve optimal data (de)coding speed and quality. Figure 6.1 shows a high level system architecture of the modem used in the O2O terminal for the Artemis 2 mission [26]. It is roughly similar to the description given above. However, in the depicted design the DLA is integrated within the modem instead of being a separate subsystem on its own in DOT. The uplink detector also is integrated within the modem instead of the OH unit.

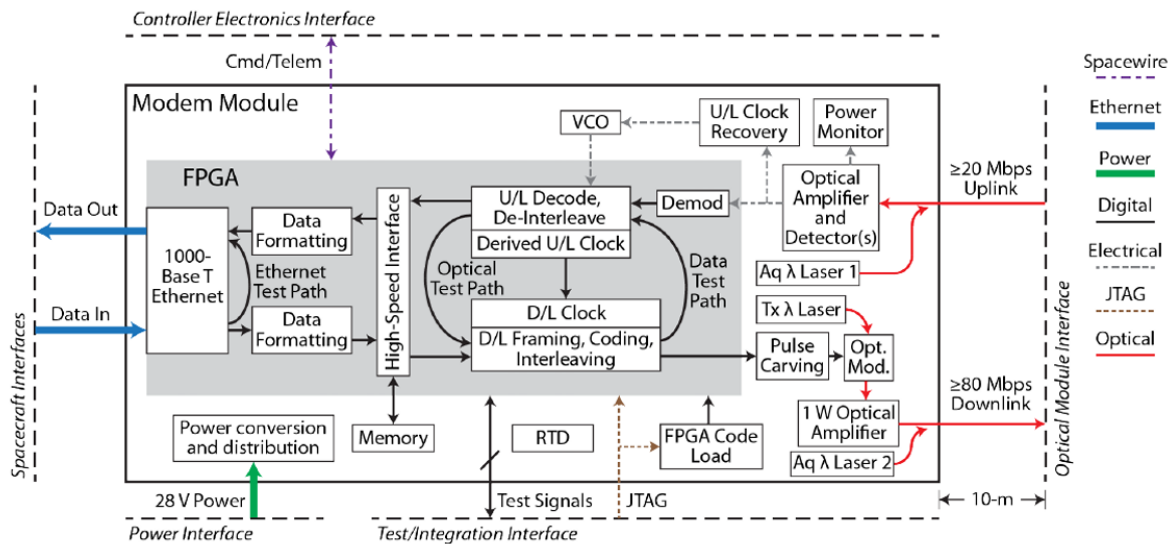


Figure 6.1: High level architecture of O2O modem [26].

TNO seems to have completed a first iteration of its deep space terminal modem recently [40]. This modem is meant to initially demonstrate a downlink speed of 400 Mbps at GEO range and afterwards increase to 1 Gbit/s. Minimal slot time is 0.25 ns.

6.3. Downlink laser assembly

The downlink laser beam is generated in the downlink laser assembly (DLA). The high power laser is then transferred towards the OH, where it enters the optical system. The DLA task list is shown below:

- Generate continuous wave seed laser
- Import binary temporally modulated data vector from the modem
- Carve binary vector onto laser beam with modulator
- Amplify laser beam up to desired power
- Filter for wavelength pass band
- Pass downlink laser on to OH

A PPM capable laser at 1550 nm is required. The laser would need a high modulation rate capacity of 8 GHz. A modulation of 16 PPM requires a maximum laser power of 30 W. Such high peak to average power (PTAP) ratios will increase SNR and lower BER which is desired. The typical low spectral efficiency of PPM modulation and high peak to average power ratios go well with average power limited laser assemblies which buffer optical power during inactivity and release it in a pulsed slot. This, together with subsystem modularity, calls for pumped fiber amplifiers in the assembly. A high extinction ratio is also needed, >30 dB [100][134], to prevent uncontrolled amplified spontaneous emission (ASE) events and maintain high PTAP.

Directly modulating a seed laser at these rates is impossible and would give bad extinction ratios. Q-switched lasers as alternative are also not an option because of limited repetition rates [50][59]. The extremely high clock rate requires externally modulating a seed laser. A Master Oscillator Power Amplifier (MOPA) architecture with external modulator would be the best option, often used in DSOC terminals [25][26][41][51].

The MOPA starts with a fiber coupled seed laser that generates a continuous wave at 1550 nm, typically at a low 10-100 mW power level. This will probably be a Distributed Feedback laser (DFB), often used for optical communication, because of its tunable characteristic, low noise and narrow spectral wavelength bandwidth [55]. This is followed by a high speed electro-optic intensity modulator. Fiber amplifier architectures are capable of reaching high extinction ratios of 30 dB [50][100][134]. The

modulator will preferably support similar extinction levels. For intensity modulation, this typically is a fiber coupled lithium niobate ($LiNbO_3$) modulator. These are based on Mach-Zehnder interferometers, where the fiber is split in two arms which are phase modulated by electric fields and recombined, resulting in a net intensity modulation through constructive and destructive interference [108][134]. This is possible in bandwidths up to 40 GHz, more than enough for DOT [132].

The device is controlled by the modem downlink signal output in the form of a temporally coded binary vector indicating active and inactive laser slots. A concept MOPA configuration has been created which is depicted in figure 6.2. Two seed lasers and modulators are included for redundancy. The modulators are subsequently followed by doped fiber amplifier stages (xDFA) that enhance optical power up to the desired level. For safety and redundancy reasons, this would best be done in a staged configuration with intermediate optical isolators (indicated with arrows) to mitigate reflections, and parallel taps that monitor forward output power and backward reflections through photodiodes (PD) [26]. Inserting additional ASE filters in between amplifier stages will improve signal gain and reduce noise [34].

Often Erbium Doped Fiber Amplifiers (EDFA) are used for the 1550 nm wavelength with a 980 nm pump wavelength [41]. However since the required optical power will probably be relatively high, Erbium Ytterbium Doped Fiber Amplifiers (EYDFA) might instead be needed as these can achieve higher gains [82]. Advantages of co-doping with Ytterbium (Yb) include a higher pump absorption efficiency, and a higher Yb doping capacity of typically used silica fibers in xDFAs, compared with Er [76]. Yb ions are also called sensitizer ions since they cause a higher gain medium sensitivity for pump light. Pumping happens at absorption peak wavelength of 975 nm which primarily excites Yb ions that subsequently pass on the energy to nearby Er ions, which then release 1550 nm radiation. Earlier mentioned ASE includes unwanted radiation by the Yb ions around $1 \mu m$. This is mitigated by the ASE filters and by optimizing doping concentrations [109]. Especially the DFB laser combined with pure EDFA amplifier is reported to be very inefficient while EYDFA offers a much better power conversion efficiency. This also enables using much shorter length fiber amplifiers which is beneficial for lower SWAP [110]. A combination of both may also be applied [41][26].

Depending on amplifier gain, more than two stages might be needed to reach required average power. Implementing redundancy and monitoring in these MOPA architectures is of high importance to maintain quality and safety. Since the doped fiber amplifiers are radiation sensitive, the DLA will be located within SC shielding while transferring the DL by fiber to the OH.

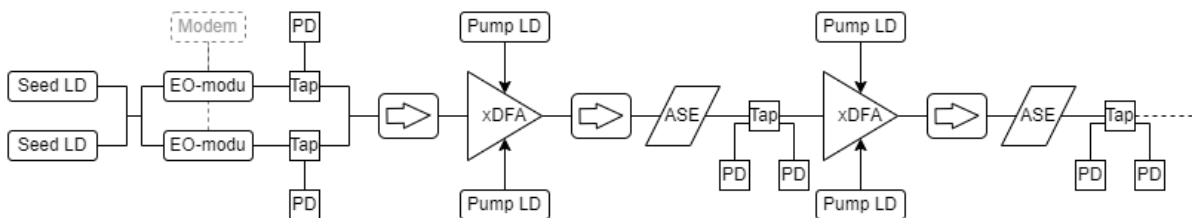


Figure 6.2: Concept MOPA architecture.

6.4. Optical head

The optical head (OH) guides the transmit and receive beams on the border between the system and space. It includes an optical system with (steering) mirrors and beam splitters that stabilize, point and combine optical paths. It includes a detector for uplink acquisition, tracking and data communication. It also includes a telescope for beam expansion as part of the CPA. Finally it will include a vibration isolation system. The OH task list is seen below:

- Import downlink laser (DL) from DLA
- Free space couple DL into optical system
- Point ahead, guide, stabilize, expand and transmit DL
- Catch uplink laser (UL) with CPA
- Condense, guide, stabilize the UL

- Detect the UL with spatial detector array
- Pass on detector signal towards the modem and CE
- Provide CE with PAT data through sensors
- Perform PAT tasks as commanded by CE
- Suppress and correct for SC platform, actuator and other vibrational disturbances

The DOT optical head (OH) will consist of two main areas: backend optics (BO) and the Course Pointing Assembly (CPA). These are mounted in a vibration isolation frame. The backend optics (BO) will reside within the spacecraft to limit radiation exposure. It is in close proximity with the CPA and telescope, located just outside the spacecraft. The OH entirety will thus cross the spacecraft skin.

Uplink detector

Earlier determined modulation settings result in a required timing jitter of <200 ps and count rate of 50 MHz for the uplink detector. A detector trade is shown in table 6.1. Three options for single photon detectors (SPD) were considered: the Superconducting Nanowire Single Photon Detector (SNSPD), the photo-multiplier tube (PMT) and the avalanche photodiode (APD). The SNSPD scores slightly higher than the APD. However, it is not realistic to implement it in the terminal due to bulky required cryogenic infrastructure. For the downlink, this does seem to be the best option as seen in table C.1. It seems the APD would be the best option for DOT.

Table 6.1: Uplink detector trade.

Uplink		<i>Options ></i>		
<i>Criteria V</i>	<i>Weight (1-5)</i>	SNSPD	PMT	APD (InGaAs)
Timing jitter	5	<10 ps	3 ns	300 ps
Quantum efficiency	4	85%	2%	75%
Dark counts	1	1 Hz	25 Hz	kHz
SWAP	3	Big	Medium	Small
Counting rate	2	>500 MHz	50 MHz	800 MHz
Score		36	8	34

Backend optics

A potential design setup for the BO bench has been created and can be seen from above in figure 6.3. Regarding the downlink path, the Tx fiber will enter the BO from the DLA. It is free space coupled into the optical system and then guided onto the point ahead mirror (PAM). The PAM is controlled by the CE which calculates required PAA using relative velocities and orientation of receive and transmit terminals. The Tx beam encounters a beam splitter (BS) which directs most optical power further into the system but allows a very small quantity to pass. The small Tx beam is bounced back by a retro-reflector and guided by the same BS towards the 4QD APD Array detector. The detector is primarily meant for Rx detection but in this case for Tx PAA verification. The main Tx beam is guided towards the fast steering mirror (FSM) after first BS encounter. The FSM finely points Tx and Rx beams and corrects for disturbances. It is controlled by the CE and actuated based on tracking data gathered by the detector array and by an inertial measurement unit (IMU) located within the OH. Subsequently the Tx beam passes the fold mirror by which it is folded into the CPA relay system discussed later.

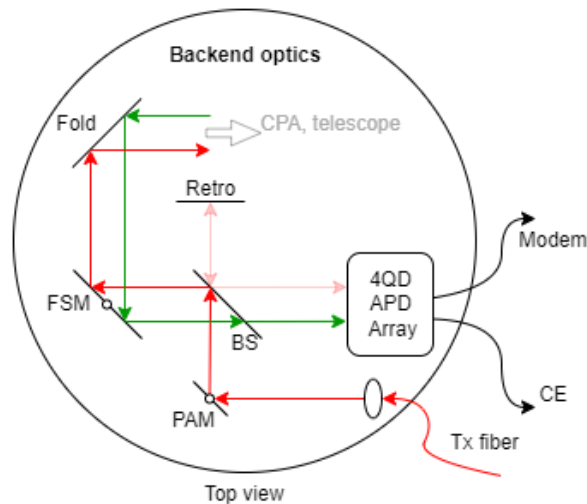


Figure 6.3: Backend optics.

The uplink beam enters the BO from the CPA relay through the fold mirror. Similar to the Tx, it passes the FSM which stabilizes the beam and directs it through the BS, which doesn't affect the Rx wavelength. FSM and fold mirror could be combined into one, but has not been done in this example to maintain clarity. The Rx beam then falls onto the 4QD APD detector array. This detector is expected to perform beam PAT and data communication simultaneously. Although often these two activities are separated among different detectors, integrating these into one device would simplify the optical system and maintain uplink optical power in one beam instead of dividing it among two detectors. Additionally the detector is preferred to be able of verifying the Tx PAA, therefore it has to be sensitive to both wavelengths. This allows for verifying the spatial direction and magnitude of the PAA relative to the uplink beam, implementing additional redundancy. Data gathered by the array will be transferred towards the modem for data decoding and the CE for PAT purposes respectively.

In this design two steering mirrors would be required for the FSM and PAM. These mirrors are commercially available and have been developed by TNO. Their FSM is capable of control bandwidths over 1 kHz at an accuracy of less than $1 \mu\text{rad}$ [72]. Regular space qualified mirrors and lenses are also commercially available. The APD array capable of multiple functionalities is not commercially available and will have to be developed. Considering sensitivity to both wavelengths, the detector would have to be InGaAs based since Si is insensitive to 1550 nm. It is foreseen that the entire BO assembly will be thermally stabilized by the CE and mechanically by a surrounding vibration isolation system, which will additionally stabilize the CPA. Materials of choice preferably have a low thermal expansion coefficient, high conductivity to avoid gradients, low mass, low cost, high stiffness and radiation hardness. A typically used material for space optical components is Zerodur.

Tracking

The main challenge in tracking is SC platform disturbance. Uncorrected pointing jitter caused by platform disturbance typically is in the order of 10-20 μrad [65] and practically proven around 16 μrad RMS average for the Silex and ETS-VI spacecraft platforms [131]. This requires closing a gap up to 15 μrad or more with correcting systems. Figure 6.4 shows a typical power spectral density of SC platform vibration. The graph shows that SC vibrations occur at a variety of frequencies with most high magnitude disturbances below 10 Hz. Disturbance correction will be a combined effort of multiple subsystems operating at different parts of the disturbance spectrum. Low frequency disturbances (0-1 Hz) are measured with the optical head 4QD sensor that senses angular offsets between incoming beacon and CPA attitude. The terminal may furthermore be informed about these through SC attitude data and star trackers. Correction for these can be done by actuating the CPA or even the SC AOCS system when required with large disturbances.

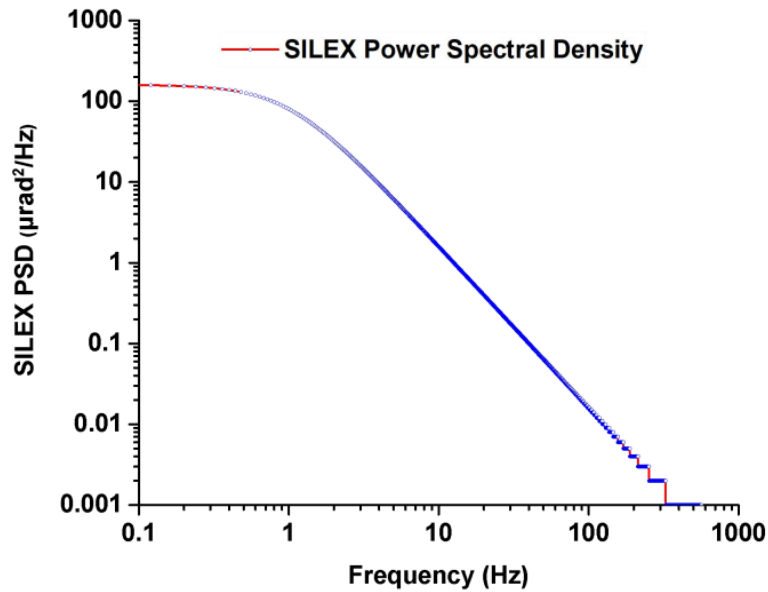


Figure 6.4: Power spectral density for SILEX spacecraft platform vibration [131].

Disturbances at frequencies in the middle part of the spectrum (1-1000 Hz) will also be measured by the 4QD sensor but may need help through an inertial measurement unit (IMU) [11]. This unit measures fast accelerations of the optical head and can process this data through a control loop that actuates Fast Steering Mirrors (FSM) in the OH to keep the optical beams stabilized. The TNO FSM is able to correct at bandwidths over 1 kHz at an accuracy of $1 \mu\text{rad}$ [72]. The datasheet even claims accuracies down to $0.3 \mu\text{rad}$ at platform excitations of $16 \mu\text{rad}$, similar to Silex [33]. As a reference, LLCD had a closed loop accuracy up to 300 Hz. Implementing the TNO FSM into DOT will prove very useful and may ease requirements on the vibration isolation system due to its high active control bandwidth.

Very high frequency disturbances (>kHz) are small in magnitude but difficult to actively detect and correct, see figure 6.4. To mitigate these, vibration isolation systems are implemented. These systems also aid in suppression of middle frequency vibrations. An overview of spectral disturbance coverage methods for DOT can be seen in figure 6.5.

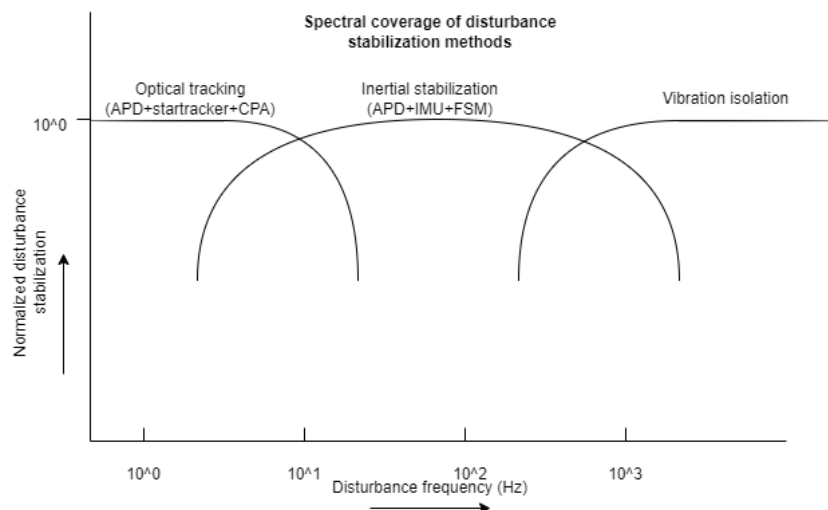


Figure 6.5: Disturbance stabilization spectral coverage.

Point ahead

As SC terminal and OGS will have different relative velocities, a point ahead angle will be needed to account for this, which can be calculated by equation 6.1 [13], where v is tangential velocity and c is light speed. Figure 6.6 depicts this method for the OGS.

$$\phi = \frac{2v_t}{c} \tag{6.1}$$

Lunar PAA will roughly be in the order of 20 μrad [11], but will vary as function of attitude, link window and ephemeris and would need to be updated by the control electronics. PAA can be performed in two ways, the first being a unique FSM that acts as point ahead mirror (PAM). The mirror will at all times direct the downlink beam with correct PAA and can also correct for disturbances or changes in attitude. The second way is an actuator system at the coupling of Tx fiber into free space optical system of the OH. The piezo electric actuators may spatially alter the fiber and thus the way light enters the downlink train. This method has been performed in the LLCD system [11]. While it seems complex, it would also simplify optical assembly setup.

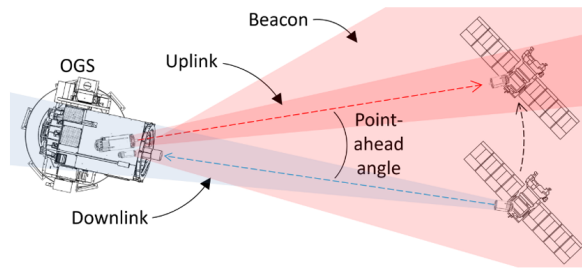


Figure 6.6: Point ahead angle [13].

Course Pointing Assembly

Transmitter aperture diameter is probably the most important system parameter. A lot of system functionalities and architectures depend heavily on this one and it thus needs careful consideration. A trade-off is shown in table 6.2 which is used to determine the optimal aperture diameter. Most important trade-off criteria can be seen vertically and potential diameter options are listed horizontally.

Table 6.2: Aperture diameter trade.

Aperture diameter		Options (cm) >							
Criteria V	Weight (1-3)	7	8	9	10	11	12	13	14
L_{pt} (dB)	2	-0.99728	-1.30257	-1.64856	-2.03526	-2.46267	-2.93078	-3.4396	-3.98912
m_{CPA} (kg)	1	3.1	4.6	6.6	9.0	12.0	15.6	19.9	24.8
P_{av} (W)	3	2.357	1.936	1.657	1.467	1.338	1.252	1.199	1.174
Score		9	12	15	16	13	12	9	9

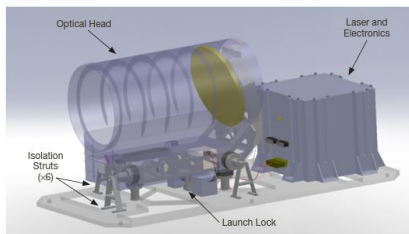
Pointing loss is determined by a combination of pointing system accuracy and aperture D , in this case, a jitter error of 1 μrad RMS is assumed [72]. The acceptable limit was deemed to be 2 dB for deep space applications, as recommended by NASA. Aperture diameter is also connected to system SWAP, in this case represented by CPA mass. A numerical relation was determined from data on similar systems, acquired by market study, in the form $mass = KD^3$, with D in cm and K in kg/cm^3 [119][45][33][77][53][99][88][126][53][129][1]. K herein turned out to be $9E-3$, based on nine data points. A CPA mass above 10 kg was determined to be too high to stay within system requirements. Laser power was determined using the earlier discussed constant EIRP formula as a function of D and pointing loss. Breakpoint here was defined at $\pm 50\%$ of similar systems to keep required laser performance realistic.

The trade table concludes the best option is a 10 cm aperture. This size results in an acceptable pointing loss around 2 dB and excellent values for mass and laser power. This size is similar to the

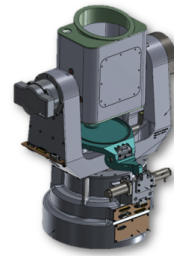
apertures used in LLCD and O2O terminals [9][121]. The same size is recommended for lunar terminals according to a study report on deep space optical communications architecture performed by ESA and RUAG [39]. It is additionally a nice rounded size which might prove useful when opting for COTS components. Figure 5.16 shows that an average laser power of 1.5 W will be needed. This happens to be the same laser power mentioned in [32], which TNO has said to be in development. In combination with 16-PPM modulation, a peak power of at least 30 W is required.

Two options are considered for the CPA: body pointing and independent pointing. The latter includes several distinctive design options: 2-axis gimbal assemblies based on a single mirror in figure 6.8a [99], a periscope in figure 6.8b [49] and a moving head design [45] in figure 6.7b.

CPA by body pointing makes the system less complicated, it uses less SWAP and is less failure sensitive. Course pointing would be done using the satellite AOCS system. This option is chosen for the DSOC terminal onboard the Psyche spacecraft in figure 6.7a [41]. It is definitely useful in situations where there is less room for error, SWAP is more critical and course pointing is less dynamic due to large deep space ranges beyond cis-lunar orbit. It does put more performance constraints on platform AOCS system.



(a) DSOC body pointing optical terminal [41].



(b) Moving head CPA for ISS optical communication and Artemis II systems [45].

Figure 6.7: Body mounted and moving head CPAs.

CPA by a hemispherical gimbal system has been applied more often. Its mechanism is based on a system where two rotating axes with mirrors provide large pointing coverage. It is useful in near earth and cis-lunar environment where course pointing is more dynamic with relatively high slew rates. It is primarily useful in relay systems where satellite nodes operate in a constellation. Nodes in these networks connect with multiple other nodes, therefore requiring multiple terminals with their own pointing system because sole platform AOCS cannot facilitate in these complicated situations. It furthermore puts less pressure on platform attitude requirements overall. SWAP and system complexity often increases though. A system trade-off can be seen in table 6.3.



(a) A single mirror CPA [99].



(b) Periscope Tesat LCT 135 lasercom terminal [49].

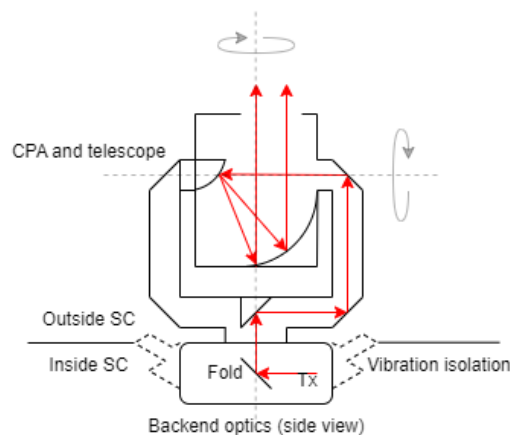
Figure 6.8: Single mirror and periscope CPA.

Table 6.3: CPA trade.

Coarse pointing assembly		Options >				Comments
Criteria V	Weight (1-9)	2-axis mirror	2-axis periscope	2-axis moving head	Body mounted (within SC)	
Dynamic complexity	7	1	2	5>	0	# Coarse moving mirrors
Range	8	Subhemi-sphere	Hemi-sphere	Hyper-hemisphere	Full	
Inertia	5	Low	Low	Low	High	Body mounted needs to turn whole SC
Independence	9	Yes	Yes	Yes	No	For redundancy and constellation potential
Dynamic imbalance	6	No	Yes	No	No	Asymmetric periscope
Telescope scalability	4	Internal	Internal	External	Internal	For D change
Optical exposure	3	High	Medium	Medium	Low	Radiation, thermal etc
Power consumption	1	Yes	Yes	Yes	No	
Size	2	+	+	-	++	Relative
Score		87	86	105	90	Red = 0, yellow = 1, blue = 2, green = 3

The trade-off shows that the 2-axis moving head design is most favorable, although being a complex system. Major benefits are its hyper-hemispherical reach and scalability. This setup can be used in a variety of applications, is independent of the spacecraft platform and can therefore also be used in future lunar constellations.

The CPA is chosen to be based on a moving head design. A concept drawing can be seen in figure 6.9 where a cross section of a side view is shown. For clarity only the downlink beam path has been drawn. The image shows how the beams are folded into the CPA relay system and expanded within the telescope, which is mounted in the gimbal structure. The rays follow a Coudé path through the gimbal arm instead of going straight through the middle. This allows for its unique hyper-hemispherical reach. This is best combined with a Schiefspiegler off-axis reflective telescope [73]. Advantage is that the beam does not encounter any secondary mirror blocking obstruction, increasing throughput and efficiency [51]. A disadvantage is that more aberrations occur due to the asymmetric design. This can however be mitigated by careful relay mirror and lens design.

**Figure 6.9:** CPA and telescope mounted in a vibration isolation frame.

The CPA will be stiffly attached to the BO to maintain optical path alignment. Both systems together are mounted in a vibration isolation structure that is connected to the SC shell. This vibration isolation structure will stabilize the OH and filter away platform distortions, primarily high frequency ones. The CPA and telescope are modular and therefore facilitate easy customization. Mounting on top of the BO, outside of the SC furthermore facilitates scaling of the assembly without affecting SC internals.

This subsystem is the only dynamic part of the terminal. A fail safe and redundant design will be important. Facilitating accurate and fast gimbal motor operations without induced stresses or material binding is essential. Choice of materials therefore highly depends on materials used in the motors. A similar thermal expansion coefficient is required and like before, a high thermal conduction will avoid gradients and thus mechanical stresses. In 2020 a new CPA motor has been developed by TNO which combines a switched reluctance motor and magnetic hall sensor for actuation and sensing respectively [70]. Its tracking error is lower than $4 \mu\text{rad}$ and when combined with the TNO FSM [72] reduces to smaller than $1 \mu\text{rad}$ in accordance with earlier made assumptions.

As for redundancy, one might opt for a terminal design where the gimbal assembly can be rejected in the case of a CPA total loss or induced damage, and operations can continue in limited body pointing configuration. In this case another subsystem layer may be integrated between the BO and CPA consisting of a double inverse telescope assembly imaged in figure 6.10. The idea is that a compact Cassegrain telescope fully expands the beams after the fold mirror, up to 10cm in this case, or incomplete expansion to save volume and ease required SC AOCS accuracy in the body pointing scenario. A similar but opposite facing telescope will condense the beam again before entering the CPA relay system. In case of CPA total loss, the upper telescope with CPA on top can be rejected at the release line and link operations may continue with a single telescope using SC body pointing.

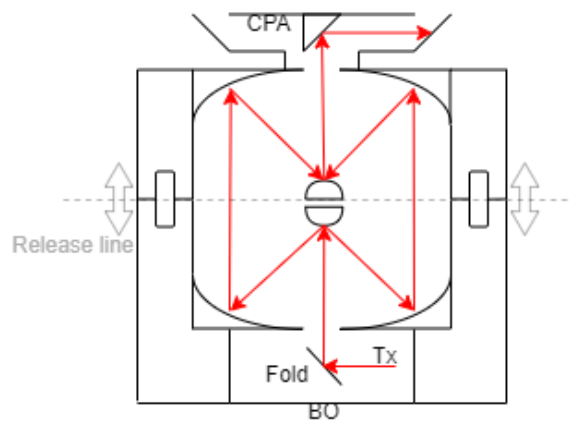


Figure 6.10: Redundant double inverse telescope assembly concept.

6.5. Power unit

The power unit (PU) will collect power from the SC platform and distribute it among DOT subsystems. The PU task list is given below:

- Import DOT system power supply from platform
- Supply and power up CE
- Receive and execute CE commands for power distribution
- Condition and distribute power among DOT subsystems

The power unit (PU) is considered to be closely related to the CE but still a subsystem on its own. Power units are available commercially in all shapes and sizes. Isispace develops their own cubesat power units in house. Isispace's Modular Electric Power System is meant for systems of sizes over 3U and includes a battery pack for storage, battery unit for battery management, conditioning unit for

incoming power conditioning and distribution unit towards the subsystems [57]. These can be seen in figure 6.11. The system is modular, redundant and can easily be scaled by stacking sub-units.

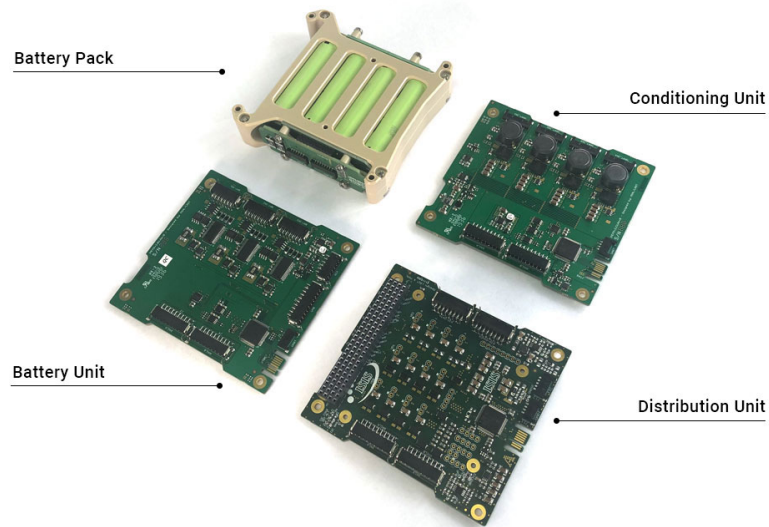


Figure 6.11: Isispace MEPS elements [57].

This chapter discussed the physical opto-mechanical design and subsystems of the DOT which are needed to realize earlier discussed link design in order to meet identified system requirements. The next chapter will review the integrated system design by discussing the downlink budget, system budgets and interfaces.

7

System design

This chapter will combine discussed design iterations into one system design and performance description. In the V-model in figure 4.1, this is the result of the design arrow coming from the system requirements. A product tree is given which shows the hierarchical architecture of the DOT system within a spacecraft. Budgets for these subsystems are estimated and subsequently interfaces between these are quantified. Finally derived specifications for the subsystems are summarized.

7.1. Product tree

A product tree overview is produced and shown in figure 7.1. The schematic was made to visually explain the hierarchical and functional position of DOT in a hypothetical spacecraft, including its subsystems. The image includes the upper level lunar orbiter on which DOT could be mounted and demonstrated for the first time. Typical platform subsystems and example payloads, as discussed in the use cases, have also been depicted. In the first demonstration mission, the terminal will both be part of the spacecraft platform as communication subsystem, but also a spacecraft payload, since the system still has to be demonstrated in orbit. When the system has been successfully proven, it can be treated as a regular platform subsystem in later missions and not as payload anymore.

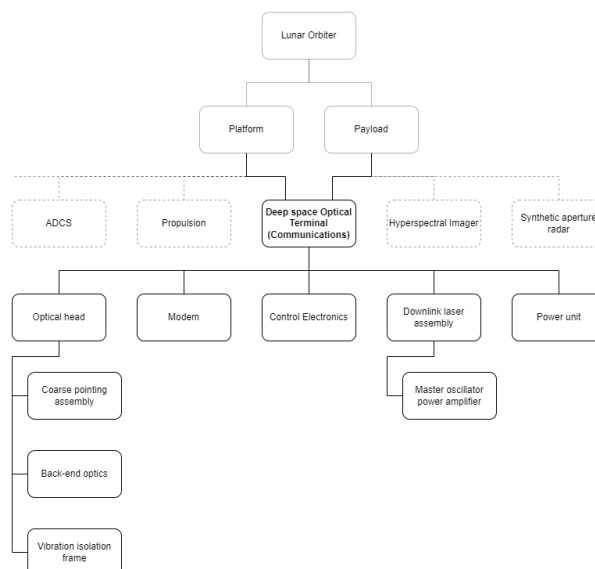


Figure 7.1: DOT product tree.

The five subsystems of DOT are shown, including their respective subsystems. This level deeper only applies for the optical head and the downlink laser assembly as these were the focus of chapter

6 and SQ3. This thesis covers the concept design down to the current level. It is recommended that further design stages will expand this tree into even more detail.

7.2. Link Budget

A downlink budget has been made which is shown in table 7.1. The budget uses values defined earlier in table 5.6. The link budget combines results of the link analysis and required modulation settings for maximum downlink data rate. As seen, the link is closed with practically no margin since average signal and required power are very similar, although a margin of 3 dB is already included within the 5 dB accounting for implementation loss. The required EIRP of 134 dBm is realized with a 1.5 W average laser power, a 10 cm aperture and a pointing loss of 2 dB. Although average noise power is higher than average signal power, a sufficient SNR is obtained due to application of buffering fiber amplifiers and focusing of the optical energy in one of 20 PPM slots each symbol, where the noise power is smeared out equally over all slots. As the table shows, this means that the OGS detector will on average count approximately one noise photon per non pulsed slot and one noise photon + approximately five signal photons for every pulsed slot.

Table 7.1: DOT downlink budget.

Segment	Parameter	Value	Decibel
Space	Average transmit power	1.5 W	32 dBm
	Transmitter gain	4.1E10	106 dB
	Pointing loss	0.63	-2 dB
	Transmitter loss	0.7	-1.5 dB
	EIRP	2.7E10 W	134 dBm
Channel	Free space loss	1.03E-31	-310 dB
	Atmospheric transmission loss	0.7	-1.5 dB
	Wavefront error	0.8	-0.97 dB
	Scintillation loss	0.47	-3.3 dB
Ground	Receiver gain	2.63E12	124 dB
	Receiver loss	0.5	-3 dB
	Detector efficiency	0.85	-0.7 dB
	Implementation loss	0.3	-5 dB
Total	Average signal power	2.59E-10 W	-65.9 dBm
	Required average signal power (Matlab sim)	2.56E-10	-65.9 dBm
	Average noise power	9.9E-10	-60 dBm
Data	PPM order	16	
	bits/symbol	4	
	Slot time	0.125 ns	
	Symbol time	2.5 ns	
	Symbol rate	4E8 Hz	
	Throughput	1.6E9 bits	
	Coding rate	2/3	
SNR	Netto data rate	1.07E9 bits/s	
	Signal ph/symbol	5.1	
	Noise ph/slot	0.96	
	Symbol SNR	5.2	7.2 dB

7.3. SWAP budgets

This section will estimate system budgets of all the subsystems of DOT which together make up the physical hardware of the integrated system. This is important in order to verify if DOT-SR-05 and 06 are met.

7.3.1. Control electronics

Because of the required capabilities regarding commands, data handling, and real time control systems, it was chosen to assume an OBC like system for small sat applications. The Amethyst OBC by Airbus

would be a feasible option. SWAP is 11x24x17 cm, 3.5 kg and 20-50 W respectively [118]. Another OBC by Airbus is the OSCAR OBC which is CCSDS compliant and primarily used for data handling. SWAP is 23x16x20 cm, 5 kg and 15 W max [117]. From various sources it is known that CE for the O2O mission will be produced by SEAKR [135], a space hardware manufacturer that is often contracted by NASA [35]. They offer catalog small sat OBCs that would be feasible in this case. Their latest generation has a SWAP of 27.7x19.9x11 cm, 5.3 kg, and 14 W power consumption [120]. During the LLCD demonstration in 2013, CE were used that will probably be similar to that of DOT. LLCD space terminal subsystems can be seen in figure 7.2 with CE on the left. Not a lot is known about those CE but regarding SWAP, it was approximately 26x20x15 cm, 10 kg and had a 30 W power consumption [106]. NASA's laser communications relay demonstration (LCRD) platform which combines optical PPM and DPSK for high data rate relay from GEO, uses control electronics designed by Moog [35]. They have an extended product line of OBCs and avionics for LEO missions up to interplanetary. Their main avionics controller (MAC) would be feasible for DOT having a SWAP of 23.6x23.5x8.8 cm, 5.8 kg and 12-40 W power consumption [91]. For an estimation, middle ground will be taken resulting in a SWAP of 25.04x20.1x12.36 cm, 5.94 kg and 24 W power consumption for DOT budgetting.

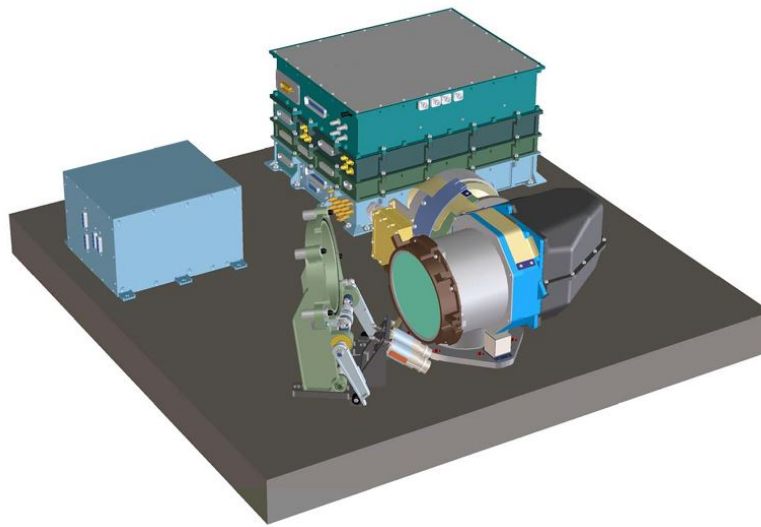


Figure 7.2: LLCD space terminal subsystems with the CE left, Modem above and OH below [9].

7.3.2. Modem

To estimate modem SWAP, already verified modem designs used in LLCD and O2O will be analysed and extrapolated for DOT. The LLCD modem design can be seen in figure 7.3. Weight and size can be seen and it had a total power consumption of 78 W. It produced a 0.5 W average power downlink laser with data rate of 622 Mbit/s and received a 22 Mbit/s uplink. The modem was divided in several different functional slices [25]. Note that this modem includes the downlink laser assembly and uplink detector assembly where the DOT modem will not. The DOT modem will thus have a much smaller SWAP.

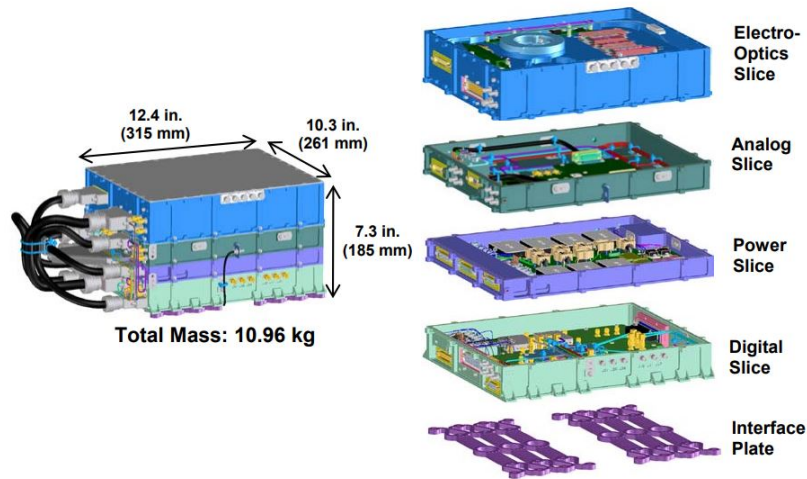


Figure 7.3: LLCOD modem design [25].

The O2O modem has a similar design in a sense that it includes several stacked functional slices, as can be seen in figure 7.4. SWAP is 27.4x34.3x20.3 cm, 11.36 kg and power consumption is 62 W [26]. It produces a 1 W average power downlink laser at 260 Mbit/s and receives a 21 Mbit/s uplink.

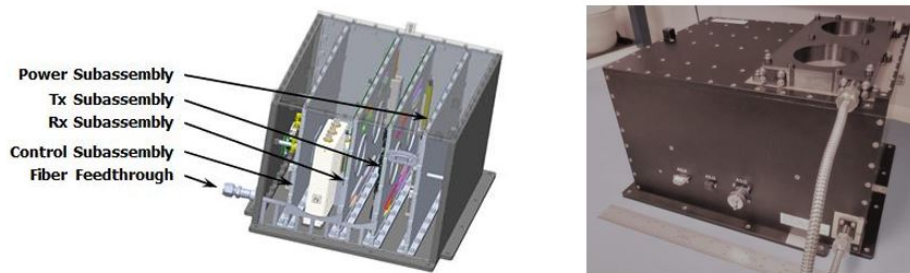


Figure 7.4: O2O modem [26].

DOT modem design will be a lot different. Electro-optics will not be included since the laser generator will be integrated in the DLA and the uplink detector is located in the OH. Thus the DOT modem will solely consist of electronics. The DOT modem can thus be compared with just the digital/control slices seen in the figures. Taking one slice, DOT modem volume is estimated to be about 32x26x5 cm. Most of the mass in mentioned modems comes from the electro-optics and power sub-assemblies. It is estimated that approximately 10% of the discussed modems mass makes up the coding hardware, about 1.1 kg. Power use of this modem is difficult to predict and is not to be underestimated. For LLCOD and O2O it is 60-70 W but that includes all electro-optics. For DOT it will probably be somewhere between 10-30 W, with most being consumed by the FPGAs. 20 W will be assumed for now.

7.3.3. Downlink laser assembly

DLA power use is due to the seed laser and fiber amplifier stages. Assuming a low efficiency for amplifier stages of 10% and neglecting initial seed laser power, amplifiers will take up 15 W [50]. A typical 40 mW seed laser requires a max power input of 10 W, adding up to 25 W for the DLA [96][97]. Most of the volume within the DLA will be taken up by the doped fiber amplifiers as these are relatively long in length, sometimes up to meters, and cannot be bent very sharply. These will be bound up in circular bundles with a diameter of approximately 20 cm, which means volume is minimally 20 cm squared x height. A linear optical train setup as shown in figure 6.2 will thus not be possible. The electro-optics slice from the LLCOD modem, including MOPA assembly and supporting elements was around 31.5x26.1x7 cm and 3 kg [9], similar for O2O. State of the art laser assemblies at similar power

level are of the same order in size at 26x25x6 cm with a mass of 8 kg [87]. Taking the average gives an estimation for DOT DLA of 30.6x26.2x6.3 cm and 5.5 kg.

7.3.4. Optical head

To estimate SWAP of the OH casing, a scaled Solidworks model was created which can be seen in figure 7.5. The model consists of 2 mm thin walled beryllium. Beryllium was chosen because it has a similar coefficient of thermal expansion as the stainless steel used in the motors, it is very stiff, lightweight and has high thermal conduction [95][121]. The two cylinders below would contain the BO and one of the two motors. Mass of this assembly is approximately 1.8 kg and volume is 10,452.4 cm^3 . This does not yet include the optical components of the BO.

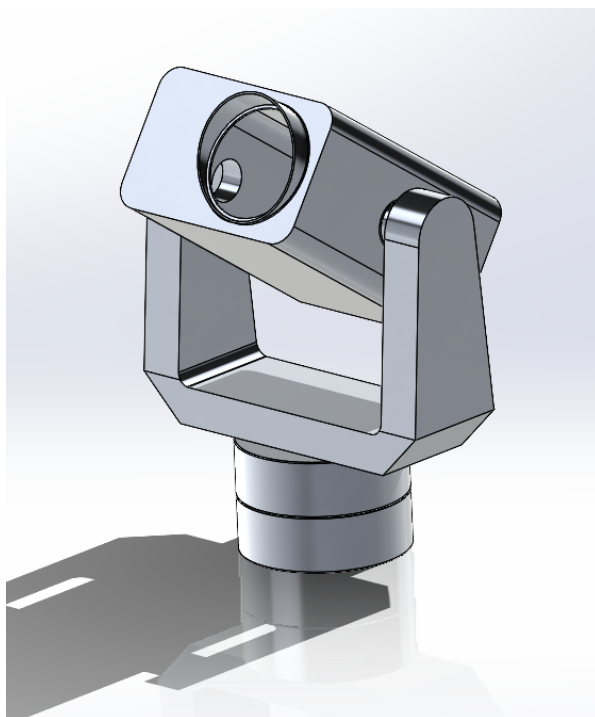


Figure 7.5: Solidworks model of the OH.

Regarding optical components, an inventarisation was made including large and smaller mirrors for the telescope, CPA relay and BO using data from the optical elements catalog of Thorlabs. Additionally beam splitter, TNOs fast steering mirrors [72], a 4QD detector module and axis motors [70] were taken into account. Summing these and rounding up gives a mass of 2.5 kg, resulting in a total mass of 4.3 kg. As for power use, the only consuming components are the axis motors, FSMs and the detector module. The two FSMs take up 50 mW max, the APD module 1 W max [143][142] and the motors 5 W max [70], summing up to 6.05 W maximum.

7.3.5. Power unit

The total system will have a power use approximately over 80 W during downlink, according to above analysis. Looking at the Ispispace modular EPS, the power battery unit has a maximum output of 64 W, which will not be enough. Two of these might be required. PU mass will be 0.5 kg and have a volume of 0.5U [57]. Power dissipation is not mentioned for the unit but is probably negligible.

7.3.6. Summary

The above SWAP analysis is summarized in tables 7.2, 7.3 and 7.4 below. Total maximum SWAP in the worst case scenario is summarized in table 7.5. Calculated values were inventoried and its estimation model was given an uncertainty parameter A, B or C, with A the most certain and C uncertain. These parameters have margins 5%, 10% and 15% respectively. Similar margins are used by Ispispace system engineers to calculate CubeSat SWAP budgets. However, Ispispace uses smaller margins of

2, 5 and 10% respectively for uncertainties A, B and C, based on TRL and heritage. In the current analysis, larger margins have been considered due to estimation uncertainties and system novelty.

If the actual system SWAP values are maintained below those calculated for the worst case scenario, they would comply with system requirements for mass and power. Figure 7.6 shows a Solidworks model of all DOT subsystems together on a 1 m² plate to give a sense of volume of the system. Left is the OH, top the CE, below the PU, and right the modem and DLA stacked on top of each other.

Table 7.2: DOT size budget with estimation model uncertainties causing the margin. Variables A, B and C have uncertainties of 5, 10 and 15% respectively.

<i>Subsystem V</i>	<i>Size (cm³)</i>	<i>Model certainty</i>	<i>Margin (cm³)</i>	<i>Size + Margin (cm³)</i>
Control electronics	6180	A	309	6489
Modem	4160	B	416	4576
Downlink laser assembly	5051	A	253	5303
Optical head	10452	B	1045	11497
Power unit	500	A	25	525
Total	26343		2048	28390
Total (liters)	26.3		2.0	28.4

Table 7.3: DOT mass budget with estimation model uncertainties causing the margin. Variables A, B and C have uncertainties of 5, 10 and 15% respectively.

<i>Subsystem V</i>	<i>Mass (kg)</i>	<i>Model certainty</i>	<i>Margin (kg)</i>	<i>Mass + Margin (kg)</i>
Control electronics	5.9	C	0.891	6.83
Modem	1.1	C	0.165	1.27
Downlink laser assembly	5.5	B	0.55	6.05
Optical head	4.3	C	0.645	4.95
Power unit	0.5	A	0.025	0.525
Total	17		2.3	19.6

Table 7.4: DOT power budget with estimation model uncertainties causing the margin. Variables A, B and C have uncertainties of 5, 10 and 15% respectively.

<i>Subsystem V</i>	<i>Power (W)</i>	<i>Model certainty</i>	<i>Margin (W)</i>	<i>Power + Margin (W)</i>
Control electronics	24	C	3.6	27.6
Modem	20	C	3	23
Downlink laser assembly	25	B	2.5	27.5
Optical head	6.05	B	0.6	6.66
Power unit	0	A	0	0
Total	75		9.7	84.8

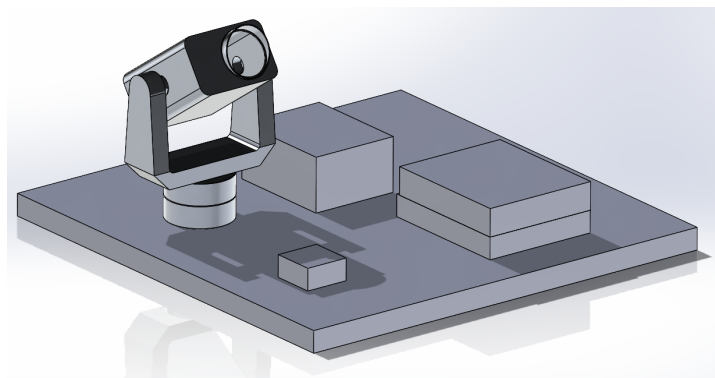


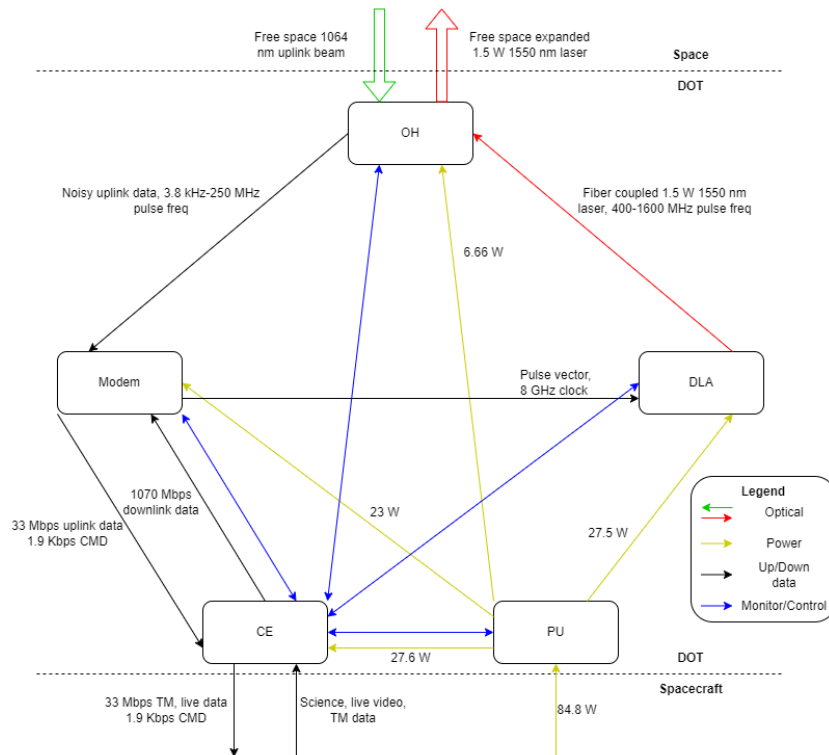
Figure 7.6: Solidworks model of all DOT subsystems scaled on a 1m² plate.

Table 7.5: Maximum SWAP budget.

Subsystem V	Size (cm ³)	Weight (kg)	Power (W)
Control electronics	6489	6.83	27.6
Modem	4576	1.27	23
Downlink laser assembly	5303	6.05	27.5
Optical head	11497	4.95	6.66
Power unit	525	0.525	0
Total	28390	19.6	84.8
	28.4 liters		

7.4. Interfaces

A high level DOT (sub)system interface (IF) schematic can be seen in figure 7.7. Yellow arrows indicate power lines, black arrows communication data IF, red and green arrows optical IF and blue lines indicate monitor and control IF. The last thus also includes data but are different from the black lines since blue IF are meant for subsystem control and not for the up or downlink data flow. The schematic shows the case of maximum data rate performance. The up and downlink raw data and optical flows show a pulse frequency domain since the actual spread of the PPM pulses vary depending on bit sequence. The optical interface between DOT and space show hollow arrows which means the link is free space coupled instead of fiber coupled.

**Figure 7.7:** High level interface overview.

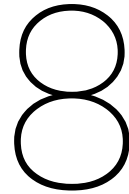
7.5. Derived specifications

This section will summarize and list some of the lower level specifications to which the DOT will need to adhere. These were deduced as a result of the design iterations and trade-offs. The DOT subsystem specifications include those shown in table 7.6. This level in design is the deepest this thesis will discuss.

Table 7.6: Derived system specifications.

Subsystem	Specification code	Derived system specification
General	DOT-GEN-01	Downlink wavelength shall be 1550 nm
	DOT-GEN-02	Uplink wavelength shall be 1064 nm
Modem	DOT-MOD-01	DOT will use SCPPM modulation and coding
	DOT-MOD-02	The modem shall be able of 16 PPM coding
	DOT-MOD-03	The modem shall at least be able of 2 and 4 PPM decoding
	DOT-MOD-04	Modem shall at least accommodate slot times of 0.125 ns for the downlink
	DOT-MOD-05	Modem shall be able to identify nested uplink modulation schemes
	DOT-MOD-06	Modem shall have a storage to facilitate variable interleaving
Control electronics	DOT-CE-01	CE shall be able of passing a 1067 Mbps downlink datarate to the modem
	DOT-CE-02	CE shall be able of receiving a 33 Mbps datarate uplink from the modem
Optical head	DOT-OH-01	The OH shall be duplex
	DOT-OH-02	The OH uplink detector shall perform tracking, data comms and PAA verification simultaneously
	DOT-OH-03	OH CPA shall be based on a moving head design
	DOT-OH-04	OH shall have a vibration isolation system
	DOT-OH-05	OH shall have an aperture size of 10 cm
Downlink laser assembly	DOT-DLA-01	DLA shall be able to produce a downlink laser with average power of 1.5 W
	DOT-DLA-02	DLA architecture shall be MOPA based
	DOT-DLA-03	DLA shall be able to facilitate slot times of 0.125 ns
	DOT-DLA-04	Maximum timing jitter shall be 12.5 ps
	DOT-DLA-05	DLA clock rate shall be able of 8 GHz
	DOT-DLA-06	DLA shall facilitate a maximum pulse frequency of 1600 MHz
	DOT-DLA-07	Peak power shall be at least 30 W
	DOT-DLA-08	Extinction ratio shall be at least 30 dB
Power unit	DOT-PU-01	PU shall be able to deliver 84.8 W to different subsystems

This chapter has discussed the integrated DOT system design as a result of the performed design iterations. The next chapter will verify if these iterations have been performed properly and if the system requirements are met.



Verification

This chapter will verify the system requirements along the design iterations performed. In figure 4.1, this chapter thus represents the verification arrow to the left from system design and performance description to system requirements.

In order to verify the initial system requirements listed in table 3.2, a compliance analysis is made in this chapter. The system requirements compliance matrix can be seen in table 8.1. The concept design made in this thesis shows compliance to 6 out of 6 of the initial system requirements. Verification in general can be proven with four different methods: test, analysis, review of design and inspection. The methods used in this thesis include only analysis and review of design as no hardware can be inspected and testing on software or hardware has not been performed.

Table 8.1: System requirements compliance matrix.

Code	System requirement	Compliance	Reference	Verification method
DOT-SR-01	DOT shall be able to downlink 1 Gbit/s through optical communication from the Moon to Earth	Yes	Chapter 5.4.2	Design review
DOT-SR-02	BER shall be equal or lower than 10^{-6} for the optical downlink from the Moon to Earth after error correction	Yes	Chapter 5.6.2	Design review
DOT-SR-03	DOT shall be able to receive 30 Mbit/s of high data rate optical uplink from Earth	Yes	Chapter 5.4.3	Design review
DOT-SR-04	DOT design shall follow CCSDS high photon efficiency standards	Yes	Chapter 7.5	Design review
DOT-SR-05	DOT shall consume less than 89.6 Watt of power	Yes	Chapter 7.3.6	Analysis
DOT-SR-06	DOT shall have a mass less than 24 kg	Yes	Chapter 7.3.6	Analysis

Design review of figure 5.6 indicates that DOT-SR-01 can be met using modulation settings of 16-PPM, 0.125 ns slot time and coding rate of 2/3. Design review of figure 5.14 indicates that DOT-SR-02 can be met by realizing an average optical power of 3 dB photons/ns at the receiver. Design review of figure 5.7 indicates DOT-SR-03 can be met by using modulation settings of 4-PPM, 2 ns slot time and coding rate of 2/3. Design review of table 7.6 shows that wavelength, coding, slot times, and modulation settings all comply with CCSDS HPE standards and that DOT-SR-04 is met. Finally, analysis of table 7.5 indicates that proposed the estimated DOT system budgets would stay below 24 kg and consume less than 89.6 W of power, thus meeting DOT-SR-05 and 06.

9

Conclusion

This chapter will first conclude the thesis research before discussing and evaluating the performed work. Finally recommendations will be made. In the V-model in figure 4.1, this chapter represents the system capability block, going one level upwards from system design and performance description. Answering the initial RQ and SQs as derived from the stakeholder need, this chapter is the result of the design arrow to the right from system need and stakeholder requirements. It is validated in the sense that the need of Isispace for DSOC system knowledge expansion has been met.

9.1. Conclusion

In order to conclude and answer the main research question, the sub-questions will first be revisited. The first sub-question was: *What are the system requirements related to link and opto-mechanical design for a spacecraft terminal that facilitates a high data rate optical communication link between the Moon and Earth?* The system requirements for DOT in this thesis were derived from the stakeholder requirements, which were formed based on use case analysis in chapter 2. The system requirements, formulated in table 3.2, do not include all relevant system requirements, but only those relevant for link and opto-mechanical design of the terminal, within the scope of the research question.

The second sub-question was: *What link design is needed for a high data rate optical communication system between the Moon and Earth?* The system requirements derived in SQ1 provided the required performance level of this link design. SQ2 discusses how this link would work. Key aspects in this link design are wavelength, coding, modulation, slot time, pointing, and EIRP. These have been discussed elaborately in chapter 5. However, a summary of the optical link design for the maximum performance case is given in table 9.1.

Table 9.1: DOT link design.

Link parameter	DOT design
Wavelength	1550 nm down and 1064 nm up
Coding (rate)	Serially Concatenated Pulse Position Modulation (2/3)
Modulation	16-PPM down and 4-PPM up
Slot time	0.125 ns down and 2 ns up
Effective Isotropic Radiated Power	134 dBm
Netto data rate	1067 Mbit/s down and 33.3 Mbit/s up

The third sub-question was: *What are the opto-mechanical subsystems of the optical communication terminal aboard the lunar orbital spacecraft?* The entire DOT system was divided into five subsystems: the Control Electronics, the Modem, the Downlink Laser Assembly, the Optical Head and the Power Unit. These identified subsystems have been discussed elaborately in chapter 6. In line with the main RQ and the scope of this thesis, focus in this part primarily lies on the opto-mechanical subsystems, thus the DLA and the OH, although the other subsystems are also discussed.

The main research question was: *What optical link and opto-mechanical design is needed for a terminal aboard a lunar orbital spacecraft, enabling high data rate optical communication with Earth?* This question is answered by combining the answers of sub-questions two and three.

9.2. Discussion

The research performed in this thesis is theoretical. Practical experiments would be needed in further research to verify if the theory lines up with reality. Furthermore, the focus and scope of this thesis was merely to generate a concept design of the link and opto-mechanics of the optical terminal as a method for leveraging Isispace DSOC knowledge. There are many more relevant aspects of the terminal which have not been discussed here, but that would take more than a single MSc thesis.

Practical applications of DSOC are relatively new. A significant effort was put into study of theory, systems and gathering of data. However because of its novelty, useful data is scarce. Verification and validation offers a challenge, especially because of the theoretical nature of this thesis. Verification mainly concerned review of the design steps taken. Validation of the concept design is not addressed. Because the design of DOT relies on assumptions made based on the limited amount of similar systems, validation of design results by comparison with the same limited pool of similar systems would be invalid. Further practical research is needed for validation.

The models made in this thesis rely on several assumptions that were made based on literature and similar systems. For the noise constraint for example, an estimation was made for all noise sources under a single variable. A more accurate way to approach this would be to evaluate every single noise source and make realistic estimations for these. More examples of generalized assumptions can be found throughout the thesis. Given the multidisciplinary nature of DSOC however, there was not enough time to dive into the details of every discipline and science related to this subject. The systems engineering approach inherently highlights the manner in which the many disciplines and subsystems tie into each other to achieve a common goal. Assumptions and analyses made on individual disciplines may therefore sometimes seem somewhat superficial.

9.3. Recommendations

Recommendations for Isispace would be to focus on the company's expertise and apply that to DSOC. In this case that would probably concern development of Control Electronics and Modem subsystems. These kind of systems involve CDHS, pointing, coding and modulation hardware and software. General recommendations would include to focus on DSOC disadvantages and try to solve these. An example would be the atmospheric sensitivity of optical communication and its effect on link availability. Significant efforts will have to be made in order to expand existing ground segment systems to increase availability and facilitate DSOC video calls in the future. Furthermore, the low efficiency of laser modules in general offers a big opportunity for improvement. If this can be resolved, it would enable more efficient systems with increased optical power, allowing for higher data rates at higher quality. Finally it is recommended to design future DSOC systems to be adaptable, inter-operable and resilient to cope with challenging deep space environments.

The system complexity of DSOC requires a lot of investments. Currently, the main driver for development of DSOC is scientific research of deep space and enhanced payloads generating more data in more efficient spacecraft. Hence development is driven by agencies, governments and public funding, while commercial investments are still lacking, which is actually where the momentum lies. The initiative will have to come from agencies to create demand for DSOC and in response, industry will follow. Future plans for returning to the Moon by several agencies will hopefully boost DSOC development.

Deep space optical communications is merely a tool. But it is a tool that will prove to be essential to support deep space exploration and to find answers to some of humanities biggest questions. It is therefore of high importance to increase development efforts of this technology. Pushing the boundaries of this multidisciplinary tool will collaterally prove to be of significant contribution to science not only in space, but also on Earth in different fields and applications, as has been historically proven by technological development for space.

References

- [1] Aage Skullestad. *Pointing Mechanism for Optical Communication*. Tech. rep. Kongsberg Defence & Aerospace.
- [2] Abhijit Biswas et al. *Deep-space Optical Terminals (DOT) Systems Engineering*. Tech. rep. JPL, Nov. 2010.
- [3] Emmanuel Domfeh Aboagye and Shun Ping Chen. “Deep space optical communications (DSOC) downlink simulation with varying PPM order”. In: *Optical and Quantum Electronics* 53.10 (2021). ISSN: 1572817X. DOI: 10.1007/s11082-021-03232-z.
- [4] Felix Arnold et al. “Ground receiver unit for optical communication between LADEE spacecraft and ESA ground station”. In: *Free-Space Laser Communication and Atmospheric Propagation XXVI*. Vol. 8971. 2014. DOI: 10.1117/12.2039959.
- [5] Archit Arora et al. “Multiprobe Mission Architecture Options for a Uranus Flagship Mission”. In: *Journal of Spacecraft and Rockets* 58.3 (2021). ISSN: 0022-4650. DOI: 10.2514/1.a34960.
- [6] Brian Aull. *Geiger-mode avalanche photodiode arrays integrated to all-digital CMOS circuits*. 2016. DOI: 10.3390/s16040495.
- [7] Laurens Bierens, Rob van Heijster, and Hans van Bezouwen. *DATA REDUCTION USING REAL-TIME ON-BOARD SATELLITE SAR PROCESSING*. Tech. rep. the Hague: TNO, 1994.
- [8] Bradley G. Boone et al. “Optical communications development for spacecraft applications”. In: *Johns Hopkins APL Technical Digest (Applied Physics Laboratory)* 25.4 (2004). ISSN: 02705214.
- [9] Don M. Boroson and Bryan S. Robinson. *The Lunar Laser Communication Demonstration: NASA’s First Step Toward Very High Data Rate Support of Science and Exploration Missions*. 2014. DOI: 10.1007/s11214-014-0122-y.
- [10] Benjamin Buck et al. “Photon counting camera for the NASA deep space optical communication demonstration on the PSYCHE mission.” In: 2019. DOI: 10.1117/12.2520617.
- [11] Jamie W. Burnside et al. “Design of an inertially stabilized telescope for the LLCDC”. In: *Free-Space Laser Communication Technologies XXIII*. Vol. 7923. 2011. DOI: 10.1117/12.878926.
- [12] Sonja Caldwell. *9.0 Communications*. July 2023.
- [13] Alberto Carrasco-Casado. “Free-space optical links for space communication networks”. In: *Springer handbook of optical networks*. Tokyo: Springer, 2022. Chap. 8.
- [14] CCSDS secretariat. *OPTICAL COMMUNICATIONS CODING AND SYNCHRONIZATION*. 1st ed. Vol. 1. Washington DC: NASA, Aug. 2019.
- [15] CCSDS secretariat. *OPTICAL COMMUNICATIONS PHYSICAL LAYER*. 1st ed. Vol. 1. Washington DC: NASA, Aug. 2019.
- [16] CCSDS secretariat. *OPTICAL HIGH DATA RATE (HDR) COMMUNICATION— 1550 NM*. 1st ed. Vol. 1. Washington DC: NASA, June 2022.
- [17] C Chen et al. *System Requirements for a Deep Space Optical Transceiver*. Tech. rep. Pasadena: JPL, Jan. 1999.
- [18] Shun Ping Chen. “Investigations of free space and deep space optical communication scenarios”. In: *CEAS Space Journal* 14.2 (2022). ISSN: 18682510. DOI: 10.1007/s12567-021-00388-y.
- [19] Shun Ping Chen. “Performance analysis of near-earth, lunar and interplanetary optical communication links”. In: *Optical and Quantum Electronics* 54.9 (2022). ISSN: 1572817X. DOI: 10.1007/s11082-022-03987-z.

- [20] Michael K. Cheng et al. "Implementation of a coded modulation for deep space optical communications". In: *GLOBECOM - IEEE Global Telecommunications Conference*. 2006. DOI: 10.1109/GLOCOM.2006.529.
- [21] Gordon Chin et al. "Lunar reconnaissance orbiter overview: The instrument suite and mission". In: *Space Science Reviews* 129.4 (2007). ISSN: 00386308. DOI: 10.1007/s11214-007-9153-y.
- [22] R. K. Choudhary et al. "Dual frequency radio science experiment onboard chandrayaan-2: A radio occultation technique to study temporal and spatial variations in the surface-bound ionosphere of the Moon". In: *Current Science* 118.2 (2020). ISSN: 00113891. DOI: 10.18520/cs/v118/i2/210-218.
- [23] Arup Roy Chowdhury et al. "Imaging infrared spectrometer onboard Chandrayaan-2 orbiter". In: *Current Science* 118.3 (2020). ISSN: 00113891. DOI: 10.18520/cs/v118/i3/368-375.
- [24] Arup Roy Chowdhury et al. "Orbiter high resolution camera onboard chandrayaan-2 orbiter". In: *Current Science* 118.4 (2020). ISSN: 00113891. DOI: 10.18520/cs/v118/i4/560-565.
- [25] Steven Constantine et al. "Design of a high-speed space modem for the lunar laser communications demonstration". In: *Free-Space Laser Communication Technologies XXIII*. Vol. 7923. 2011. DOI: 10.1117/12.878927.
- [26] James M. Dailey et al. "Optical modem enabling broadband datacom links for crewed cis-lunar missions". In: 2022. DOI: 10.1117/12.2613748.
- [27] Ngoc T. Dang and Anh T. Pham. "Performance improvement of FSO/CDMA systems over dispersive turbulence channel using multi-wavelength PPM signaling". In: *Optics Express* 20.24 (2012). ISSN: 10944087. DOI: 10.1364/oe.20.026786.
- [28] Tirtha Pratim Das et al. "CHandra's Atmospheric Composition Explorer-2 onboard Chandrayaan-2 to study the lunar neutral exosphere". In: *Current Science* 118.2 (2020). ISSN: 00113891. DOI: 10.18520/cs/v118/i2/202-209.
- [29] David Israel. *Draft LunaNet Interoperability Specification*. Tech. rep. NASA, July 2021.
- [30] Dariush Divsalar et al. "Wavelength division multiple access for deep space optical communications". In: *IEEE Aerospace Conference Proceedings*. 2020. DOI: 10.1109/AERO47225.2020.9172472.
- [31] Sam Dolinar. *A note on deep space optical communication link parameters*. Tech. rep. Pasadena: Communications Systems Research Section JPL, May 1982, pp. 42-70.
- [32] M. Dresscher et al. "Design of Moon to Earth Optical Trunk Datalink for 400 Mbps". In: *Proceedings of the International Astronautical Congress, IAC*. Vol. B2. 2021.
- [33] M. Dresscher et al. "Key Challenges and Results in the Design of Cubesat Laser Terminals, Optical Heads and Coarse Pointing Assemblies". In: *2019 IEEE International Conference on Space Optical Systems and Applications, ICSOS 2019*. 2019. DOI: 10.1109/ICSOS45490.2019.8978976.
- [34] Vasuki Durairaj. "Amplification in Ytterbium-doped fibers". PhD thesis. Aalto: Aalto University, May 2013.
- [35] Bernie Edwards et al. "Challenges, Lessons Learned, and Methodologies from the LCRD Optical Communication System AIT". In: *2022 IEEE International Conference on Space Optical Systems and Applications, ICSOS 2022*. 2022. DOI: 10.1109/ICSOS53063.2022.9749730.
- [36] Taissir Y. Elganimi. "Studying the BER performance, power- and bandwidth- efficiency for FSO communication systems under various modulation schemes". In: *2013 IEEE Jordan Conference on Applied Electrical Engineering and Computing Technologies, AEECT 2013*. 2013. DOI: 10.1109/AEECT.2013.6716426.
- [37] ESA. *FOUR-QUADRANT INGAAS AVALANCHE PHOTODIODES FOR LEO DIRECT-TO-EARTH OPTICAL GROUND STATION (ARTES 6C.016)*. Dec. 2021.
- [38] ESA. *Moonlight*. 2023.

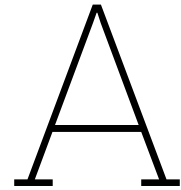
- [39] ESA and RUAG. *DOCOMAS Deep Space Optical Communications Architecture Study*. Tech. rep. ESA, Mar. 2016.
- [40] Ewa Kadziolka. *TNO & partners bring deep-space communication a step closer*. June 2023.
- [41] William Farr et al. "Overview and design of the DOT flight laser transceiver". In: *IPN Progress Report 42* (2011).
- [42] Jeff Foust. *NASA developing larger cubesat payload adapter for SLS*. Logan, Aug. 2023.
- [43] Sean Fuller et al. "Gateway program status and overview". In: *Journal of Space Safety Engineering* 9.4 (2022). ISSN: 24688967. DOI: 10.1016/j.jssse.2022.07.008.
- [44] Eberhard Gill. *AE4-S12-01-Introduction to Systems Engineering-V24*. Sept. 2020.
- [45] Steven R. Gillmer et al. "Demonstration of a modular, scalable, laser communication terminal for human spaceflight missions". In: 2021. DOI: 10.1117/12.2599014.
- [46] GVEC internet services. *STREAMING VIDEO DATA USAGE: WHAT INTERNET SPEED DO I NEED TO STREAM?* July 2021.
- [47] Christine M. Hartzell et al. "Data system design for a hyperspectral imaging mission concept". In: *IEEE Aerospace Conference Proceedings*. 2009. DOI: 10.1109/AERO.2009.4839507.
- [48] Harald Hauschildt et al. "European data relay system goes global". In: *2017 IEEE International Conference on Space Optical Systems and Applications, ICSOS 2017*. 2018. DOI: 10.1109/ICSOS.2017.8357204.
- [49] F. Heine et al. "Optical inter-satellite communication operational". In: *Proceedings - IEEE Military Communications Conference MILCOM*. 2010. DOI: 10.1109/MILCOM.2010.5680175.
- [50] Hamid Hemmati. *Deep Space Optical Communications DEEP SPACE COMMUNICATIONS AND NAVIGATION SERIES*. Tech. rep. JPL, Oct. 2005.
- [51] Hamid Hemmati, Abhijit Biswas, and Ivan B. Djordjevic. "Deep-space optical communications: Future perspectives and applications". In: *Proceedings of the IEEE* 99.11 (2011). ISSN: 00189219. DOI: 10.1109/JPROC.2011.2160609.
- [52] Kelsey Herndon, Franz Meyer, and Africa Flores. *What is Synthetic Aperture Radar?* 2023.
- [53] Honeywell. *OISL Coarse Pointing Assembly*. Oct. 2020.
- [54] Ben Hudson. *Synthetic Aperture Radar Concept of Operations*. Tech. rep. Open Source Satellite, July 2021.
- [55] INPhenix. *Everything You Need to Know About DFB Laser*. 2023.
- [56] Isispace. *Deep Space Deployer*. 2023.
- [57] Isispace Group. *Modular Electrical Power System*. 2023.
- [58] Hristo Ivanov et al. "Experimental characterization of SNSPD receiver technology for deep space FSO under laboratory testbed conditions". In: *Optik* 195 (2019). ISSN: 00304026. DOI: 10.1016/j.ijleo.2019.163101.
- [59] Michal Jachura et al. "Optimizing deep-space optical communication under power constraints". In: 2018. DOI: 10.1117/12.2289653.
- [60] Ben Jai et al. "The Mars Reconnaissance Orbiter mission operations: Architecture and approach". In: *SpaceOps 2006 Conference*. 2006.
- [61] Andrew Jones. *NASA and China are eyeing the same landing sites near the lunar south pole*. Aug. 2022.
- [62] JPL. *Psyche mission*. Jan. 2023.
- [63] Ewa Kadziolka. *Laser satellite communication*. 2023.
- [64] Rajesh Karki. "Reliability of Renewable Power Systems". In: *Encyclopedia of Sustainable Technologies*. 2017. DOI: 10.1016/B978-0-12-409548-9.10147-2.
- [65] Hemani Kaushal and Georges Kaddoum. *Optical Communication in Space: Challenges and Mitigation Techniques*. 2017. DOI: 10.1109/COMST.2016.2603518.
- [66] Herbert Kramer. *KPLO (Korean Pathfinder Lunar Orbiter)*. Oct. 2021.

- [67] Herbert Kramer. *LADEE (Lunar Atmosphere and Dust Environment Explorer)*. 2023.
- [68] Herbert Kramer. *LRO (Lunar Reconnaissance Orbiter)*. Nov. 2013.
- [69] Herbert Kramer. *PRISMA (Hyperspectral)*. June 2012.
- [70] Lukas Kramer et al. "Novel motorization axis for a coarse pointing assembly in optical communication systems". In: *IFAC-PapersOnLine*. Vol. 53. 2. 2020. DOI: 10.1016/j.ifacol.2020.12.1437.
- [71] U. Krüger et al. "A power and bandwidth efficient modulation for diffuse wireless infrared communication". In: *Journal of Optical Communications* 22.4 (2001). ISSN: 01734911. DOI: 10.1515/JOC.2001.22.4.139.
- [72] Stefan Kuiper et al. "High-Bandwidth and Compact Fine Steering Mirror Development for Laser Communications". In: *Esmats.Eu* September (2017).
- [73] Anton Kutter. *The Schiefspiegler*. Tech. rep. Biberach an der Riss: Sky publishing corporation, Dec. 1958.
- [74] Michelangelo L'Abbate et al. "From Mbps to Gbps: Evolution of Payload Data Handling and Transmission system for future earth observation missions". In: *2014 IEEE International Workshop on Metrology for Aerospace, MetroAeroSpace 2014 - Proceedings*. 2014. DOI: 10.1109/MetroAeroSpace.2014.6865991.
- [75] *Laser communication in space*. Feb. 2023.
- [76] Ingrida Lavrinovica and Jurgis Porins. "An improvement of EDFA efficiency by using ytterbium co-doped optical fibers". In: *2016 IEEE International Black Sea Conference on Communications and Networking, BlackSeaCom 2016*. 2017. DOI: 10.1109/BlackSeaCom.2016.7901584.
- [77] Rui Li et al. "A Survey on Laser Space Network: Terminals, Links, and Architectures". In: *IEEE Access* 10 (2022). ISSN: 21693536. DOI: 10.1109/ACCESS.2022.3162917.
- [78] Dawei Liang and Joana Almeida. "Highly efficient solar-pumped Nd:YAG laser". In: *Optics Express* 19.27 (2011). ISSN: 10944087. DOI: 10.1364/oe.19.026399.
- [79] Dawei Liang et al. "Most efficient simultaneous solar laser emissions from three Ce:Nd:YAG rods within a single pump cavity". In: *Solar Energy Materials and Solar Cells* 246 (2022). ISSN: 09270248. DOI: 10.1016/j.solmat.2022.111921.
- [80] Sarah Loff. *Artemis Program*. Apr. 2023.
- [81] Shannon M. MacKenzie et al. "The enceladus orbilander mission concept: Balancing return and resources in the search for life". In: *Planetary Science Journal* 2.2 (Apr. 2021). ISSN: 26323338. DOI: 10.3847/PSJ/abe4da.
- [82] O. Mahran and Moustafa H. Aly. "High performance characteristics of dual pumped Er³⁺/Yb³⁺ Co-doped/Raman hybrid optical amplifier". In: *Journal of Optoelectronics and Advanced Materials* 18.7-8 (2016). ISSN: 14544164.
- [83] Micah Maidenberg. *The Global Race to Water at the Moon's South Pole*. Aug. 2023.
- [84] Nathan Mathura. *Performance comparison of Digital Modulation techniques*. Apr. 2010.
- [85] Matlab. *End-to-End CCSDS SCPPM Simulation Using Deep Space Poisson Channel*. 2023.
- [86] Alfred S. McEwen et al. "The High Resolution Imaging Science Experiment (HiRISE) during MRO's Primary Science Phase (PSP)". In: *Icarus* 205.1 (2010). ISSN: 00191035. DOI: 10.1016/j.icarus.2009.04.023.
- [87] Menhir photonics. *MENHIR-1550 SERIES*. 2023.
- [88] Eric D. Miller et al. "A prototype coarse pointing mechanism for laser communication". In: *Free-Space Laser Communication and Atmospheric Propagation XXIX*. Vol. 10096. 2017. DOI: 10.1117/12.2264086.
- [89] Mitsubishi. *Mitsubishi Electric Develops World's First Laser Communication Terminal Integrating Space Optical Communication and Spatial Acquisition*. May 2022.
- [90] Bruce Moision and Jon Hamkins. "Deep-Space Optical Communications Downlink Budget: Modulation and Coding". In: *IPN progress report* 42.154 (2003).

- [91] Moog. *Spacecraft Avionics*. 2023.
- [92] Sangman Moon and Chang-Kyoon Kim. *Korea pathfinder lunar orbiter X-band downlink validation using X-band downlink test set*. Tech. rep. Jan. 2019.
- [93] NASA. "Small spacecraft avionics". In: vol. 1. NASA, 2023. Chap. 8, pp. 202–229.
- [94] Chandra M. Natarajan, Michael G. Tanner, and Robert H. Hadfield. *Superconducting nanowire single-photon detectors: Physics and applications*. 2012. DOI: 10.1088/0953-2048/25/6/063001.
- [95] Kate E. Nevin, Keith B. Doyle, and Allen D. Pillsbury. "Optomechanical design and analysis for the LLCD space terminal telescope". In: *Optical Modeling and Performance Predictions V*. Vol. 8127. 2011. DOI: 10.1117/12.890204.
- [96] NKT photonics. *Koheras BOOSTIK – fiber amplifier line card*. 2023.
- [97] NKT photonics. *Koheras MIKRO – single-frequency OEM lasers*. 2023.
- [98] Ian O'Neill. *NASA's Deep Space Optical Comm Demo Sends, Receives First Data*. Nov. 2023.
- [99] Oerlikon. *Coarse Pointing Assembly (CPA)*. Jan. 2007.
- [100] Optica. *Deep-space optical communication demonstration project forges ahead*. Dec. 2022.
- [101] G Ortiz, J Sandusky, and A Biswas. *Design of an opto-electronic receiver for deep-space optical communications*. Tech. rep. Pasadena: JPL, Aug. 2000, pp. 42–142.
- [102] P.Carril. *Inter-satellite laser links*. Feb. 2016.
- [103] Robert Pappalardo et al. "The Europa Clipper Mission: Understanding Icy World Habitability and Blazing a Path for Future Exploration". In: *Bulletin of the AAS 53.4* (2021). DOI: 10.3847/25c2cfeb.08489926.
- [104] V. Radhakrishna et al. "Chandrayaan-2 large area soft X-ray spectrometer". In: *Current Science 118.2* (2020). ISSN: 00113891. DOI: 10.18520/cs/v118/i2/219-225.
- [105] D. Renker. "Geiger-mode avalanche photodiodes, history, properties and problems". In: *Nuclear Instruments and Methods in Physics Research, Section A: Accelerators, Spectrometers, Detectors and Associated Equipment 567.1* SPEC. ISS. (2006). ISSN: 01689002. DOI: 10.1016/j.nima.2006.05.060.
- [106] B. S. Robinson et al. "Overview of the lunar laser communications demonstration". In: *Free-Space Laser Communication Technologies XXIII*. Vol. 7923. 2011. DOI: 10.1117/12.878313.
- [107] Bryan S. Robinson et al. "The lunar laser communications demonstration". In: *2011 International Conference on Space Optical Systems and Applications, ICSOS'11*. 2011. DOI: 10.1109/ICSOS.2011.5783709.
- [108] Rudiger Paschotta. *Electro-optic modulators*. 2022.
- [109] Rudiger Paschotta. *Erbium-ytterbium-doped Laser Gain Media*. 2023.
- [110] Rudiger Paschotta. *Rare-earth-doped Fibers*. 2023.
- [111] Rudolf Saathof. *AE4880 Laser Satellite Communications*. Delft, Mar. 2023.
- [112] Rudolf Saathof, Stefano Speretta, and Jian Guo. *Fundamental Challenges for Laser Satellite Communications and Quantum Key Distribution*. Tech. rep. Delft University of Tehcnology.
- [113] Rudolf Saathof et al. "In orbit demonstration plans for an optical satellite link between a CubeSat and a ground terminal at TNO". In: 2021. DOI: 10.1117/12.2583381.
- [114] Rudolf Saathof et al. "Optical technologies for terabit/s-throughput feeder link". In: *2017 IEEE International Conference on Space Optical Systems and Applications, ICSOS 2017*. 2018. DOI: 10.1109/ICSOS.2017.8357221.
- [115] Hirobumi Saito et al. "Proto-flight model test results of synthetic aperture radar for 100kg class small satellite". In: *Proceedings of the International Astronautical Congress, IAC*. Vol. 2019-October. 2019.
- [116] Marc Sans et al. "Design of the ESA Optical Ground Station for Participation in LLCD". In: *Proceedings of the International Workshop on Space Optical Systems and Applications 3-1* (2012).

- [117] Satsearch. *OSCAR*. Mar. 2022.
- [118] Satsearch. *PureLine Amethyst*. Mar. 2022.
- [119] Joseph J. Scozzafava et al. "Design of a very small inertially stabilized optical space terminal". In: *Free-Space Laser Communications VII*. Vol. 6709. 2007. DOI: 10.1117/12.738384.
- [120] SEAKR. *SEAKR®'s third generation Command & Data Handling system*. 2023.
- [121] Tina Shih et al. "A modular, agile, scalable optical terminal architecture for space communications". In: *2017 IEEE International Conference on Space Optical Systems and Applications, ICSOS 2017*. 2018. DOI: 10.1109/ICSOS.2017.8357236.
- [122] Zoran Sodnik et al. "Deep-space Optical Communication System (DOCS) for ESA's Space Weather mission to Lagrange orbit L5". In: *2017 IEEE International Conference on Space Optical Systems and Applications, ICSOS 2017*. 2018. DOI: 10.1109/ICSOS.2017.8357207.
- [123] Zoran Sodnik et al. "Results from a Lunar Laser Communication Experiment between NASA's LADEE Satellite and ESA's Optical Ground Station". In: *International Conference on Space Optical Systems and Applications (ICSOS) 9*. May (2014).
- [124] SpaceX. *MARS & BEYOND*. Sept. 2023.
- [125] Linda Spilker. *Cassini-Huygens' exploration of the Saturn system: 13 years of discovery*. 2019. DOI: 10.1126/science.aat3760.
- [126] Steve Wolter. *CrossBeam® Optical Communication Terminal*. Mar. 2023.
- [127] Venkatesan Sundararajan. "Overview and technical architecture of india's Chandrayaan-2 mission to the moon". In: *AIAA Aerospace Sciences Meeting, 2018*. 2018. DOI: 10.2514/6.2018-2178.
- [128] Aaron J. Swank et al. "Beaconless pointing for deep-space optical communication". In: *34th AIAA International Communications Satellite Systems Conference, 2016*. 2016. DOI: 10.2514/6.2016-5708.
- [129] Amnon G. Talmor, Harvard Harding, and Chien-Chung Chen. "Two-axis gimbal for air-to-air and air-to-ground laser communications". In: *Free-Space Laser Communication and Atmospheric Propagation XXVIII*. Vol. 9739. 2016. DOI: 10.1117/12.2218097.
- [130] Jim Taylor, Laura Sakamoto, and Chao-Jen Wong. *Cassini Orbiter/Huygens Probe Telecommunications*. Tech. rep. Pasadena: Deep Space Communications and Systems Navigation, Jan. 2002.
- [131] Yunjie Teng, Min Zhang, and Shoufeng Tong. "The Optimization Design of Sub-Regions Scanning and Vibration Analysis for Beaconless Spatial Acquisition in the Inter-Satellite Laser Communication System". In: *IEEE Photonics Journal* 10.6 (2018). ISSN: 19430655. DOI: 10.1109/JPHOT.2018.2884718.
- [132] Thorlabs. *Lithium Niobate Electro-Optic Modulators, Fiber-Coupled (1260 nm - 1625 nm)*. 2023.
- [133] R Trautner. *ESA'S ROADMAP FOR NEXT GENERATION PAYLOAD DATA PROCESSORS*. Tech. rep. Noordwijk: ESA-ESTEC, 2011.
- [134] George N. Tzintzarov, Sunil G. Rao, and John D. Cressler. *Integrated silicon photonics for enabling next-generation space systems*. 2021. DOI: 10.3390/photonics8040131.
- [135] UK department for business & trade. *United States - O2O-2 Optical Module Control Electronics System*. Oct. 2019.
- [136] Nishanth Virushabaddoss et al. "Design of X-And Ka-Band Reflectarray Antennas for Intercelestial Communication Using CubeSat Relay". In: *2021 IEEE Space Hardware and Radio Conference, SHaRC 2021*. 2021. DOI: 10.1109/SHaRC51853.2021.9375885.
- [137] Colin. E. Webb. *Handbook of Laser Technology and Applications*. 2020. DOI: 10.1201/9780429183508.
- [138] Wikipedia. *Technische Universiteit Delft*. 2023.
- [139] David Williams. *Korea Pathfinder Lunar Orbiter*. Oct. 2022.

-
- [140] W Dan Williams, Michael Collins, and D. Boroson. "RF and Optical Communications: A Comparison of High Data Rate Returns From Deep Space in the 2020 Timeframe". In: *Nasa/Tm March* (2007).
- [141] Bram de Winter. *ACHIEVED – Assembly for Concepts in Human Interplanetary Exploration with Various Extraterrestrial Designations*. 2023.
- [142] Jin Wu et al. "64 × 64 GM-APD array-based readout integrated circuit for 3D imaging applications". In: *Science China Information Sciences* 62.6 (2019). ISSN: 18691919. DOI: 10.1007/s11432-018-9712-7.
- [143] Toshihide Yoshimatsu et al. "Compact and high-sensitivity 100-Gb/s (4 × 25 Gb/s) APD-ROSA with a LAN-WDM PLC demultiplexer". In: *European Conference on Optical Communication, ECOC*. 2012. DOI: 10.1364/oe.20.00b393.
- [144] Changming Zhao et al. "Solar pumped lasers for free space laser communication". In: *PHOTONICS 2019 - Proceedings of the 7th International Conference on Photonics, Optics and Laser Technology*. 2019. DOI: 10.5220/0007569702680275.



Matlab codes

A.1. BER plots

The code below was used to create the BER simulations for various modulation schemes as a function of SNR in figure 5.5.

```
1 close all
2
3 snr = 0:.5:25;
4 snr_lin = 10.^(snr/10);
5
6 %BPSK
7 BPSK = log10(0.5*erfc(sqrt(snr_lin)));
8
9 %DPSK
10 DPSK = log10(0.5*erfc(sqrt(snr_lin)/sqrt(2)));
11
12 %OOKnrz
13 OOKnrz = log10(0.5*erfc((1/(2*sqrt(2)))*sqrt(snr_lin)));
14
15 %OOKrz
16 OOKrz = log10(0.5*erfc(0.5*sqrt(snr_lin)));
17
18 %8 PPM
19 ppm8 = log10(0.5*erfc((1/(2*sqrt(2)))*sqrt(snr_lin*12)));
20
21 %16 PPM
22 ppm16 = log10(0.5*erfc((1/(2*sqrt(2)))*sqrt(snr_lin*32)));
23
24 %32 PPM
25 ppm32 = log10(0.5*erfc((1/(2*sqrt(2)))*sqrt(snr_lin*80)));
26
27 %qam16
28 qam16 = log10((3/8)*erfc(sqrt((6/15)*snr_lin)));
29
30 %qam64
31 qam64 = log10((7/24)*erfc(sqrt((9/63)*snr_lin)));
32
33 plot(snr, OOKnrz, 'r-h')
34 hold on
35 plot(snr, qam64, 'm-h')
36 plot(snr, OOKrz, 'g-o')
37 plot(snr, qam16, 'r-d')
38 plot(snr, DPSK, 'c-s')
39 plot(snr, BPSK, 'b-*')
40 plot(snr, ppm8, 'm-d')
41 plot(snr, ppm16, 'g-*')
42 plot(snr, ppm32, 'k-p')
43
44
45 hold on
```

```

46 axis([0 26 -10 0])
47 legend('OOKnrz = 2PPM','64QAM','OOKkrz','16QAM','DPSK = 4PPM','BPSK','8PPM','16PPM','32PPM')
48 title('Theoretical BER as function of SNR for various modulation formats')
49 xlabel('SNR (E_b/N_0) [dB]')
50 ylabel('log10(BER)')

```

A.2. Data rates

This section includes codes used for simulation of up and downlink data rates as a function of slot times and PPM orders.

A.2.1. Downlink

The code below was used for the downlink data rate simulation in figure 5.6.

```

1 close all
2
3 Ts = 0.025E-9:.001E-9:.6E-9;
4 CR = 2/3;
5 CRL = 1/2;
6 Tslot = Ts*1E9;
7
8 Rd4 = CR*((4*log2(4))./(5.*Ts*4));
9 Rd8 = CR*((4*log2(8))./(5.*Ts*8));
10 Rd16 = CR*((4*log2(16))./(5.*Ts*16));
11 Rd32 = CR*((4*log2(32))./(5.*Ts*32));
12 Rd64 = CR*((4*log2(64))./(5.*Ts*64));
13 LLCD16 = CRL*(log2(16))./(Ts*16);
14
15 plot(Tslot,(Rd4/1E9),'m')
16 hold on
17 plot(Tslot,(Rd8/1E9),'c')
18 plot(Tslot,(Rd16/1E9),'r')
19 plot(Tslot,(Rd32/1E9),'b')
20 plot(Tslot,(Rd64/1E9),'g')
21
22 xlabel('Slot time [ns]')
23 ylabel('Datarate [Gbps]')
24 legend('4-PPM','8-PPM','16-PPM','32-PPM','64-PPM')
25 title('Downlink datarate vs. slot time and PPM order at CR = 2/3')
26 ylim([0 1.5])
27 xlim([0 .5])
28 yline(1,'k--','Gbps limit','HandleVisibility','off')
29 xline(.125,'k--','0.125 ns','HandleVisibility','off')
30 xline(.25,'k--','0.25 ns','HandleVisibility','off')

```

A.2.2. Uplink

The code below was used for the uplink data rate simulation in figure 5.7.

```

1 close all
2
3 Ts = 0:.01E-9:7E-9;
4 CR = 2/3;
5 CRL = 1/2;
6 Tslot = Ts*1E9;
7
8 Rd4 = CR*((4*log2(4))./(5.*Ts*4))/4;
9 Rd8 = CR*((4*log2(8))./(5.*Ts*8))/4;
10 Rd16 = CR*((4*log2(16))./(5.*Ts*16))/4;
11 Rd32 = CR*((4*log2(32))./(5.*Ts*32))/4;
12 Rd64 = CR*((4*log2(64))./(5.*Ts*64))/4;
13 LLCD16 = CRL*(log2(16))./(Ts*16))/4;
14
15 plot(Tslot,(Rd4/1E6),'m')
16 hold on
17 plot(Tslot,(Rd8/1E6),'c')
18 plot(Tslot,(Rd16/1E6),'r')
19 plot(Tslot,(Rd32/1E6),'b')
20 plot(Tslot,(Rd64/1E6),'g')

```

```

21
22 xlabel('Slot time [ns]')
23 ylabel('Datarate [Mbps]')
24 legend('4-PPM','8-PPM','16-PPM','32-PPM','64-PPM')
25 title('Uplink datarate vs. slot time and PPM order at CR = 2/3')
26 ylim([0 40])
27 xlim([0 7])
28 %yline(20,'k--','20 Mbps limit','HandleVisibility','off')
29 yline(30,'k--','30 Mbps limit','HandleVisibility','off')
30 xline(1,'k--','1 ns','HandleVisibility','off')
31 xline(2,'k--','2 ns','HandleVisibility','off')
32 xline(4,'k--','4 ns','HandleVisibility','off')

```

A.3. Pointing

The codes in this section were used for the pointing analysis

A.3.1. Pointing loss vs. geometric loss

The code below was used for the pointing vs. geometric loss trade-off in figure 5.11.

```

1 close all
2
3 Thetap = 3E-6;
4 p0 = .001;
5 lapda = 1.550E-6;
6 Rmoon = 3.84E8;
7
8
9 thetadiv = [4E-6:.1E-6:15E-6];
10 sigmajitter1 = 1E-6;
11 Dia = (2*lapda)./(thetadiv*pi);
12 w0 = (pi*thetadiv)./lapda;
13
14 Gtx = 10*log10(((pi*Dia)/lapda).^2);
15 ptstat = 10*log10(exp(-(2*Thetap^2)./(thetadiv.^2)));
16 ptscin1 = 10*log10(p0.^((4.*sigmajitter1.^2)./(thetadiv.^2)));
17
18
19 Lfs = -310;
20 Geoloss = Gtx+Lfs;
21 ptloss1 = ptstat+ptscin1;
22 combi1 = Lfs+Gtx+ptloss1;
23
24
25
26 figure(1)
27 hold on
28 title('Tradeoff between geometric and pointing link loss')
29 xlabel('Aperture diameter [m]')
30 ylabel('Link loss [dB]')
31
32 plot(Dia, Geoloss)
33 hold on
34 plot(Dia, combi1)
35 %plot(Dia, combi2)
36 yyaxis right
37 plot(Dia, ptloss1)
38 hold on
39 ylabel('Pointing loss [dB]')
40 legend('Geometric loss G_{tx}+L_{fs}','Combined G_{tx}+L_{fs}+L_{pt} 1 urad rms','Pointing
    loss L_{pt}',Location='northeast')

```

A.3.2. Required pointing accuracy vs. Diameter

The code below was used to plot required pointing accuracy as a function of aperture diameter at various predetermined constant pointing losses in figure 5.12.

```

1 close all
2

```

```

3 p0 = .001;
4 thetastat = 3E-6;
5 lapda = 1.550E-6;
6 thetadiv = 4E-6:.01E-6:15E-6;
7 Epow = (-2*(thetastat^2))./(thetadiv.^2);
8
9
10 D = (2*lapda)./(pi*thetadiv);
11
12 sigmaj10 = sqrt(((thetadiv.^2).*((log10((10^(-1))./(exp(Epow))))/(log10(p0)))))./4);
13 sigmaj8 = sqrt(((thetadiv.^2).*((log10((10^(-4/5))./(exp(Epow))))/(log10(p0)))))./4);
14 sigmaj7 = sqrt(((thetadiv.^2).*((log10((10^(-7/10))./(exp(Epow))))/(log10(p0)))))./4);
15 sigmaj6 = sqrt(((thetadiv.^2).*((log10((10^(-3/5))./(exp(Epow))))/(log10(p0)))))./4);
16 sigmaj5 = sqrt(((thetadiv.^2).*((log10((10^(-1/2))./(exp(Epow))))/(log10(p0)))))./4);
17 sigmaj45 = sqrt(((thetadiv.^2).*((log10((10^(-8/20))./(exp(Epow))))/(log10(p0)))))./4);
18 sigmaj4 = sqrt(((thetadiv.^2).*((log10((10^(-2/5))./(exp(Epow))))/(log10(p0)))))./4);
19 sigmaj35 = sqrt(((thetadiv.^2).*((log10((10^(-7/20))./(exp(Epow))))/(log10(p0)))))./4);
20 sigmaj3 = sqrt(((thetadiv.^2).*((log10((10^(-3/10))./(exp(Epow))))/(log10(p0)))))./4);
21 sigmaj25 = sqrt(((thetadiv.^2).*((log10((10^(-5/20))./(exp(Epow))))/(log10(p0)))))./4);
22 sigmaj2 = sqrt(((thetadiv.^2).*((log10((10^(-1/5))./(exp(Epow))))/(log10(p0)))))./4);
23 sigmaj15 = sqrt(((thetadiv.^2).*((log10((10^(-3/20))./(exp(Epow))))/(log10(p0)))))./4);
24 sigmaj1 = sqrt(((thetadiv.^2).*((log10((10^(-1/10))./(exp(Epow))))/(log10(p0)))))./4);
25
26
27 figure
28 hold on
29 plot(D, sigmaj10,'b')
30 plot(D, sigmaj8,'g')
31 plot(D, sigmaj6,'r')
32 plot(D, sigmaj4,'c')
33 plot(D, sigmaj3,'y')
34 plot(D, sigmaj2,'m')
35 plot(D, sigmaj1,'k')
36
37
38 hold on
39 title('Required pointing accuracy vs. D_{ap} at constant pointing losses')
40 xlabel('Aperture diameter [m]')
41 ylabel('Required pointing accuracy [rad]')
42 legend('Loss_{pt} = -10 dB','Loss_{pt} = -8 dB','Loss_{pt} = -6 dB','Loss_{pt} = -4 dB','
         Loss_{pt} = -3 dB','Loss_{pt} = -2 dB','Loss_{pt} = -1 dB')

```

A.4. SCPPM deep space Poisson simulation

The code shown below was used for the CCSDS SCPPM deep space Poisson simulation creating the results in figure 5.14[85]. It includes Matlab commands specifically created for these kind of applications.

```

1 close all
2
3 crc32Generator = comm.CRCGenerator(...
4     Polynomial="x^32+x^29+x^18+x^14+x^3+1", ...
5     InitialConditions=1);
6 infoSize = 10046;
7
8 m = 4; % PPM order
9 M = 2^m; % PPM slots
10
11 Ts = 0.125; % PPM slot width in nanoseconds
12 pps = linspace(2,4,20)'; % Average number of signal photons per
    nano second (ns/(M*Ts))
13 ns = power(10,pps/10)*M*Ts; % Average number of signal photons per pulsed
    slot
14 nb = 1; % Average number of noise photons per slot
15
16 numFrames = 10;
17 numErrFrames = zeros(length(ns),1);
18 berEst = zeros(length(ns),1);
19 errorRate = comm.ErrorRate;
20

```

```

21 for itr = 1:length(ns)
22     rng("default")
23     for frmIdx=1:numFrames
24         % Generate input data
25         data = randi([0 1],infoSize,1);
26         crcData = crc32Generator(data); % Generate CRC
27         msgIn = [crcData; 0; 0]; % Add termination bits
28
29         % Perform SCPPM encoding
30         [encSym,info] = ccstdsSCPPMEncode(msgIn,m);
31         r = info.OuterEncoderCodeRate;
32
33         % M-ary PPM Modulation
34         modOut = zeros(length(encSym)*M,1);
35         mapIndex = (0:length(encSym)-1)*M + encSym + 1;
36         modOut(mapIndex) = 1;
37
38         % Pass through Poisson channel
39         receivedCode = HelperDeepSpacePoissonChannel(...
40             modOut,ns(itr),nb);
41
42         % SCPPM decoding
43         [decData,errFrames] = ccstdsSCPPMDecode(...
44             receivedCode,r,m);
45         errorStats = errorRate(int8(msgIn),decData);
46         numErrFrames(itr) = numErrFrames(itr)+errFrames;
47     end
48     berEst(itr) = errorStats(1);
49     reset(errorRate)
50 end
51
52 semilogy(pps,berEst,'-*')
53 xlabel("Signal photons per nano second in dB photons/ns")
54 ylabel("Bit Error Rate")
55 title(['BER for CR = 2/3, 16-PPM, nb=',num2str(nb),' ,Ts=',num2str(Ts),' ns'])

```

A.5. 3D EIRP plot

The code shown below was used to create the 3D EIRP plot in figure 5.15.

```

1 close all
2
3 lapda = 1550E-9;
4 thetap = 3E-6;
5 p0 = .001;
6 sigmaj = 1E-6;
7 EIRP = 2.64E10;
8 eta = .7;
9
10 thetadiv = [8E-6:.5E-6:20E-6];
11 D = (2*lapda)./(pi*thetadiv);
12
13 ptstat = 10*log10(exp(-(2*thetap^2)./(thetadiv.^2)));
14 ptscin = 10*log10(p0.^((4*sigmaj^2)./(thetadiv.^2)));
15 ptloss = [ptstat+ptscin]';
16
17
18 pav = EIRP./(((D.*pi)./(lapda)).^2).*eta.*(10.^(ptloss./10));
19
20 surf(D,ptloss,pav)
21 hold on
22 title('Constant EIRP surface as a function of P_{av}, D_{ap} and L_{pt}')
23 xlabel('Aperture diameter [m]')
24 ylabel('Pointing loss [dB]')
25 zlabel('Average transmit power [W]')

```

A.6. 2D EIRP plots

The code shown below was used to create the EIRP plots in section 5.6.3.

```

1 close all
2
3
4 EIRPllcd = 1.0565*10^10;
5 EIRPdot = 2.64*10^10;
6 EIRPdsoc = 2.5*10^11;
7 EIRPsaturn = 1.33*10^12;
8 Pav = [0.1:0.01:12];
9 lapda = 1.55E-6;
10 eta = 0.7;
11 etadsoc = .5;
12 Lpt = .63;
13
14 Dllcd = sqrt((EIRPllcd)./(Pav*eta*Lpt))*(lapda/pi);
15 Ddot = sqrt((EIRPdot)./(Pav*(pi/lapda)^2*eta*Lpt));
16 Ddsoc = sqrt((EIRPdsoc)./(Pav*(pi/lapda)^2*etadsoc*Lpt));
17 Dsaturn = sqrt((EIRPsaturn)./(Pav*(pi/lapda)^2*eta*Lpt));
18
19
20 figure;
21 hold on
22 title('Constant EIRP lines for DSOC systems as function of P_{av} and D_{tx}')
23 xlabel('P_{av} [W]')
24 ylabel('Transmit aperture diameter [m]')
25 plot(Pav,Dllcd,'g')
26 plot(Pav,Ddot,'c')
27 plot(Pav,Ddsoc,'r')
28 plot(Pav, Dsaturn,'b')
29 legend('LLCD EIRP = 130.2 dBm, 622 Mbps','DOT EIRP = 134.22 dBm, 1.07 Gbps','DSOC EIRP = 144
    dBm, 267 Mbps','Saturn EIRP = 151.22 dBm, 1.56 Mbps')
30 ylim([0 1])
31
32
33 figure;
34 hold on
35 title('DOT EIRP line for 1 Gbps as function of P_{av} and D_{tx}')
36 xlabel('P_{tx} [W]')
37 ylabel('Transmit aperture diameter [m]')
38 plot(Pav,Ddot)
39 legend('EIRP = 134.22 dBm, 1550 nm')
40 ylim([0.05 .4])
41
42 figure;
43 hold on
44 title('Saturn terminal EIRP line for ... as function of P_{av} and D_{tx}')
45 xlabel('P_{tx} [W]')
46 ylabel('Transmit aperture diameter [m]')
47 plot(Pav,Dsaturn)
48 legend('EIRP = 151.22 dBm, 1550 nm')
49 ylim([0.1 .8])
50 xlim([0 12])

```

B

Redundant chapter: Challenges and opportunities

Several major challenges still lie ahead in the field of deep space optical communications. These challenges will become bigger as exploration missions venture deeper into space and scale with required performance. New challenges and problems however also present new possibilities and opportunities for technological development. These will be discussed in this chapter

B.1. Challenges

This section will discuss some of the major challenges that still exist.

B.1.1. Laser and amplifier efficiency

One of the biggest problems currently is laser efficiency. Spacecraft have limited power resources and these only get scarcer as one goes deeper into space, further away from the sun. Simultaneously deeper space means larger range and thus higher required laser power. Current laser efficiencies around 10-20% [137] are very low and thus a waste of onboard power supply. This presents a lot of room for technological improvement.

B.1.2. Pointing

Despite continuous technology development and constantly improving accuracies, pointing remains a challenge in FSO due to the small beamwidths. Near Earth communications require complex dynamic gimbal pointing mechanisms in optical relay constellations with many terminals. LOS durations in LEO can be on the order of several minutes. A challenge lies in shortening the pointing and acquisition times. This can be done by improving modelling accuracy and laser ranging measurements [112]. Deep space requires a stabilized very high accuracy link. Apertures become larger to limit required laser power, producing smaller beamwidths which need high precision. Additionally uplink pointing beacons become less practical when going beyond Mars [128]. This means pointing systems would need to rely on star tracker and SC attitude data. At this range coarse pointing is more often done by SC body pointing instead of a dynamic gimbal which puts more pressure on its AOCS system [112]. Beam stabilization also is of higher priority because of the large range. This may require higher performance vibration isolation systems, especially in body pointing systems where mechanical platform interfaces are more direct than in gimbal systems.

B.1.3. Modulation slot time

To achieve a Gbps data rate with PPM, the smallest allowable CCSDS slot time of 125 ps is required. Such T_s has not yet been used practically to the best of the authors knowledge. Smallest proven T_s known was 200 ps by LLCD in 2013, ten years ago. A T_s of 125 ps requires a maximum timing jitter in the order of 10 ps for the laser modulator and for the SNSPD detector. This puts enormous performance constraints on the required HW and SW for both space terminal and OGS. Although M/4

SCPPM guard slots offer some breathing space for transmit and receive components, at 16PPM this still is only a break of 500 ps. Smaller slot times thus enable higher data rates but offer a significant challenge for hardware implementation and processing capabilities in the future.

B.1.4. Geographic diversity

Utilizing one OGS as has been assumed in this thesis may be risky regarding availability. Link performance is extremely dependent on atmospheric and weather conditions. Unlike RF communication which work all the time, clouds may block the link completely. To mitigate this it would be better to have more geographic diversity, meaning more OGS options to use for linking with DOT in case of sub-optimal environmental conditions at primary OGS site[112]. This could for example be enabled by an optical deep space network as discussed earlier in 5.1.1. Geographic OGS diversity will prove especially important for deep space since link windows may be limited depending on mission scenario. To realise this, challenges lie in infrastructure and geopolitics as link data may be sensitive.

B.1.5. Atmospheric turbulence

Geographic diversity might fix the weather problem but will not fix the challenge posed by atmospheric turbulence. Atmospheric absorption and scattering attenuates link power, while the beam is distorted by turbulence and SNR is decreased by background radiation[112][50]. These are often already taken into account using models and mitigation methods like adaptive optics. However it is still important to keep improving the state of the art and minimize atmospheric losses. This will allow more efficient systems and larger ranges for deep space.

B.1.6. Photon counting uplink detector

Currently, APDs are generally accepted to be the best option for space terminal uplink detector technology. APDs can be turned into single photon detectors by running them in geiger mode. This significantly increases detector sensitivity and allows communication in photon starved situations. Geiger mode has several disadvantages however compared to a nominal APD. Unlike nominal APDs, geiger mode cannot distinguish incoming light intensity and have sort of binary on-off responsivity. This would complicate estimation of environmental link quality for adaptive modulation. Furthermore it is subject to cross-talk and after-pulsing [6]. The latter may cause false detection caused by carriers from past events. To mitigate this dead time or reset time is significantly higher in geiger mode, which leads to either detector blocking losses or a decreased data rate due to longer symbol time [105]. It would therefore be better to operate the uplink at significant power levels so that the APD can be run in nominal mode. The future challenge lies in development of high performance, low swap space terminal detectors which can operate in photon starved conditions, especially for deep space scenarios.

B.1.7. Low spectral efficiency PPM

The low spectral or bandwidth efficiency of PPM on the one hand is key to its unrivalled power efficiency and SNR but on the other hand causes limited data rates compared to other modulation schemes. DOT modulation of 16-PPM, which is common for lunar application [26][107], and smallest allowable slot times only just reach Gbit/s rates. Which means there is currently a cap on lunar data rates using PPM. Only if slot times become smaller and if laser efficiency is improved, allowing lower PPM order, data rate can be increased with a standard PPM format. Otherwise its spectral efficiency will somehow have to be improved, or other modulation schemes are needed. Data rates keep increasing and PPM will have to adjust to keep up.

B.2. Opportunities

This section will discuss technical development opportunities that might tackle some of the challenges of DSOC.

B.2.1. Fast steering dichroic beam splitters

Dichroic mirrors in optical terminals serve the purpose of separating or combining beams of different wavelengths. They currently are only used in static mounting. In the spirit of making optical terminals more efficient, an opportunity would be to create actuated dichroic mirrors. These would point and direct a certain wavelength beam while passing another, thereby combining two functionalities of DBS

and PAM which reduces optics complexity and SWAP, see figure B.1. A challenge in this would be to design an actuation system that moves the mirror at the edges. This is necessary to allow unobstructed path for the passing wavelength. This has not been done before as most FSMs actuate the mirror from behind like the one from TNO in figure B.2. The mirror would probably similarly use piezoelectric actuators to achieve urad accuracy.

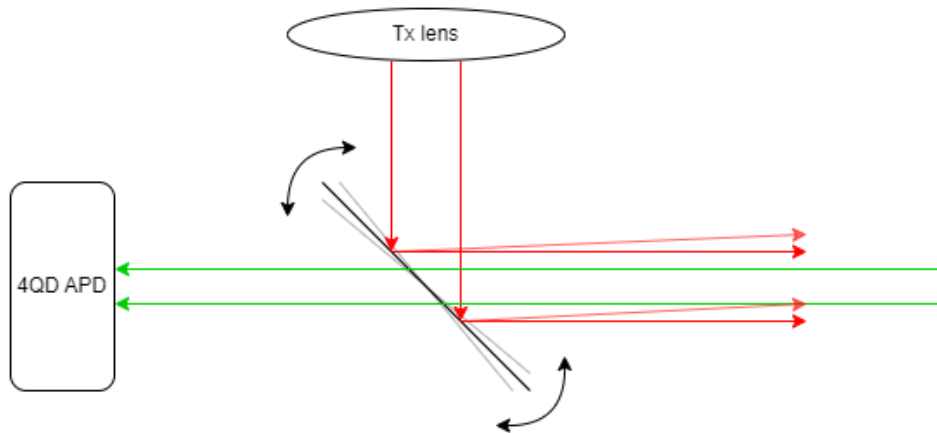


Figure B.1: Fast steering dichroic beam splitter performing PA.

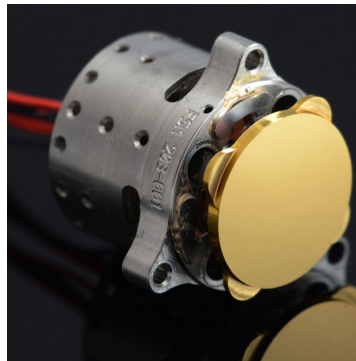


Figure B.2: TNO FSM [72].

B.2.2. Solar pumped lasers

As indicated, lasers and fiber amplifiers have very low wall plug efficiencies, causing a lot of wasted power. This low efficiency is partially caused by power conversions, namely solar to electrical to optical. Using the solar radiation directly for optical laser power would be much more efficient and logical. Solar pumped lasers (SPL) are not new, they already exist since shortly after the invention of the laser 60 years ago. It has however never been applied yet for space optical communication. In 2011, [78] managed to produce a 12.3 W Nd:YAG laser with a 0.9 diameter Fresnel lens collecting solar power, corresponding with a collection efficiency of 19.3 W/m² collector. The same researchers improved this record at the end of 2022 when they produced a 16.5 W coherent continuous wave 1064 nm laser beam [79]. This was done with a solar radiation collector area of 0.4 m² focused into a pump cavity with Nd:YAG rods. At a solar irradiance of 890 W/m² this resulted in a collection efficiency of 41.25 W/m² and a record breaking solar to laser efficiency of 4.64%. In 2017 the first terrestrial FSO link was achieved with SPL technology [144]. A similar setup was used with a 0.35 m² Fresnel lens focusing 930 W/m² solar irradiation into a gold plated optical pump cavity with a cooled Nd:YAG rod inside, see figure B.3 where the conical cavity has a length of 5 cm and diameter of 3 cm. The rod was fiber coupled and combined with a 1064 seed laser producing a 6.8 W optical output. The output was modulated by Lithium Niobate MZM and transmitted over a distance of 5 m before being decoded by an APD at data rate of 125 Mbps with BER E-6.

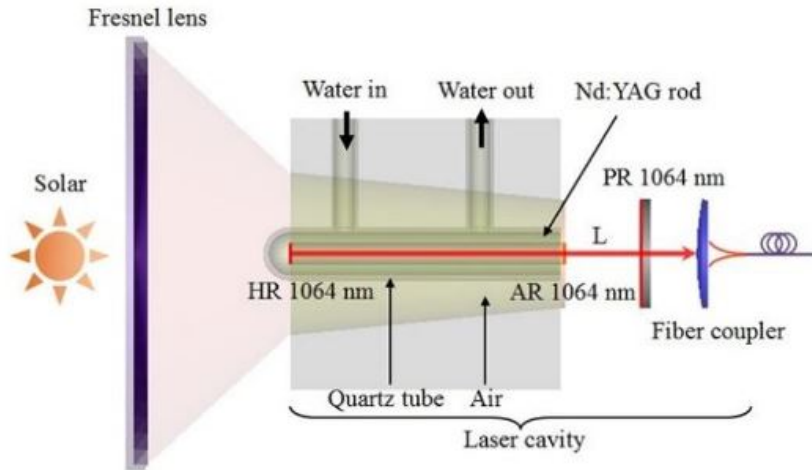


Figure B.3: SPL used for terrestrial FSO [144].

Assuming highest proven SPL efficiency of 4.64% [79] and extraterrestrial solar irradiation of 1367 W/m² [64], DOT would need 0.0236 m² collecting area or an aperture of 17.4 cm diameter, to produce up to 1.5 W optical power amplification. A SPL to power DOT will thus not take up very much SWAP and would save a significant amount of electrical power in the order of $(5 - 10)P_{tx}$, assuming regular FA efficiency of 10-20% [137]. Note this is assuming discussed technology producing a 1064 nm laser. It is yet unknown if this technology can also be applied to produce 1550 nm beams. Discussed examples worked with Nd:YAG rods doped with Cesium ions because these exhibit high absorption levels in the UV and visible spectral region which make up the larger part of solar irradiation, see figure B.4. Additionally the Ce ions perform efficient energy transfer to Nd ions. The Nd ions subsequently strongly emit radiation in the 1064 nm region. This process is very much alike to that described earlier, where the Ytterbium ions in EYDFA are effectively pumped with 975 nm light before efficient energy transfer to Er ions which then release 1550 nm radiation. A new kind of pump medium would have to be designed which is doped with ions that have optimal absorption levels in the most intense part of the solar spectrum and efficient energy transfer to Erbium ions, that can then release required 1550 nm light.

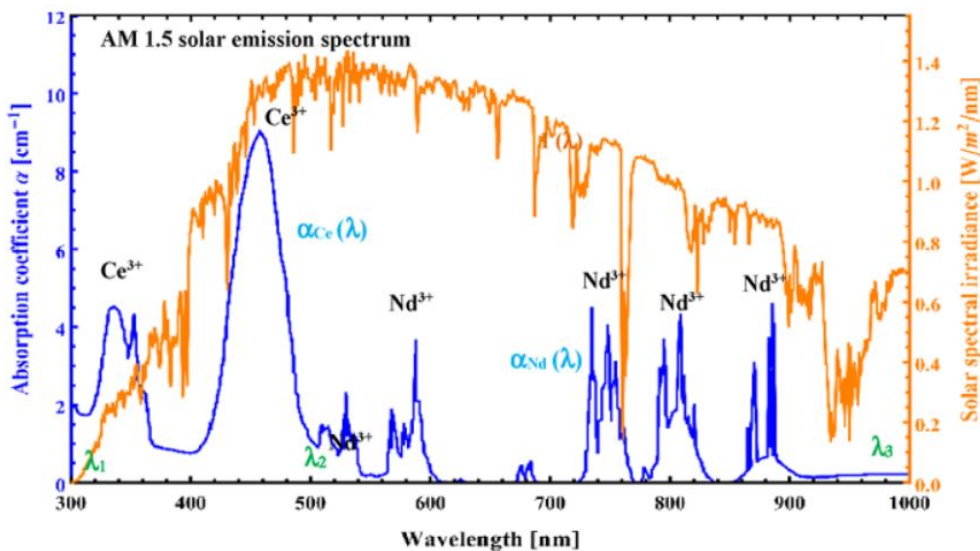


Figure B.4: Terrestrial solar irradiance spectrum along with absorption spectrum of the Ce:Nd:YAG pump medium used in [79].

This technology has a few side notes of course. While linking, the collector aperture would need to be in continuous optimal solar illumination to maintain steady laser power level, requiring not only PAT for the duplex laser beams but also for the solar pump collector. Not much is known about SPL ASE behaviour and could be quite complex to control since solar pump light involves almost the entire EM spectrum instead of only one pump wavelength. Additionally, solar irradiation decreases exponentially into deep space, so this might not be practical beyond certain distance from the sun.

B.2.3. Multidimensional pulse position modulation

A trend that can often be seen is that increase of datarate at the same BER scales linearly with average transmit power [50]. It often means making a choice between either power efficiency or bandwidth efficiency. Multidimensional PPM however is a modulation scheme that offers increased datarates at the same power levels. The idea was initiated in 2001 when [71] suggested combining regular M-PPM with K-WSK (wavelength shift keying) modulation, where in each time slot one of K wavelengths is transmitted, coding for a specific bit sequence. This was later also mentioned in [50]. Combining these effectively results in a bandwidth performance of KM order PPM modulation, using M-PPM temporal architecture. An example can be seen in figure B.5 where 4-WSK combined with 8-PPM gives 32-PPM bandwidth performance, coding 5 bits into one pulse using only 8 time slots. Regular 8-PPM only achieves 3 bits in one pulse. This comes at a price of increased system complexity caused by multiple wavelength use.

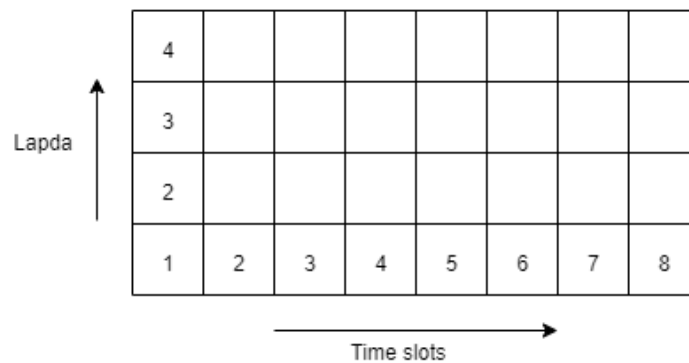


Figure B.5: Multiwavelength PPM (MWPPM) [27].

Similarly this idea can be expanded into more dimensions. Phase modulation could for example be involved as shown in figure B.6. The figure shows an expansion of two modes for phase modulation, this could either use BPSK or DPSK as baseline. Effective bandwidth in this architecture would be similar to 64-PPM, coding 6 bits into one active pulse using only 8 time slots per symbol instead of 64 slots. As a reference, if DOT would use 2 phases and 4 wavelengths additional to 16-PPM, 7 bits could be coded instead of 4 on each pulse, resulting in a net datarate of 1867 Mbps instead of 1067. One might even consider another modulation dimension like polarization [30].

This method of course has some drawbacks. While increasing datarates at constant power levels, adding more modulation dimensions would significantly complicate the system regarding both HW and SW. A higher error rate will occur due to receiver sensitivity not only to intensity but also phase and wavelength. The atmospheric channel is a highly distorting factor for phase modulation and might not be practical for photon starved deep space links, although being implemented more like DPSK from GEO in LCRD [35]. Also different wavelength modes used might lie close to each other while deep space relative velocities can be very high, resulting in measured wavelength errors due to Doppler shift.

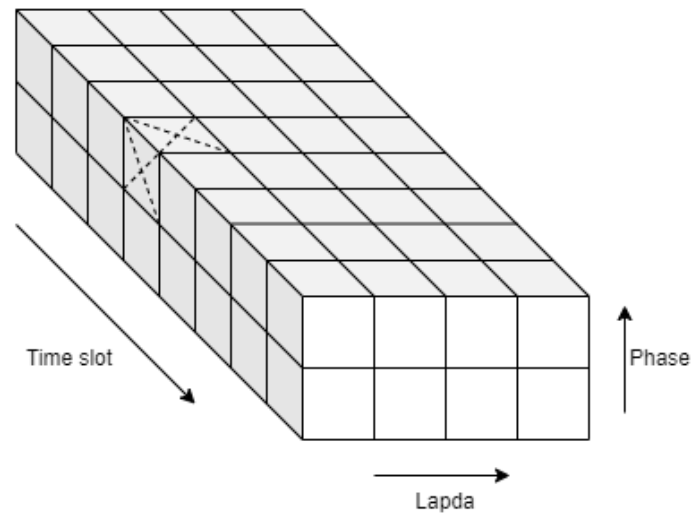


Figure B.6: Multidimensional PPM

B.2.4. Multifunctional uplink detector

As indicated, DOT terminal design relies on an uplink detector that performs PAT and data comms simultaneously. These kind of detectors are not yet available commercially but have been custom made and proven by several institutions [37][89][10] and planned for use in ESA's L5 mission [122]. Such an uplink detector significantly simplifies optical design and additionally increases link quality since part of the uplink power is not needed anymore for a separate 4QD detector path. This will furthermore save on terminal SWAP. The uplink detector will then preferably also be able of downlink point ahead verification. This means it will have to be sensitive to both wavelength regions and be able to distinguish between them. It is unknown if current APDs can distinguish between separate wavelengths.

An alternative is to fabricate mixed APD substrates which are sensitive to individual wavelengths. DOT uplink and downlink, like most optical systems currently, operate at 1064 and 1550 nm respectively. this would be done through a 4QD detector array assembly where the inner centroid part is Si based for the 1064 nm uplink is expected to be centered, and where the surrounding outer array medium is InGaAs based for the 1550 nm Tx PAA is expected off center, see figure B.7. This would promote wavelength distinction and would allow to make the Si medium spatially and high speed data comms sensitive while the outer part would only need spatial sensitivity.

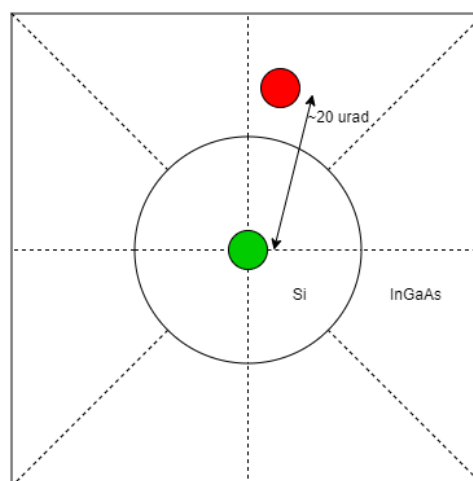


Figure B.7: Binary substrate 4QD APD array. The green circle represents uplink beam and the red circle the downlink beam PAA verification.

B.2.5. Isispace deep space deployer and optical relay

The final opportunity does not discuss a technology but more a mission architecture. Isispace recently finished development of its deep space deployer (DSD) [56]. It is especially meant for precision trajectory release of cubesats for deep space applications. This initiative comes from a growing popularity of deploying cubesats for deep space applications. NASA for example carried 10 cubesats into cislunar space on Artemis 1 [42] and the SGAC is currently designing a mission concept to explore Uranus with a main orbiter carrying several cubesats as payload [141]. Three NASA flagship missions in the upcoming 15 years include the Europa clipper [103], Uranus orbiter and probe [5] and the Enceladus orbiter [81], all exploring the outer solar system ice/gas giants and their potentially habitable moons. In contrast to traditional single spacecraft flagships like Cassini [125], cubesat swarms have a lot of advantages like flexibility, affordability, modularity and lower risk. Additionally swarms can be deployed to study different targets and moons within a planetary system at once and are able to perform unique experiments while formation flying.

There is an opportunity for Isispace to expand on their DSD and continue development for these kind of missions. One critical issue is that cubesat communication systems aren't capable of bridging interplanetary deep space ranges. That's why after deployment of the cubesats in Saturn system for example, the DSD could act as relay orbiter for the cubesats. These would use regular RF or TNO's optical Cubecat [113] to communicate with the DSD relay. The DSD would then be equipped with a deep space optical terminal that bridges a high data rate link to Earth.

Saturn use case

A case for optical communication from Saturn has been made as expansion on this technological opportunity and to estimate primary terminal characteristics.

Maximum downlink data rate from the Cassini High Gain Antenna (HGA) during Saturn tour was 166 Kbps [130]. Making a parallel with LLCD, its downlink rate of 622 Mbps was a 6.22x improvement on the 100 Mbps Lunar Reconnaissance Orbiter [68]. A downlink data rate aim for a future Saturn orbiter with laser comms will thus have a similar improvement of $7 \times 166 \text{ Kbps} = 1.162 \text{ Mbps}$. The proposed Orbiter mission to Enceladus assumes a nominal downlink rate of 40 Kbps [81] so the aimed for 1.162 Mbps will be more than enough at almost 30x higher. A data rate model has been made which is a function of PPM order and slot time which can be seen in figure B.8.

A robust CR of 1/2 has been assumed for more redundancy similar to the LLCD demonstration [25]. Minimum usable slot time is assumed to be 0.5 ns as has been previously demonstrated in LLCD and will be used in the upcoming Psyche mission. PPM orders and CCSDS recommended slot times are shown. The required data rate can easily be reached as seen. It is preferred to use a high PPM order for power efficiency and low BER. The required data rate can even be achieved with a PPM order as high as 8192 with a 0.5 ns slot time. This would be an extremely power efficient system. However, the CCSDS does not allow PPM orders higher than 256 [15]. Therefore this order will be assumed in combination with a slot time of 8 ns as seen in the figure. This slot time is chosen as it approaches aimed data rate the closest, a longer slot time of 16 ns would not reach required rate. Data rate would in this case be 1.56 Mbps, in the end almost 10x higher than Cassini.

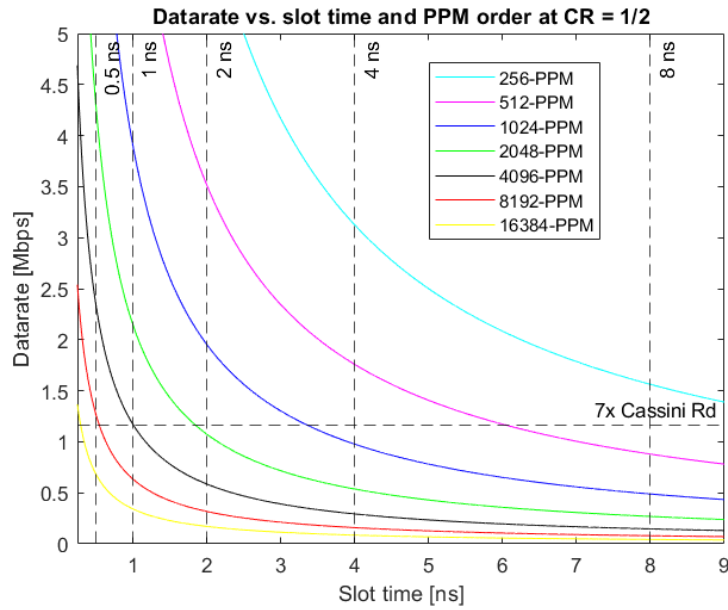


Figure B.8: Data rates as function of slot time and PPM order.

Noise rate was found harder to estimate in this situation than for DOT. For this link one would probably use a much larger telescope to catch as much signal as possible, smaller bandpass filter, smaller FOV and perform link at nighttime to limit blue sky radiance. It has similarly been assumed there will be one noise photon per PPM slot. The same Matlab CCSDS compliant SCPPM deep space poisson channel simulation was then performed and shown in figure B.9.

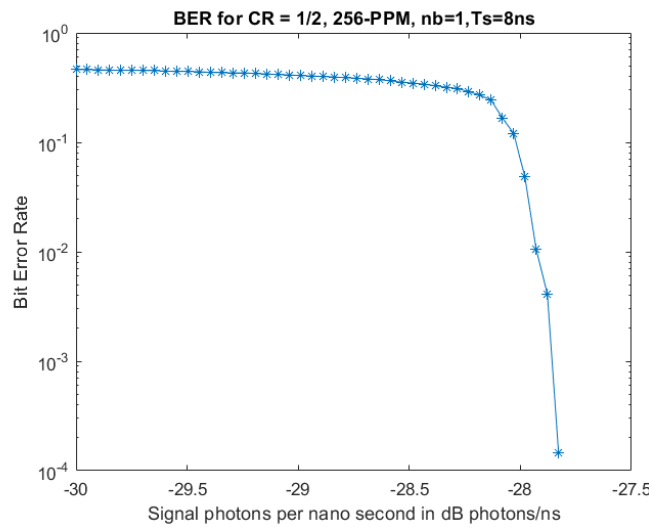


Figure B.9: CCSDS SCPPM deep space Poisson simulation for Saturn.

The simulation was performed for above discussed modulation settings, 256-PPM, 8 ns slot times, 1/2 CR and 1 noise ph/slot. As can be seen, it seems to converge towards -27.5 dB photons/ns. Most of the same link variables have been assumed as earlier in the DOT EIRP calculation except for free space loss, which is much bigger at -381.1 dB for Saturn range, and receiver gain with a 12 m OGS at 147.7 dB [51]. This results in a required EIRP of 151.22 dBm. This EIRP for a Saturn optical link has been plotted along with earlier discussed DSOC missions in figure B.10. Assuming an aperture size of 30 cm, an average laser transmit power of 8.12 Watts would be needed. In a paper comparing RF to optical for deep space applications in the 2020 timeframe [140], similar results are achieved at Saturn

range with an aperture of 26.5 cm diameter and 7.5 W for up to 10 Mbit/s. Compared with this, the analysis performed in this thesis might be considered conservative.

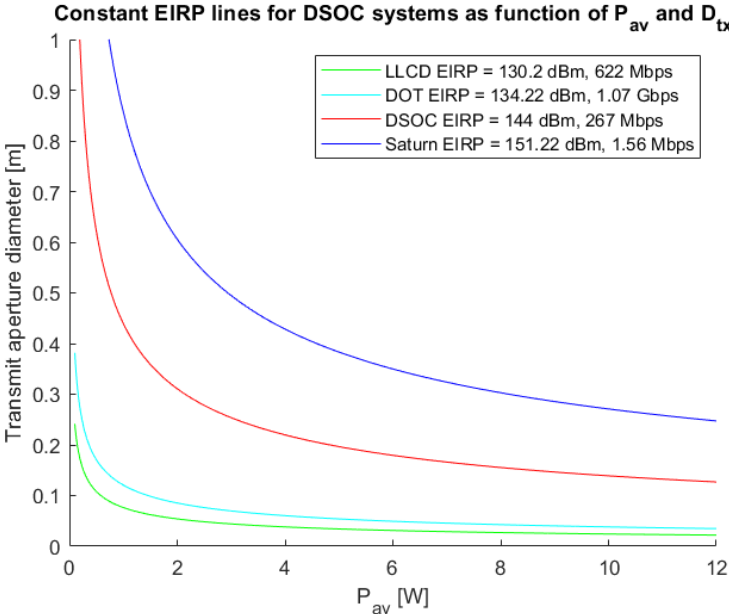


Figure B.10: Comparison of EIRP for several DSOC terminals.



Redundant work

C.1. Downlink detector

With a slot time of 0.125 ns for the downlink, the only viable option for the OGS detector is a SNSPD. It is the only detector with timing jitter in the order of several ps, which is needed for CCSDS regulations of <10% slot time. SNSPDs furthermore show superior performance in quantum efficiency for a 1550 nm wavelength around 90%, low dark count rates and highest counting rates (low reset time) exceeding GHz levels. Table C.1 shows a tradeoff table for the downlink detector.

Table C.1: Downlink detector trade.

Downlink		Options >			Comments
Criteria V	Weight (1-5)	SNSPD	PMT	APD (InGaAs)	
Timing jitter	5	<10 ps	3 ns	300 ps	
Quantum efficiency	4	90%	2%	75%	
Dark counts	2	1 Hz	25 Hz	kHz	
SWAP	1	Big	Medium	Small	
Counting rate	3	>500 MHz	50 MHz	800 MHz	
Score		43	6	27	

SNSPDs work by cryogenic cooling of composite nanowires, often sputtered niobium nitride, below their superconducting state down to several K. These nanowires are formed in a pattern within a single pixel. A current flows through it while being superconductive. When a photon hits the nanowire, energy is absorbed and a hotspot is produced. Within the hotspot, resistance is finite and the wire becomes non-superconducting. A voltage pulse is created representing a single photon count while the nanowire cools to become superconducting again and get ready for the next photon impact [94]. The mechanism is shown in figure C.1. Use of multipixel detectors allows higher count rates and even photon number resolution. It can furthermore be used for tracking purposes. Using a fiber coupled configuration instead of direct detection would allow a more flexible and modular design and is thus preferred. The beam would first hit the telescope, get corrected by AO and enter OGS optics before being coupled to fiber. SNSPD's are currently highest performance options but do require quite bulky and cryogenic infrastructure. They are therefore not an option for use in the DOT space terminal.

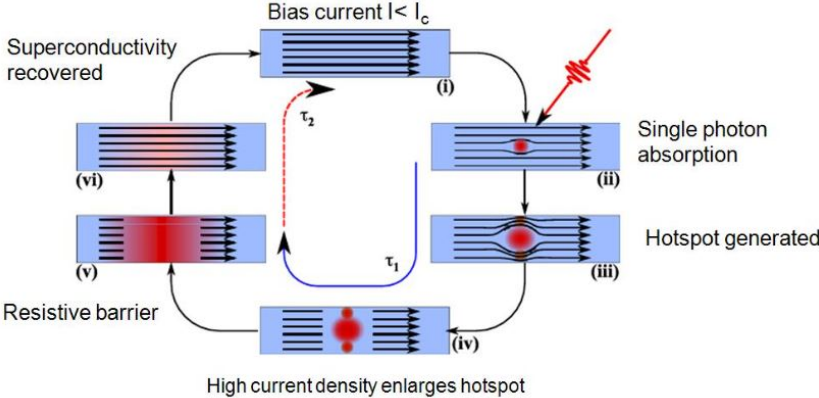


Figure C.1: SNSPD mechanism [94].

D

Simulations

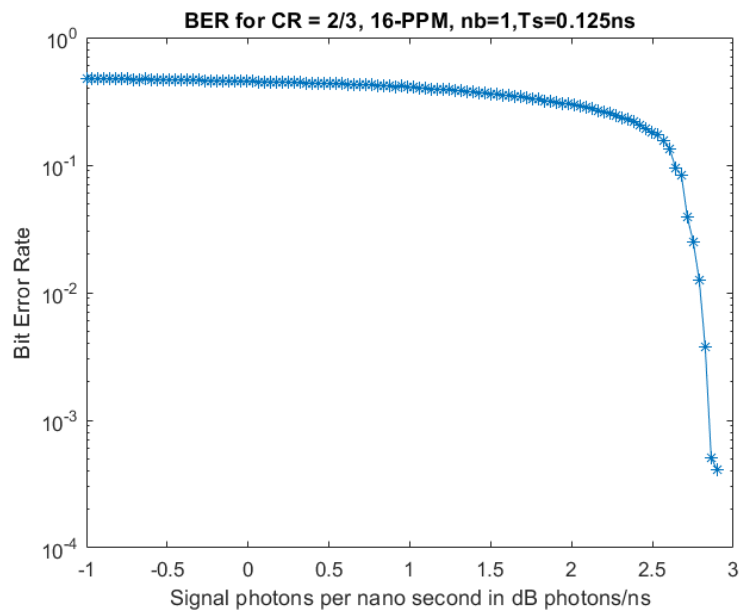


Figure D.1: SCPPM max datarate simulation 1.

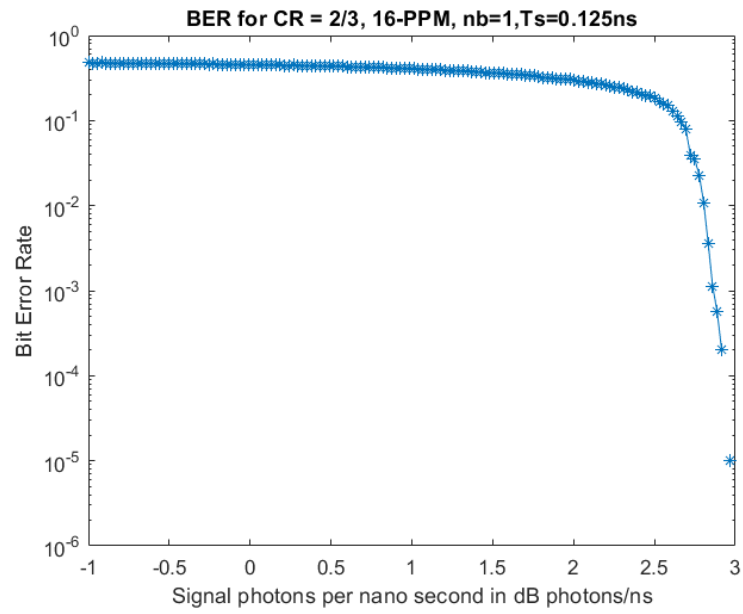


Figure D.2: SCPPM max datarate simulation 2.

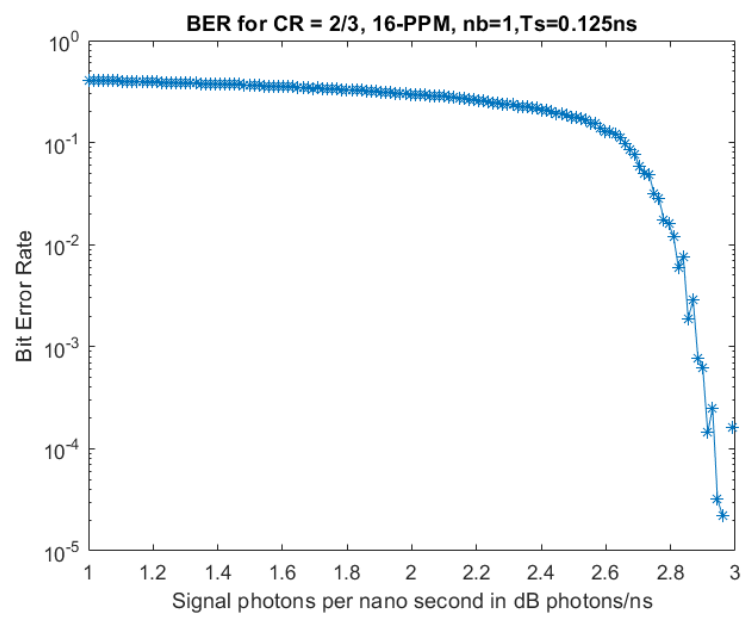


Figure D.3: SCPPM max datarate simulation 3.

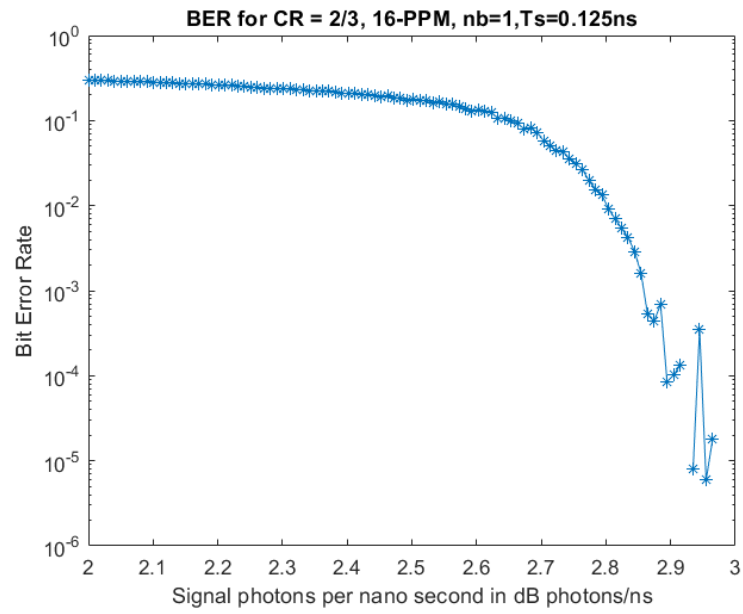


Figure D.4: SCPPM max datarate simulation 4.

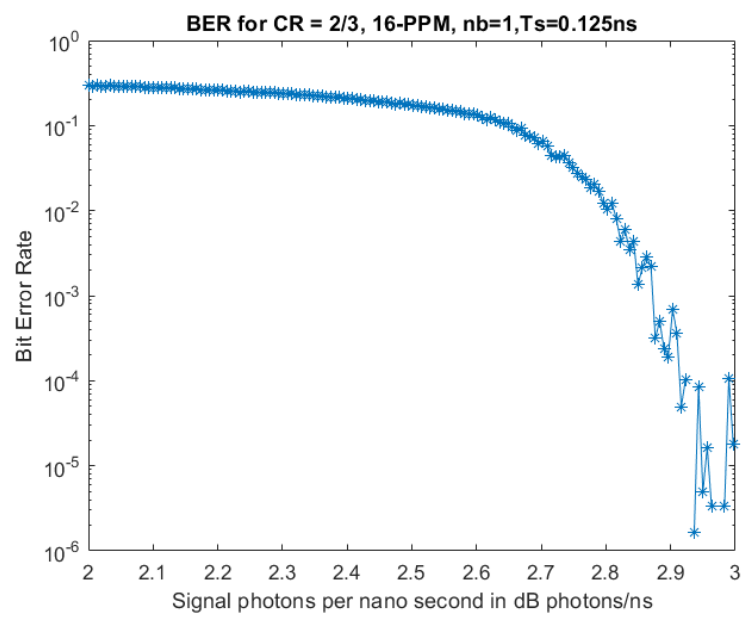


Figure D.5: SCPPM max datarate simulation 5.